NUREG/CR-6943
PNNL-16472

A Study of Remote Visual Methods to Detect Cracking in Reactor Components

Pacific Northwest National Laboratory

\

U.S. Nuclear Regulatory Commission
Office of Nuclear Regulatory Research
Washington, DC 20555-0001

NUREG/CR-6943
PNNL-16472

A Study of Remote Visual Methods to Detect Cracking in Reactor Components

Manuscript Completed: August 2007
Date Published: October 2007

Prepared by
S.E. Cumblidge, M.T. Anderson, S.R. Doctor,
F.A. Simonen, A.J. Elliott

Pacific Northwest National Laboratory
P.O. Box 999
Richland, WA 99352

W.E. Norris, NRC Project Manager

Prepared for
Division of Fuel, Engineering and Radiological Research
Office of Nuclear Regulatory Research
U.S. Nuclear Regulatory Commission
Washington, DC 20555-0001
NRC Job Code Y6604

Abstract

The U.S. Nuclear Regulatory Commission Office of Nuclear Regulatory Research funded a multiyear program at the Pacific Northwest National Laboratory (PNNL) to evaluate the reliability and accuracy of nondestructive evaluation techniques employed for inservice inspection. Recently, the U.S. nuclear industry proposed replacing current volumetric and/or surface examinations of certain components in commercial nuclear power plants, as required by the American Society of Mechanical Engineers Boiler and Pressure Vessel Code Section XI, "Inservice Inspection of Nuclear Power Plant Components," with a simpler visual testing (VT) method. The advantages of VT are that these tests generally involve much less radiation exposure and time to perform the examination than do volumetric examinations such as ultrasonic testing. Therefore, the issues relative to the reliability of VT in determining the structural integrity of reactor components were examined.

Certain piping and pressure vessel components in a nuclear power station are examined using remote VT to reduce occupational exposure as they are in high radiation fields. Other components are examined using VT because the geometry precludes the use of ultrasonic testing (UT). Nuclear utilities employ remote VT with radiation-hardened video systems to find cracks in pressure vessel cladding in pressurized water reactors and core shrouds in boiling water reactors and to investigate leaks in piping and reactor components. The utilities perform these visual tests using a wide variety of procedures and equipment, including the use of submersible closed-circuit video cameras for the remote examination of reactor components and welds.

To evaluate the reliability and effectiveness of the testing, PNNL conducted a parametric study that examined the important variables influencing the effectiveness of remote VT. The tested variables included lighting techniques, camera resolution, camera movement, and magnification. PNNL also conducted a limited laboratory test using a commercial visual testing camera system to experimentally determine the ability of the camera system to detect cracks of various widths under ideal conditions. The results of these studies and their implications are presented in this report.

Foreword

The U.S. nuclear industry has proposed replacing the volumetric and surface examination requirements of certain safety-related components specified in the ASME International Boiler and Pressure Vessel Code, Section XI, "Inservice Inspection of Nuclear Power Plant Components," with remote visual testing (VT) methods. Remote VT with radiation-hardened video systems has been used to find cracks in pressure vessel cladding in pressurized water reactors and core shrouds in boiling water reactors as well as investigate leaks in piping and reactor components. These visual tests are performed using a wide variety of procedures and equipment.

In addition to reducing occupational exposure, the time required to perform a VT inspection is less than that for volumetric inspection methods such as ultrasonic testing (UT), and can be deployed in geometries that preclude the use of UT. However, few comprehensive studies on the effectiveness and reliability of VT have been published.

Given the shortage of available information on the capabilities and effectiveness of remote VT, the U.S. Nuclear Regulatory Commission (NRC) initiated research to examine the important variables that influence the effectiveness of remote VT and to assess the effects of the variables on the ability of remote systems to detect cracks. Six parameters—crack size, lighting conditions, scanning speed, camera resolution, surface specularity, and surface conditions—were assessed.

The results indicate that crack opening displacement (COD) is the parameter that most dramatically impacts the reliability of inspections. The study concludes that a significant fraction of the cracks that have been reported in nuclear power plant components are at the lower end of the capabilities of the VT equipment currently being used. The study also suggests that inspection conditions need to be nearly ideal to detect these cracks.

Remote VT has been used extensively to inspect the reactor pressure vessel (RPV) internals in boiling water reactors (BWRs). Accordingly, the NRC evaluated the surface conditions found on these components and assessed the structural integrity of these components as related to the cracking that has been reported. The assessment showed that most of the BWR internal components can tolerate rather large cracks without compromising integrity. Some locations, however, receive special inspections because failures have occurred as a result of small cracks. Therefore, the surface conditions and quality of inspection are very important relative to the probability of detection of cracks.

The research results have been presented at several, recent symposia and shared with the cognizant ASME International Section XI committees, the Boiling Water Reactor Vessel Internals Project, and the Electric Power Research Institute.

Jennifer L. Uhle, Director
Division of Fuel, Engineering and Radiological Research
Office of Nuclear Regulatory Research
U.S. Nuclear Regulatory Commission

Contents

Abstract iii

Foreword v

Executive Summary xiii

Acknowledgments xvii

Abbreviations and Acronyms xix

1 Introduction 1.1

2 Background 2.1
- 2.1 Standards in Visual Testing 2.1
- 2.2 Previous Studies on Crack Detection 2.1
- 2.3 Cracks in Reactor Components 2.2
- 2.4 Cracks in Components 2.4
- 2.5 Factors Influencing Crack Opening Displacement 2.6
- 2.6 Primary Factors in Crack Detection 2.7
- 2.7 Determining Visual Acuity 2.9
- 2.8 Brightfield and Darkfield Imaging 2.12
- 2.9 Specular and Diffuse Reflection 2.14

3 Experimental Procedures 3.1
- 3.1 Parametric Study 3.1
- 3.2 Cameras and Lights 3.1
- 3.3 Specularity Measurements 3.3
- 3.4 Reactor Internals Samples 3.4
- 3.5 Laboratory Tests of Radiation-Hardened Cameras 3.5

4 Parametric Study of Crack Detection Using Visual Testing 4.1
- 4.1 Parametric Matrix Results 4.1
- 4.2 Inspection-Dependent Parameters 4.3
  - 4.2.1 Camera Resolution/Magnification 4.3
  - 4.2.2 Lighting Style 4.4
  - 4.2.3 Scanning Speed 4.8
- 4.3 Subject-Dependent Parameters 4.11
  - 4.3.1 Crack Opening Displacement/Crack Size 4.11
  - 4.3.2 Surface Scratching and Machine Marks 4.12
  - 4.3.3 Surface Specularity 4.13

5 Laboratory Test Results 5.1
5.1 Fixed-Focus Camera Test Results 5.1
5.2 Pan/Tilt/Zoom Camera Results 5.2

6 Conditions in Commercial Reactors 6.1
6.1 Oxide Deposits in Reactors 6.1
6.2 Effects of Oxide Layer on Crack Detectability 6.3
6.3 Surface Features and Geometry 6.5

7 Discussion 7.1
7.1 Parametric Study 7.1
7.2 Laboratory Tests 7.2
7.3 Conditions in Reactor Components 7.2
7.3.1 Reduced Specularity 7.2
7.3.2 Discoloration 7.2
7.3.3 Crack Decoration 7.3
7.3.4 Crack Masking 7.3
7.4 Integrated Results 7.3

8 Conclusions 8.1

9 References 9.1

Appendix A – Surface Conditions for Each Window Used in Limited Round Robin Test A.1

Appendix B – Images from Parametric Test Matrix B.1

Figures

2.1 Relationship of Line Visibility to Contrast Between Line and Sharpness of Background and Image 2.8

2.2 Recognition of High-Contrast Letters as a Function of Letter Size and Image Sharpness 2.8

2.3 Recognition of Reduced-Contrast Letters as a Function of Letter Size and Image Sharpness 2.9

2.4 Sample Image of a 1951 U.S. Air Force Resolving Power Target 2.11

2.5 Lighting for Brightfield and Darkfield Imaging 2.13

2.6 Crack with 12-μm Crack Opening Depth Imaged Using Both Darkfield and Brightfield Illumination 2.13

2.7 Simultaneous Brightfield and Darkfield Effects Produced by Lighting at Off Angle 2.14

2.8 Specular and Diffuse Reflection 2.14

3.1 Visual Testing Apparatus and Sample 3.2

3.2 Lights Used in Visual Testing Experiments 3.2

3.3 Dime Illuminated Using Three Lighting Techniques 3.2

3.4 Experimental Setup for Specularity Measurements 3.3

3.5 Reactor Internals Samples Used in Testing. 3.4

3.6 Cameras Used for Laboratory Tests. 3.6

3.7 Water Tanks with Specimens Prepared for Visual Inspection 3.7

4.1 12-μm COD Crack Illuminated with Diffuse On-Axis Lighting Imaged Using a 1.3-Megapixel Video Camera Set to Full Magnification. 4.5

4.2 12-μm COD Crack Illuminated with Diffuse On-Axis Lighting Imaged Using 640 × 480 Pixels of Resolution. 4.5

4.3 12-μm COD Crack Illuminated with Spotlight Imaged Using 1.3-Megapixel Video Camera Set to Full Magnification. 4.6

4.4 Images of Crack, Wire, and Scratches Taken Using Diffuse On-Axis Light, Diffuse Ring Light, and Bare-Bulb LED Spotlight 4.6

4.5 125-μm COD Crack Imaged Using Ring Light and Two Spotlights 4.7

4.6 Sample Images of a 125-mm COD Crack Imaged at Three Scanning Speeds 4.9

4.7 Effect of Scanning Speed on Grayscale Level Contrast Between Crack and Background 4.9

4.8 1951 Air Force Resolution Target Imaged at Two Scan Speeds 4.10

4.9 Effects of Scanning Speed on Resolution of Radiation-Hardened Camera 4.10

4.10 Sample Images of Three 12-μm COD Cracks 4.12

4.11 Influence of Lighting Style on Crack Detectability on Highly Specular Surface 4.14

4.12 Influence of Lighting Style on Crack Detectability on Somewhat Specular Surface 4.14

4.13 Influence of Spotlighting Angle on Crack Detectability on Somewhat Specular Surface 4.15

6.1 Examples of Deposit Layers from BWR and PWR 6.2

6.2 Bottom of PWR Pressure Vessel 6.2

6.3 A Crack Before and After Cleaning Loose Oxide Layer from Surface 6.3

6.4 Mechanical Fatigue Crack with Black Oxide Decorating One End of Crack 6.4

6.5 Mechanical Fatigue Crack Made Visible by Disturbance in Loose Oxide Layer 6.4

6.6 Stress Corrosion Crack Through Stainless Steel Made More Visible by Oxide Decoration 6.5

6.7 Mottled Surface with Varying Color and Specularity Across Surface 6.6

6.8 Complex Surface Geometry and Deposit Layering on BWR Component 6.6

6.9 Complex Surface Deposit Layering On and Near BWR Weld 6.7

Tables

2.1 Crack Widths in Stainless Steel Components 2.2

2.2 Crack Shape Versus Crack Type 2.3

2.3 Number of Turns per Millimeter Versus Crack Type 2.3

2.4 Examples of Calculated Lengths for Acceptable Flaws Detected by VT Examinations 2.5

2.5 Number of Lines per Millimeter by Group and Element in a 1951 U.S. Air Force Resolving Power Target 2.11

4.1 Subjective Evaluation Results for Parametric Matrix for Samples 1-9 ..... 4.1

4.2 Matrix Results for Lighting Techniques 4.7

4.3 Effects of Crack COD on Crack Detectability 4.11

4.4 Effects of Surface Conditions on Crack Detectability 4.13

5.1 Probability of Detection by Inspector Using Fixed-Focal Length Camera 5.1

5.2 Probability of Detection Versus Crack COD Results Using Fixed-Focal Length Camera 5.2

5.3 Probability of Detection Versus Crack COD Results Using the Pan/Tilt/Zoom Camera 5.2

Executive Summary

Reactor pressure vessel internal components in boiling water reactors (BWR) are presently examined using remote visual testing (VT). Recently, the U.S. nuclear industry proposed to expand the use of visual testing by replacing current volumetric and/or surface examinations of certain components in commercial nuclear power plants, as required by the American Society of Mechanical Engineers Boiler and Pressure Vessel Code (ASME Code) Section XI, Inservice Inspection of Nuclear Power Plant Components, with a simpler VT method. The advantages of VT are that these tests generally involve much less radiation exposure and time to perform the examination than do volumetric examinations such as ultrasonic testing (UT). A study of the issues associated with the reliability of VT in determining the structural integrity of reactor components was initiated in response to the proposal to expand the use of VT.

Parametric Study

Pacific Northwest National Laboratory (PNNL) conducted a study on the effects of various parameters on the ability of a mechanical system to image cracks on a stainless steel surface. Six parameters—crack size, lighting conditions, scanning speed, camera resolution, surface specularity, and surface conditions—were assessed from the standpoint of the inspector being able to control them and parameters that are sample-dependent.

The parameter that appeared to have the largest effect on the inspection reliability is the crack opening displacement (COD). The test matrix results and the other examinations showed that cracks with CODs above 100 μm (0.004 in.) are generally detectable unless the inspection parameters and surface conditions are very unfavorable. Cracks with CODs less than 20 μm (0.0008 in.) were difficult to detect under all but the most favorable conditions.

Between these two extremes in crack COD, things become more difficult to quantify. When the other parameters are taken into account, the matrix study showed little difference in the reliability in detecting cracks between 20–40 μm (0.0008–0.0016 in.) and 40–100 μm (0.0016–0.004 in.). How well one can detect these cracks appears to be very dependent on other test conditions.

Limited Laboratory Test

PNNL also conducted a limited laboratory test to determine the ability of radiation-hardened cameras to detect cracks on stainless steel components. Four inspectors examined 30 areas to determine if they could find a series of cracks. The tests were carried out under water to partially simulate the reactor environment. The limited test substantiated previous laboratory results in that cracks above 100 μm (0.004 in.) were relatively easy to detect, and cracks below 20 μm (0.0008 in.) were extremely difficult to detect. The quality of the examinations and camera systems was of great importance in the reliability of detecting cracks with CODs between 20–100 μm (0.0008–0.004 in.). Careful inspections using good lighting and stationary cameras allowed good detection of the cracks in this range, while quick scanning resulted in very poor crack detection.

Review of Reactor Internals

PNNL also conducted a review of the surface conditions found on components in commercial nuclear power plants. It was determined that the welds are often in as-welded conditions with weld beads and weld toe intact. The surfaces of the internals are not polished smooth and have a variety of scratches, grinding marks, and machining marks. Some cladding styles leave ripples along the surfaces. Also, the surfaces become oxidized and may be covered in an oxide layer. Finally, suspended material from the primary water may be deposited.

As a result of the above factors, cracks in stainless steel reactor internals in operating BWRs and pressurized water reactors (PWRs) can be difficult to detect. The weld beads, scratches, grinding and machining marks can hide a crack. In addition, these surfaces are usually covered by a surface layer of deposits. This layer of deposits is made up of colloidal corrosion products from the primary water. These corrosion products are a mix of oxides, consisting of Fe_2O_3, Fe_3O_4, Fe_2CoO_4, Fe_2NiO_4, and other metal oxides. The layer in BWRs, which have highly oxidizing conditions in the primary system, tends to consist primarily of Fe_2O_3 (hematite). In PWRs, the layer tends to be primarily M_3O_4, with M being made up of Fe, Ni, and Co (Kim 2003). It could reasonably be assumed that the oxide layer would assist in crack detection because the lighting would not create a glare on the dull oxide layer. However, it could also be reasonably argued that the oxide layer would impede crack detection by "covering up" the crack. This aspect has not yet been analyzed as part of this study and, as such, is not addressed in this report.

Previous Studies on Crack Detection

Few comprehensive studies of the probability of various video systems used for remote VT to detect cracks relative to crack opening displacement (COD) have been published to date. A visual system was used in Sweden to test crack detectability in reactor components, and the reported detectable limit for flaws was 20 μm (0.0008 in.) (Efsing et al. 2001). Useful information on the evaluation of remote VT was found in a recent human factors study performed in Sweden (Enkvist 2003). A series of cracked ceramic specimens, molded to reproduce the surface appearance of a welded region, was examined underwater by 10 operators using a high-resolution 752- × 582-pixel video camera with an 18X optical zoom and lighting provided by two 15-W halogen lamps. Cracks larger than 40 μm (0.0016 in.) COD were detected easily, while cracks less than 20 μm (0.0008 in.) COD had, at best, a 20% probability of detection using the "Lenient" grading scale defined by Enkvist (2003).

A study on the detectability of tight thermal fatigue cracks (Virkkunen et al. 2004) under normal inspection conditions was performed using a commercially available remote camera system. This work showed that the smallest cracks that could be reliably detected with their system were 100 μm (0.0039 in.) COD or larger, and the smallest defects possible to detect were 40 μm (0.0016 in.) COD. The detection rate for cracks smaller than 100 μm (0.0039 in.) COD were approximately 20%.

Discussion

The results of the PNNL parametric study were in good agreement with the limited round-robin test, the Swedish human factors study, and the Finnish camera test. The results of these studies show that large cracks can be defined as cracks with a COD larger than 100 μm (0.004 in.), tight cracks can be defined as

cracks with a COD smaller than 20 μm (0.0008 in.), and the mid-range cracks fall between these extremes.

This mid range of 20 μm to 100 μm (0.0008 in. to 0.004 in.) is somewhat troubling as many of the types of cracks that may occur in nuclear power plant components have a median COD on the order of 16 to 30 μm (0.0006 to 0.0012 in.). This suggests that a significant fraction of the cracks being reported in nuclear power plant components are at the lower end of the capabilities of the equipment currently being used. In addition, the studies suggest that inspection conditions need to be nearly ideal to detect these cracks. Careful inspections using good lighting and stationary cameras allowed good detection of the tight cracks, while quick scanning resulted in very poor crack detection in this range of COD sizes. The higher magnification used in the Swedish study was one reason why it may have found higher performance for crack detection in this range when compared to the PNNL study using the fixed-focus camera.

Conclusions

Based on the results achieved in both the parametric and laboratory studies, the following conclusions can be drawn:

- The current radiation-hardened video cameras being used in the field can be expected to reliably find cracks with CODs greater than 100 μm (0.004 in.), provided surface conditions are not overly unfavorable, adequate lighting is achieved, and sufficiently slow scan rates are applied.

- The current radiation-hardened video cameras being used in the field are not capable of effectively detecting cracks with CODs smaller than 20 μm (0.0008 in.).

- The reliability of detecting cracks with CODs between 20 and 100 μm (0.0008 and 0.004 in.) using current radiation-hardened video cameras under field conditions inspecting normal fabricated components is strongly dependent on the camera magnification, lighting, inspector training, and inspector vigilance.

- The scanning rate of a video camera over a surface strongly affects the visual acuity of the camera. At low speeds, the camera suffers little loss of visual acuity, but at high rates, the image becomes severely degraded.

- Diffuse lighting helps to increase the contrast between a crack and the metal surface while decreasing the contrast from scratches and machining marks in the metal surface.

- Reliable detection of tight cracks in nuclear components may require higher-resolution cameras.

- Although the oxide layer in reactors can aid in crack detection, the overall effects of the oxide layer are not known and need to be understood regarding influence on crack detectability.

Acknowledgments

This work is being sponsored by the U.S. Nuclear Regulatory Commission under Contract DE-AC06-76RL01830; NRC JCN Y6604; Mr. Wallace Norris, NRC Program Monitor.

PNNL would also like to thank the Imaging and Sensing Technology Corporation, especially Mark Moeser and Jonathan Quartly, for providing the radiation-hardened camera systems for the laboratory tests and parametric tests.

Abbreviations and Acronyms

ASME	American Society of Mechanical Engineers
ASME Code	ASME Boiler and Pressure Vessel Code
ASNT	American Society of Nondestructive Testing
AWS	American Welding Society
BWR	boiling water reactor
BWRVIP-03	BWR Vessel and Internals Project-3
CCTV	closed-circuit television
COD	crack opening displacement
CRDM	control rod drive mechanism
EPRI	Electric Power Research Institute
EVT	enhanced visual testing
IEEE	Institute of Electrical and Electronics Engineers
IGSCC	intergranular stress corrosion cracking
ISI	inservice inspection
ISO	International Organization for Standardization
LED	light-emitting diode
MTF	modulation transfer function
NDE	nondestructive examination
NRC	U.S. Nuclear Regulatory Commission
PNNL	Pacific Northwest National Laboratory
PWR	pressurized water reactor
RMS	root mean square
SCC	stress corrosion crack
SRCS	sensitivity, resolution, and contrast standard
UT	ultrasonic testing
VT	visual testing

1 Introduction

Visual testing (VT) is widely used as a primary inspection technique or to provide complementary information for other, more indirect nondestructive examination (NDE) methods. The human eye is highly adept at detecting small features or irregularities on the surfaces of materials, and direct VT, if applied under specific parameters, with appropriate optical tools and lighting, can exhibit highly reliable inspection results. Many VT applications use remotely operated video camera systems due to factors such as the location, size, and geometry of the parts or adverse environments surrounding the surfaces to be inspected. Because VT appears to be fundamentally simple and straightforward, and remote VT systems are convenient to deploy for periodic inspections, greater reliance is being placed on VT to determine the structural integrity of nuclear power plant components. However, the variables associated with VT personnel and equipment are often times not well defined. A better understanding of the effects of the variables on VT is required in order to determine their overall capabilities and limitations in detecting the targeted degradation.

In the commercial nuclear power industry, remote VT is used to examine components in the primary coolant system, including internal surfaces of the reactor pressure vessel and core support structures. These examinations are conducted either as part of an established inservice inspection (ISI) program required by Title 10, Part 50 of the *Code of Federal Regulations* or under licensee regulatory commitments such as the Boiling Water Reactor Vessels Internals Project (BWRVIP). Examinations conducted as part of an ISI program are performed in accordance with Section V and Section XI of the American Society of Mechanical Engineers Boiler and Pressure Vessel Code (ASME Code). The examinations performed in accordance with the BWRVIP adhere to the 150+ guidance documents that have been developed since the program's inception. Implementation variables such as the frequency of examinations, visual resolution, lighting parameters, acceptance criteria, and examiner qualifications are detailed in the ASME Code, Sections V and XI. The U.S. Nuclear Regulatory Commission (NRC) reviews and approves applicable ASME Code Editions for use at operating nuclear plants and ensures that ISI programs comply with NRC-approved ISI programs. The NRC also reviews and approves the requisite BWRVIP documents, and the NRC and the Institute for Nuclear Power Operations (INPO) routinely audit the plants to ensure compliance. Current ISI programs at operating reactors rely heavily on NDE to detect the presence of service-induced degradation that may lead to a breach of the pressure boundary or affect structural integrity; remote VT is one in a suite of NDE techniques that are deployed for this purpose.

The materials used in the design of safety-related components at commercial operating plants are robust; they were selected to provide good corrosion resistance, high strength, and fracture toughness. The most advanced forming and welding processes available were used under the auspices of high quality control programs during the fabrication of important components. Operating and residual tensile stresses are usually highest on the surfaces of the components near structural discontinuities such as welds or thickness transitions. For these reasons, it is commonly believed that service degradation will be initiated on the surfaces (not from embedded fabrication flaw growth) and will most likely occur first on the internal surfaces exposed to environments that could accelerate flaw initiation and growth. Therefore, in many cases, known degradation processes are expected to result in crack initiation on the internal surface of safety-related system components. For remote VT to be considered effective, inspection systems and implementation practices must be capable of detecting small cracks before they grow to a size that could challenge the leak-tightness of the pressure boundary.

To reduce some of the burden associated with ISI, the U.S. nuclear industry has increasingly been developing options to volumetric examinations (e.g., ultrasonic or radiographic testing) and surface examinations (e.g., electromagnetic, liquid penetrant, or magnetic particle testing) for certain components in commercial nuclear power plants by implementing remote visual tests. The advantages of using remote VT are that these tests generally involve much less radiation exposure and reduced inspection times than do the current volumetric and surface techniques. Because of geometry considerations, VT is used for some components because transducer access is limited or not possible. In some cases, the industry has proposed to perform "enhanced" remote visual examinations as alternatives to existing volumetric and/or surface tests.(1) This enhancement is based on the ability of the system to resolve a wire 12 μm (0.0005 in.) in diameter, intended as a baseline system calibration. With regard to using VT rather than volumetric methods, an analysis of all the pertinent issues is needed relative to the reliability of remote VT in determining the structural integrity of reactor components.

This report expands on the work performed earlier by Pacific Northwest National Laboratory (Cumblidge et al. 2004; NUREG/CR-6860) for the NRC. It is intended to provide a basis for describing the technical issues that must be addressed when applying remote VT to detect cracking phenomena by highlighting the inherent capabilities and limitations associated with current system deployment. The work has been aimed at nuclear power plant components; however, these issues exist for all industries where remote VT is expected to reliably detect small flaws.

Section 2 provides important background information on visual testing, defines terms, and explains concepts that will be used later in the report; it also covers the characteristics of flaws found in stainless steels and nickel alloys as well as a representative range of the sizes of tolerable flaws in nuclear reactors. Section 3 describes the experimental apparatus used to conduct the parametric studies and the laboratory tests on commercially used remote visual testing cameras. Section 4 presents and discusses the results of the parametric study. Section 5 describes the results of the laboratory tests on the commercially available camera systems that were used to detect a series of cracks. Section 6 describes the conditions found in commercial nuclear reactors. The visual testing results are described in Section 7, and conclusions are given in Section 8.

(1) Dorman WJ. Correspondence, Carolina Power and Light to U.S. Nuclear Regulatory Commission. "Brunswick Steam Electric Plant, Units 1 and 2, Docket Nos. 50-325 and 50-324, License Nos. DPR-71 and DPR-62, Request for Approval of Revised Relief Request for the Third 10-Year Inservice Inspection Program," August 7, 2000.

2 Background

As reactor components in a nuclear power plant are generally maintained underwater and/or reside in high radiation fields, remote examination with watertight radiation-hardened video systems is necessary. Remote VT has been used successfully to find cracks in pressure vessel cladding in PWRs and core shrouds in BWRs and to investigate leaks in reactor and piping components. These visual tests are performed using a wide variety of procedures and equipment. Techniques generally include the use of submersible closed-circuit high-resolution video cameras to examine reactor components. Numerous industrial camera systems are available for this purpose. These systems have video resolutions ranging from 470 to 600 vertical lines on the screen, roughly equivalent to a 640 × 480-pixel count, and most systems typically possess zoom capability to achieve fields of view of 24 mm × 18 mm (0.9 in. × 0.7 in.) or smaller. There is no standard method for visual test lighting. The cameras typically have a pair of spotlights mounted near the lens to provide illumination. The authors are aware of at least one system that has a light-emitting diode (LED) ring light mounted around the lens. The camera is normally manipulated by operators standing on the refueling bridge using an arrangement of poles and/or ropes. The inspection is primarily performed via a live view of the video on a monitor. The video data with an operator voice-over is typically stored digitally as it is taken for later review.

2.1 Standards in Visual Testing

Nuclear utilities today follow guidelines for remote VT found in the Electric Power Research Institute (EPRI) BWR Vessel and Internals Project-03 (BWRVIP-03; EPRI 2005). These guidelines specify that examined surfaces must be clean, and for underwater testing, that the water be clean and clear. The BWRVIP guidelines also describe training requirements for personnel and specify which areas around a weld should be examined, how to measure the sizes of indications found, and how to test the resolving power of the visual equipment used for the test. There are no guidelines dealing with scanning speed or field of view used during the inspection. To test the visual acuity of the camera system and lighting, the EPRI guidelines call for the camera system to image a sensitivity, resolution, and contrast standard (SRCS) before and after the inspection. This SRCS typically contains two perpendicular wires 12 μm (0.0005 in.) in diameter as a resolution calibration standard. If the camera and lighting are sufficient to detect the wires, then the camera system is deemed to have a resolution sufficiently high for the inspection. The very important issue of lighting is also presumed covered by this line detection test.

2.2 Previous Studies on Crack Detection

Few comprehensive studies of the probability of various video systems used for remote VT to detect cracks relative to crack opening displacement (COD) have been published to date. A visual system was used in Sweden to test crack detectability in reactor components, and the reported detectable limit for flaws was 20 μm (0.0008 in.) (Efsing et al. 2001). Useful information on the evaluation of remote VT was found in a recent human factors study performed in Sweden (Enkvist 2003). A series of cracked ceramic specimens, molded to reproduce the surface appearance of a welded region, was examined underwater by 10 operators using a high-resolution 752- × 582-pixel video camera with an 18X optical zoom and lighting provided by two 15-W halogen lamps. Only one viewing angle and a single distance of 200 mm (7.9 in.) from the test samples were used, so the tests were more restrictive than actual field VT. The area inspected by the system at maximum magnification was 47 × 35 mm (1.85 × 1.46 in.), with

a resulting pixel size of 60 μm (0.0024 in.). Cracks larger than 40 μm (0.0016 in.) COD were detected easily, while cracks less than 20 μm (0.0008 in.) COD had, at best, a 20% probability of detection using the "Lenient" grading scale defined by Enkvist (2003).

A study on the detectability of tight thermal fatigue cracks (Virkkunen et al. 2004) under normal inspection conditions was performed using a commercially available remote camera system. The cracks ranged in COD from less than 20 μm to 200 μm (<0.0008 to 0.008 in.). In this study, the camera was focused on an area 60 × 45 mm (2.36 × 1.77 in.). The cracked area was scanned at 2 cm (0.8 in.) per second, the data recorded, and the images later reviewed frame by frame. Identified areas of interest were then re-examined statically with a focal area of 12 × 9 mm (0.47 × 0.35 in.). This careful scanning, evaluation, and re-evaluation showed that the smallest cracks that could be reliably detected were 100 μm (0.0039 in.) COD or larger, and the smallest defects possible to detect were 40 μm (0.0016 in.) COD. The detection rate for cracks smaller than 100 μm (0.0039 in.) COD was approximately 20%.

2.3 Cracks in Reactor Components

To determine if a remote VT system is capable of detecting actual cracks, a discussion of typical service-induced crack dimensions is needed. The primary feature of a crack to be visually detected is its width, or COD. The COD is a function of several factors, some of which are material hardness, applied loads, crack length, residual stresses around the crack opening, and the degree of corrosive attack at the crack opening. The specific variables of most importance to COD depend on the type of crack involved. For instance, literature reports that the width of intergranular stress corrosion cracking (IGSCC) is fairly random and is primarily a factor of how many grain boundaries at the crack opening are affected.

Several hundred cracks of various types and origins in many materials have been characterized and documented in the literature in the United States and in Europe (Ekström and Wåle 1995; Wåle 2006). The results show that the CODs of inservice-generated cracks are highly variable over most crack types and materials, and several outlier sizes were found that increase the range of the datasets. However, it was found that most reported CODs tend to be populated around a mean, or median, crack width. Table 2.1 provides a compilation of COD ranges for various types of service-induced degradation.

Table 2.1 Crack Widths in Stainless Steel Components

	IGSCC SS	IGSCC Ni	IDSCC Ni	TGSCC SS	Thermal Fatigue	Mechanical Fatigue	Hot Cracks
Total Cracks	65	14	14	25	29	15	17
Minimum (μm)	3	4	0	3	5	3	2
Maximum (μm)	160	260	120	500	380	450	250
Mean (μm)	37.7	42.4	33.4	49.9	51.4	79.4	38.6
Median (μm)	30	17.5	21	20	30	16	25
RMS (μm)	47.2	77.8	48.5	110	85.4	144	67.3
Standard Deviation (μm)	28.7	67.7	36.4	99.6	69.3	125	56.8

It is important to note that the median values for these cracks are very tight, with CODs on the order of 16 to 30 μm (0.0006 to 0.0012 in.). The results show that COD is highly variable over all crack types and materials. This presents a significant challenge when attempting to detect cracks using remote video camera systems.

Equally important, the findings also show that COD is largely independent of the crack through-wall depth and crack length. Thus, judging the overall crack depth by COD is not reliable (Ekström and Wåle 1995). Also, one cannot assume that long cracks have a wider COD than short cracks. Therefore, even if the COD is large enough to be detected visually, other volumetric NDE methods must be used to fully characterize the crack boundaries.

Another factor that aids in crack detection is crack tortuosity (a less technical term might be "crookedness") and branching frequency. Crack tortuosity is a measure of the number of bends in the crack per unit length, and branching describes how often the crack branches off per unit length. A perfectly straight crack that does not branch may be more difficult to detect than one that has many bends and branches, as the bends and branches help to distinguish the cracks from innocuous surface features. One crack morphology occasionally seen with thermal fatigue cracking is called "cobblestone" cracking, which consists of several cracks in close proximity. Cobblestone cracking affects a region and creates Crack shape versus crack type is shown in Table 2.2 while the number of turns per mm vs. crack type is shown in Table 2.3.

Table 2.2 Crack Shape Versus Crack Type

	IGSCC SS	IGSCC Ni	IDSCC Ni	TGSCC SS	Thermal Fatigue	Mechanical Fatigue	Solidification Cracking
Total Cracks	39	4	15	15	28	14	5
Straight, %	64	75	85	60	44	100	80
Winding, %	26	25	15	13	33	0	20
Bent, %	10	0	0	13	0	0	0
Branched, %	0	0	0	13	0	0	0
Cobblestone, %	0	0	0	0	22	0	0

Table 2.3 Number of Turns per Millimeter Versus Crack Type

	IGSCC SS	IGSCC Ni	IDSCC Ni	TGSCC SS	Thermal Fatigue	Mechanical Fatigue	Solidification Cracking
Total Cracks	38	3	5	5	14	4	14
Minimum	4	16	2.7	5	1	1	1
Maximum	40	128	8.5	16	12	6	46
Mean	12.7	65.7	5.7	10.3	3.61	4	12.6
Median	9.9	53	7	8	3	4.5	9.5
RMS	15.2	80.5	6.14	11.2	4.54	4.53	17
Standard Deviation	8.51	57.1	2.55	4.88	2.87	2.45	11.8

2.4 Cracks in Components

When a crack is detected in a component, several issues need to be addressed such as the structural significance of the crack, continued operation, and inspection frequency. Many components can contain relatively long cracks without significantly affecting plant safety. The effect of a flaw on structural integrity and its acceptability for continued operation is based on the structural mechanics of the system and the theoretical crack growth rate of the degradation mechanism. Each individual reactor typically produces a set of flaw tolerance guidelines for each system based on the stresses and actual configuration of individual components.

Fracture mechanics analyses have been performed relative to postulated critical flaw sizes for BWR reactor vessel internal components. PNNL has analyzed representative acceptable lengths of flaws detected by VT examinations in BWR reactor vessel internal components. VT methods applied for inservice inspection should detect flaws before they grow to a critical size with a high level of reliability. The reviewed documents included both BWRVIP reports prepared by EPRI (EPRI 2003, 2005) and calculations from two representative BWRs.

The BWRVIP documented evaluations were based on ASME Section XI approaches that were developed originally for flaws in stainless steel piping. Although some of the components were not strictly ASME Code pressure boundary components, the calculational methods have been reviewed and accepted by the NRC. Given that VT examinations provide no measurements of flaw depth dimensions, all calculations conservatively assumed that the unmeasured flaw depths extended through the entire wall thickness.

Limit load calculations have evaluated flaws in stainless steel base metal and in welds made without the use of welding fluxes. Consistent with ASME Section XI, conservative calculations have been performed for flux-type welding processes (shielded metal arc or submerged arc). These calculations accounted for reduced material toughness (Z factor approach) and included stresses from thermal expansion bending moments as a primary stress that can contribute to unstable crack growth.

The acceptable flaw lengths have accounted for flaw growth (due to stress corrosion cracking or fatigue) between successive inspections and have addressed uncertainties in VT measurements of flaw lengths. These adjustments have been relatively small. Flaw growth rates have been taken to be 25.4×10^{-5} mm/hr (10^{-5} in./hr). This gives 4.45 mm/year (0.175 in./year) increase in the flaw length, which accounts for the growth from both ends of a through-wall crack.

The calculations address two concerns. The primary concern has been that of unstable crack growth by ductile tearing. The second concern has addressed the leakage flow rate through the crack. This second calculation has predicted leakage flows that are small relative to the flow required for the component to perform its intended safety function.

Plant-specific calculations of acceptable flaw lengths are proprietary. The representative examples analyzed by PNNL are given in Table 2.4. Even though a limited number of examples were analyzed, the results nevertheless show some interesting trends, as discussed in the following paragraphs.

Table 2.4 Examples of Calculated Lengths for Acceptable Flaws Detected by VT Examinations

Component	Material	Diameter	Weld Length	Thermal Expansion Stress	Total Stress	Acceptable Flaw Length	Acceptable Flaw Length Fraction of Weld Length
Core Shroud – Vertical Weld	304L		251 cm (98.8 in.)	-	3.0	162 cm (63.6 in.)	0.64
Jet Pump – Thermal Shield to Elbow Weld (Limit Load Failure)	304	10 in., Sch 40	~ 79 cm (31 in.)	-	-	36.3 cm (14.3 in.)	0.46
Jet Pump – Thermal Shield to Elbow Weld (Onset of Fatigue Crack Growth)	304	10 in., Sch 40	~ 79 cm (31 in.)	-	-	14.6 cm (5.75 in)	0.19
Core Spray Line – Non Flux Weld	304	13 cm (5 in.)	~ 38 cm (15 in.)	23 MPa (3.3 ksi)	32 MPa (4.6 ksi)	25.0 cm (9.86 in.)	0.66
Core Spray Line – Flux Weld	304	13 cm (5 in.)	~ 38 cm (15 in.)	220 MPa (32 ksi)	234 MPa (34 ksi)	3.30 cm (1.3 in.)	0.09
Core Spray Line – Non Flux Weld	304	13 cm (5 in.)	~ 38 cm (15 in.)	23 MPa (3.3 ksi)	32 MPa (4.6 ksi)	18.8 cm (7.42 in.)	0.49
Core Spray Line – Flux Weld	304	13 cm (5 in.)	~ 38 cm (15 in.)	64 MPa (9.3 ksi)	83 MPa (12 ksi)	15.1 cm (5.95 in.)	0.40
Sparger– Example 1	304	13 cm (5 in.)	~ 28 cm (11 in.)	9.6 MPa (1.4 ksi)	17 MPa (2.5 ksi)	16.5 cm (6.48 in.)	0.59
Sparger– Example 2	304	13 cm (5 in.)	~ 28 cm (11 in.)	9.6 MPa (1.4 ksi)	17 MPa (2.5 ksi)	16.1 cm (6.33 in.)	0.58

Vertical Weld of Core Shroud – This calculation conservatively takes no credit for the integrity of the circumferential welds (360-degree through-wall cracking) such that each shell course was treated as a separate component. The most embrittled shell course was evaluated for a through-wall vertical (axial) crack based on a fracture toughness of 165 MPa-$m^{1/2}$ (150 ksi-$in.^{1/2}$). Both normal operating and faulted conditions were addressed that gave a relatively low governing hoop stress of 21 MPa (3 ksi). The acceptable flaw length was calculated to be 162 cm (63.6 in.) compared to the 251 cm (98.8 in.) vertical length of the shell course.

Jet Pump Weld of Thermal Shield to Elbow – This calculation for the second sample BWR addressed cracking of the weld in the jet pump that joins the thermal shield and elbow. A circumferential crack was assumed to extend through the full wall thickness. Two allowable flaw lengths were calculated. A length of 14.6 cm (5.75 in.) assumed that the onset of fatigue crack growth was the governing consideration. A

larger flaw length of 36.3 cm (14.3 in.) was established for the assumption that limit load failure was the sole consideration for structural integrity.

Core Spray Line – These calculations, performed for the two sampled BWRs, which are for 13-cm (5-in.) outside diameter Schedule 40 stainless steel piping (EPRI 2005) and assumed a through-wall circumferential crack. Separate calculations were performed for the two BWRs and for flux welds versus non-flux welds. Acceptable flaw lengths ranged from 3.3 cm (1.30 in.) to 25.0 cm (9.86 in.).

Sparger – These calculations performed for the two BWRs were for 8.9 cm (3.5 in.) outside diameter Schedule 40 stainless steel piping (EPRI 2005) and assumed a through-wall circumferential crack. The acceptable flaw lengths were calculated to be 16.0 cm (6.33 in.) and 16.5 cm (6.48 in.) for the two BWRs, respectively.

The review addressed a sample of BWR reactor internal components and considered locations where cracking has been observed or has a potential to occur. The calculations of acceptable crack lengths have been based on conservative considerations including an assumption of through-wall crack depths for the flaws as detected by VT examinations, application of ASME Code safety factors, and the assumption in some cases of lower-toughness flux-type welds. Even with these conservative assumptions, most of the calculated crack lengths were several inches long, although the most limiting example had a calculated flaw length of 3.3 cm (1.30 in.).

It should be noted, however, that there have numerous reports of cracking in certain components of the jet pump assembly and for some component areas, the acceptable crack lengths are in the mid-range of cracks described in this report (i.e., at the lower end of the capabilities of the equipment). In addition, UT is not a viable option in some of these locations either because of geometry or because of the high number of locations that require inspection. Therefore, it is critical to perform VT inspections of the highest quality.

2.5 Factors Influencing Crack Opening Displacement

For thermal and mechanical fatigue cracks, the largest factor governing the crack COD is the stress acting perpendicular to the crack opening (Yoneyama et al. 2000; Kim et al. 2003; Xaio et al. 2002). According to the Westergaard stress function, the maximum COD of a semicircular crack is given by Chen et al. (1996) as

$$COD = \frac{4a\sigma}{E} \tag{2.1}$$

where a is the crack depth (and one half the crack length), σ is the stress on the material, and E is Young's modulus. In a fatigue crack, the COD strongly depends on the state of the material when the crack is measured. If a mechanical fatigue crack is examined when the material is not in tension, the crack can be closed entirely. Without a stress σ, the theoretical COD is zero. Often, the only stress available to hold a fatigue crack open is the residual stress causing the crack formation or resulting from fabrication processes. As the residual and other stresses at a given point are not generally known, one cannot use the COD to predict the through-wall depth of a crack.

It is worth noting that nuclear reactor components are examined during outages when systems are not at operating temperature and pressure. Some of the main sources of stress are not present when the components are examined. With all of the pressure relieved and the differential temperatures across components eliminated when the reactor is shut down, the COD of the cracks in the reactor will most likely decrease to a minimum size.

The factors influencing the CODs for stress corrosion cracks are more complex than for fatigue cracks. Stress corrosion cracks (SCC) form because of an interaction between a sensitized material, a corrosive environment, and stresses in the material. When SCC occurs, the opening size may depend on the susceptibility of the material and the residual stresses around the crack. A stress corrosion crack can have a very small COD if one grain boundary is affected in a lightly susceptible material or a very large COD in a very susceptible material when several surface grains are dislodged from the crack (Garcia et al. 2001). A highly sensitized material can form many SCCs in the same area, which may then link up and form a crack with a large COD. A less sensitized region will have fewer and tighter SCCs. There is no reliable way to gage the depth of a SCC based on its COD.

2.6 Primary Factors in Crack Detection

The challenge faced by inspectors using standard and remote VT is to find and correctly identify cracks on the surfaces of nuclear components. This problem can be broken down into three primary parameters—contrast, recognition, and discrimination.

For crack detection to occur, sufficient contrast must exist between a crack and the background. A high-contrast crack is easily seen and easier to identify. A low-contrast crack is easy to miss or to confuse with other features. Any factor that increases the contrast between the crack and the background will improve detectability, while anything that decreases the contrast will reduce the detectability.

When one is discussing contrast as it relates to video cameras and other automated systems, it is important to understand how the cameras capture and transmit the image to the inspector. High-quality video cameras and digital cameras have 8 bits of dynamic range. This means that each color that the camera collects has 256 levels of brightness. For a black-and-white camera, this translates into 256 shades of gray. A human eye can distinguish between 100 to 200 levels of grey, which is less than the camera systems. Figure 2.1 shows a gray box (grayscale level 146 of 256) with a series of vertical lines arranged inside. Each line is progressively one grayscale level (out of 256) darker than the previous, with an additional line on the left, which is 210 levels separated from the background. Figure 2.1 shows that at less then 10 levels of separation from the background line, detection is very difficult. At between 10–20 levels separation from the background, the lines are faintly detectable, and above 20 levels separation from the background, the lines are clearly visible. It should also be noted that the higher the system acuity, the higher the contrast in the image. When the image is slightly blurred, the overall contrast levels drop. The blurred lines are still detectable but are slightly more difficult to see because of the lower contrast.

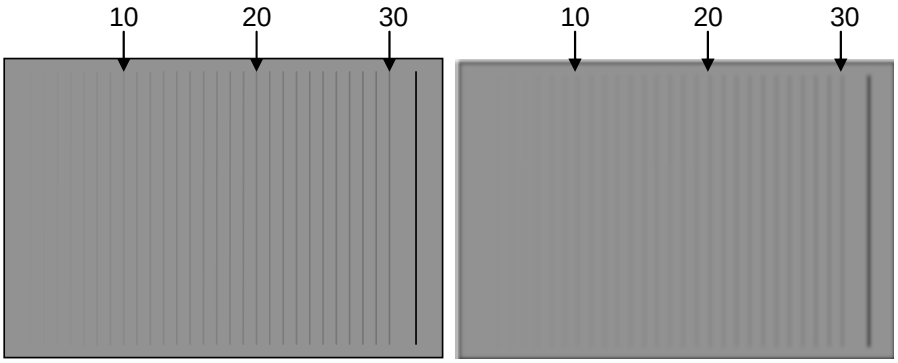

Figure 2.1 Relationship of Line Visibility to Contrast Between Line and Sharpness of Background and Image

For crack recognition to occur, the system also needs sufficient visual acuity to accurately image the morphology of the crack. Cracks come in a variety of shapes, depending on the type of crack and the material. In general, cracks have a slightly-to-very zigzagged appearance, with or without branching. A system interrogating a surface needs be able to distinguish these characteristics to allow the inspector to identify the detected image as a crack.

An example of the difference between recognition and detection and how recognition is affected by visual acuity is shown in Figure 2.2. The effects of reduced contrast and reduced acuity are shown in Figure 2.3.

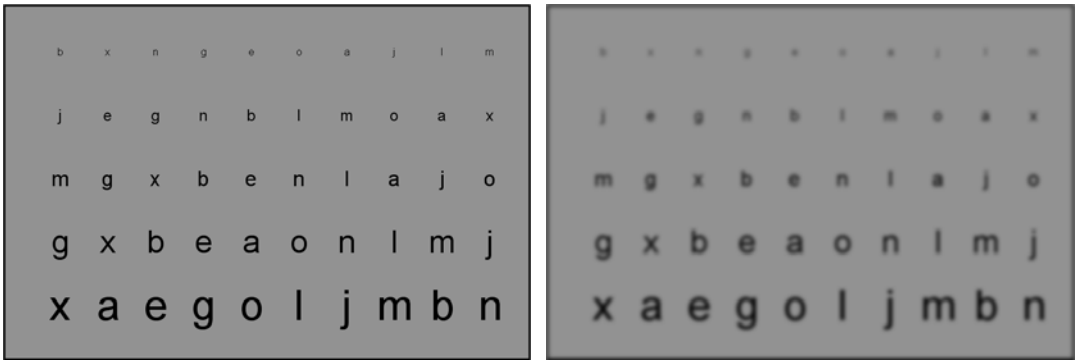

Figure 2.2 Recognition of High-Contrast Letters as a Function of Letter Size and Image Sharpness

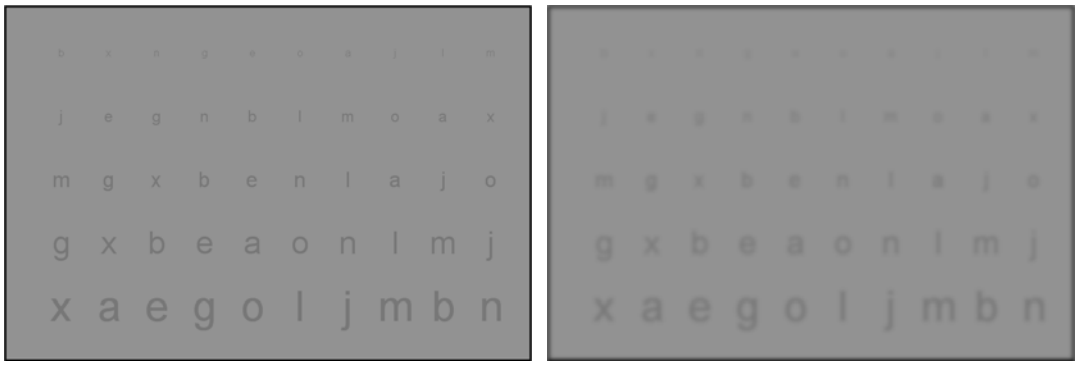

Figure 2.3 Recognition of Reduced-Contrast Letters as a Function of Letter Size and Image Sharpness

Finally, if the crack is detectable and recognizable, the crack must be distinguishable from the surrounding innocuous features such as geometry and scratches. Common issues that can mask a crack include machining marks, grinding marks, scratches, weld conditions, corners and joints, and other geometrical conditions. A crack surrounded by parallel scratches or machining marks can be much more challenging than a crack on a smooth surface. A crack along a weld may be difficult to separate from the weld root or crown, and a crack in a tight corner may be difficult to detect. Geometry can provide other effects such as casting shadows over areas of interest.

The parameters described in this report will be described in terms of how they affect the three primary factors of contrast, recognition, and discrimination.

2.7 Determining Visual Acuity

Any system used in VT, ranging from the naked eye to a digital closed-circuit television (CCTV) system, will have a measurable visual acuity. The visual acuity of a system has four pseudo-independent measures (De Petris and Macro 2000):

- visible minimum – the smallest dot the system can detect
- separable minimum (resolution) – the smallest separation between two lines the system can detect
- visual acuity by Vernier – the ability to perceive spatial variation between two objects
- readable minimum (recognition capability) – the ability to recognize complex shapes such as letters or numbers.

These visual acuity parameters describe what a system can detect and discern. A system with a detection limit of 10 μm (0.0004 in.) and a resolution limit of 30 μm (0.0012 in.) at a given distance can "see" a line 10 μm (0.0004 in.) wide on a sheet of paper but cannot resolve a 10-μm (0.0004-in.) gap between two 10-μm (0.0004-in.) lines. A letter or number will appear to be a dot if it is larger than the visible

minimum of a system but below the readable minimum of the system. The letter will be identifiable only when it is above the recognition capability of the system.

A human eye with 20/20 vision is able to resolve features as small as 75 μm (0.003 in.) in size at a distance of 25 cm (10 in.) (Allgaier et al. 1993). This limit is based on the density of rods in the retina of the eye and on the diffraction limit imposed by the size of the eye. The eye is also, however, able to detect features too small to be accurately resolved. It is possible under perfect conditions to detect a crack with a surface width, or COD, as small as 10 μm (0.0004 in.) on a mirror-polished surface (Allgaier et al. 1993). The minimum detectable COD becomes much larger if the surface is rough or not perfectly clean. These limits do not account for factors such as scratches, machining marks, or any camouflaging effects offered by a macroscopic feature such as a weld root or crown.

The image sharpness produced by mechanical visual systems such as still and video cameras can be described in terms of their modulation transfer function (MTF). The MTF is a measure of the detected versus the actual contrast ratio as a function of the spatial frequency of the indications. For example, a camera will generally show nearly 100% contrast on two black lines on a white background when the lines are far apart (low spatial frequency); however, if the lines are very close together (high spatial frequency), the system can blur the lines and the spaces between the lines together, reducing the contrast and thus reducing the MTF. Measuring the MTF of a system as a function of spatial frequency is a very reproducible and objective way to measure the visual sharpness of a camera system.

A resolution test is another common technique used to characterize the visual acuity of a system. A resolution test determines the smallest distance between two lines that can be discerned by the system. A resolution target generally has several sets of parallel or converging lines with notations on how many lines per millimeter are present at each point. Performing a resolution test consists of making an image of a standard resolution target and determining the point at which the system can no longer separate the lines. The main problem with resolution tests is that they rely on the observer to determine which lines are separable and which are not, adding an element of subjectivity to this measurement. However, a resolution test has the advantage of being faster and easier to administer than a test of system MTF. Examples of commercially available resolution targets include the Institute of Electrical and Electronics Engineers (IEEE) Resolution Target, which conforms to the standard STD 208-1995, “Measurement of Resolution of Camera Systems,” the 1951 U.S. Air Force Resolving Power Target and the International Organization for Standardization (ISO) Camera Resolution Chart. The details of which targets conform to which standard can be found in Sine Patterns L.L.C. (2004).

As the 1951 U.S. Air Force resolution target has been used to test the various cameras used in the PNNL experiments for the parametric and laboratory tests, it bears further description. The 1951 Air Force resolution target consists of a series of increasingly narrow horizontal and vertical lines. The lines are arranged in groups made up of six elements. A sample image of a 1951 Air Force resolution chart is shown in Figure 2.4.

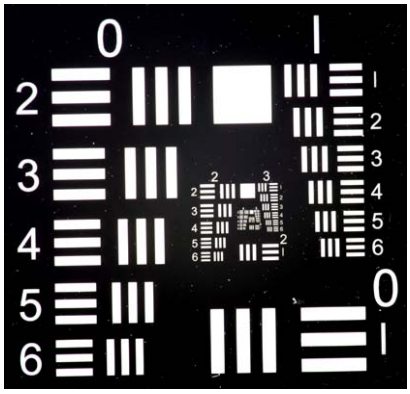

Figure 2.4 Sample Image of a 1951 U.S. Air Force Resolving Power Target

Each element is smaller than the previous by a factor of the sixth root of two (0.891). This progression is designed so that the size of the lines is halved (and the number of lines per millimeters is doubled) every six elements. Thus, each group of six is one half the size of the proceeding group. The number of line pairs per millimeter for a series of groups and elements is given in Table 2.5.

Table 2.5 Number of Lines per Millimeter by Group and Element in a 1951 U.S. Air Force Resolving Power Target

	Group Number					
Element	**0**	**1**	**2**	**3**	**4**	**5**
1	1.00	2.00	4.00	8.00	16.00	32.00
2	1.12	2.24	4.49	8.98	17.96	35.92
3	1.26	2.52	5.04	10.08	20.16	40.32
4	1.41	2.83	5.66	11.31	22.63	45.25
5	1.59	3.17	6.35	12.70	25.40	50.80
6	1.78	3.56	7.13	14.25	28.51	57.02

The maximum visual acuity of an analog or digital video system can be described by comparing the native resolution of the system to the size of the area on which the system is focused. This measure of acuity assumes perfect optics and a perfect electronic capture of the image. Using this method, a 1-megapixel (1200 × 800 pixels) camera that can focus on an area 75 mm × 50 mm (3 in. × 2 in.) would have a pixel size of 0.0625 mm/pixel (0.0025 in./pixel). Any indications that fall below this size would be pixilated and recorded as a lower-contrast shadow in the larger pixel, as the contrast from the indication is averaged with the background in the pixel. The color and shading of the pixel is dependent on the contrast between the indication and the background and on the MTF of the camera. With analog and digital video systems, one needs, as a theoretical minimum, at least one pixel (or line) width between two lines to resolve them, assuming the lines are perfectly aligned with the camera. In practice, this corresponds to at least 1.4 pixels between two lines to always be able to resolve them, regardless of the angle and orientation of the lines.

Another important variable in visual acuity is the speed at which the imaging detector is moving over the inspected area. The term *kinetic vision acuity* is used for the acuity of a given system when scanning a moving target. The loss of visual acuity as a function of scan speed is highly dependent on the technology used to capture the images. A high-speed film camera can produce sharp images of a bullet in flight, while a poor video system can show noticeable blur at slow scan speeds. A captured image picture is typically sharper when the camera is stationary (system normal visual acuity) over a zone as opposed to moving (system kinetic visual acuity).

2.8 Brightfield and Darkfield Imaging

Two ways to use light to examine features on the surface are using reflected darkfield and reflected brightfield imaging. The most common way to image a surface for visual testing is with brightfield imaging. Brightfield imaging is performed by directly illuminating the surface. The surface will be a bright background with features appearing as bright or dark depending on their reflectivity or color relative to the background. With brightfield imaging, cracks look like a dark indication against the brighter background. Scratches can appear as dark or light indications depending on their depth and the angle of illumination.

Darkfield illumination is performed when one shines light on the inspected surface at an oblique angle. Absent discontinuities on the surface, none of the light should reach the camera, and the background will appear dark. Surface features such as cracks and scratches will appear as bright indications, as the light reflects off the indications and reaches the camera. Darkfield imaging can be a very powerful tool in crack detection under good conditions and is commonly used to look for cracks in airplane wing panels and to resolve other inspection issues.

Examples of how one would illuminate a surface with dark and brightfield lighting are shown in Figure 2.5. Examples of a crack illuminated using both darkfield and lightfield illumination are shown in Figure 2.6. In the darkfield-lit image, the crack shows up clearly as a bright indication. The scratches are also well imaged by the darkfield illumination. The brightfield image clearly shows the crack as a dark image against the bright background.

Darkfield lighting is primarily only useful on smooth and flat surfaces. Curved specimens, welded specimens, and machined surfaces make darkfield illumination challenging. For this reason, all remote visual testing is performed as brightfield examinations. Direct visual inspections where one has use of a flashlight can be and often are performed using darkfield imaging as an adjunct to brightfield examinations.

If light is coming from certain angles relative to the surface, the crack can produce both brightfield and darkfield effects. An example of this effect is shown in Figure 2.7. The edge of the crack can reflect light and produce a bright indication, and the center of the crack will still produce a dark indication relative to the background. This combination of brightfield and darkfield effects can be both an aid and a hindrance for detecting a feature. If the feature is large relative to the visual acuity of the system, the two forms of lighting can help brightly outline a dark feature, which often makes the feature very easy to detect. If the feature is small relative to system visual acuity, then there is a danger the brightfield and darkfield effects will overlap in the image and cancel each other out, hiding the feature.

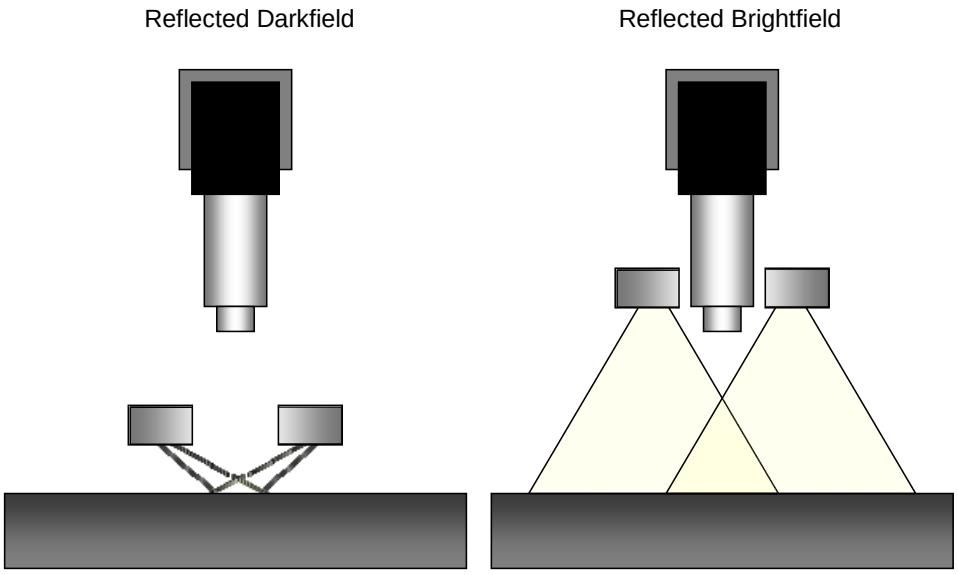

Figure 2.5 Lighting for Brightfield and Darkfield Imaging

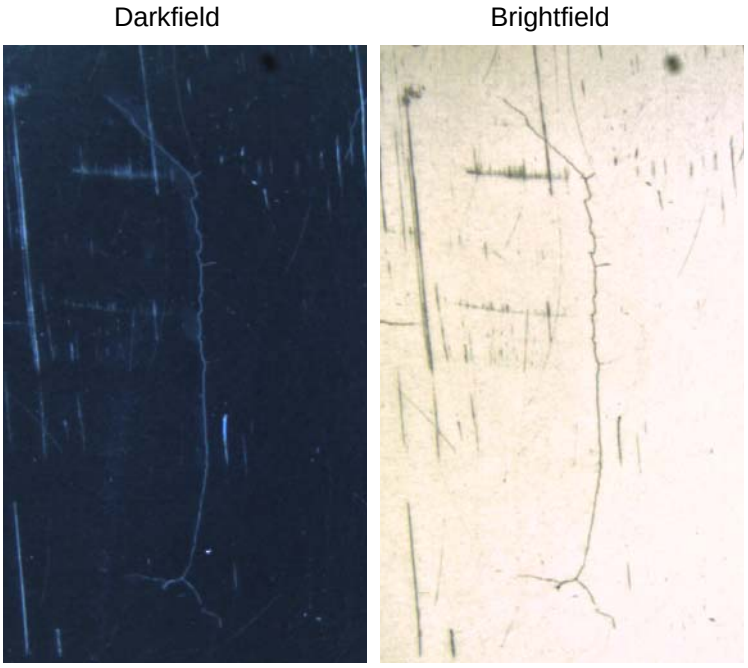

Figure 2.6 Crack with 12-µm Crack Opening Depth Imaged Using Both Darkfield and Brightfield Illumination

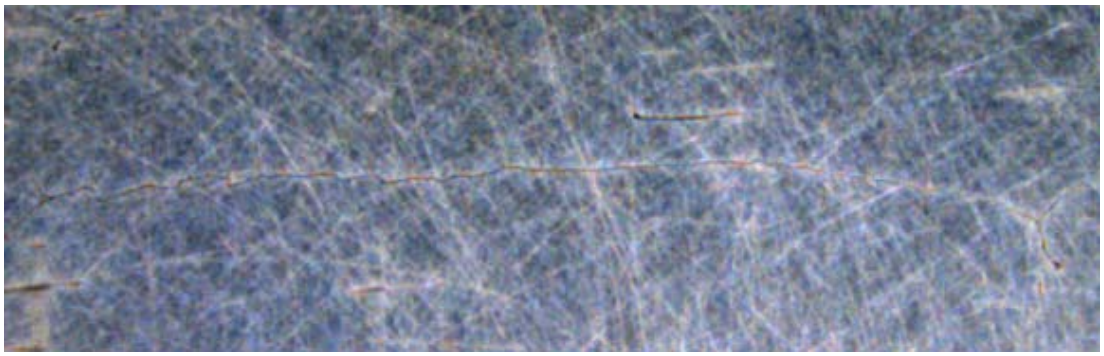

Figure 2.7 Simultaneous Brightfield and Darkfield Effects Produced by Lighting at Off Angle

2.9 Specular and Diffuse Reflection

Light reflection from a given surface has two modes, specular and diffuse. In specular reflection, light reflects from the surface at the same angle as the angle of incidence. In diffuse reflection, the light reflected from the surface has no relation to the angle of incidence and is emitted isotropically. The two modes of reflection are shown in Figure 2.8.

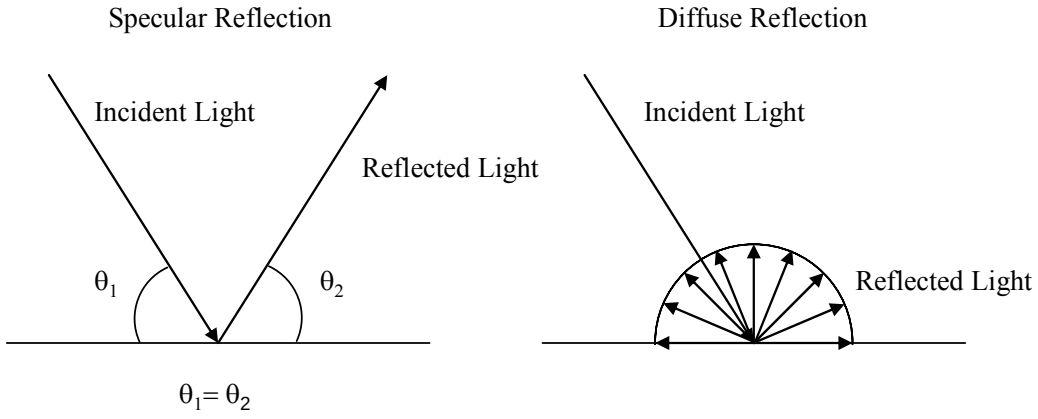

Figure 2.8 Specular and Diffuse Reflection. When light strikes a highly specular surface (left), the light is reflected away at the incident angle. When light strikes a diffusely reflecting surface (right), it reflects isotropically.

For many surfaces, one finds that some of the light reflects specularly and some of the light reflects in a diffuse fashion. This condition is often seen on a slightly oxidized stainless steel surface or a rough metallic surface. One can also find this condition on a scratched surface that would normally be very specular. An important measurement is the ratio between specularly reflected light and diffusely reflected light. For a very diffusely-reflecting surface with virtually no specularity, such as a typical piece of paper, the amount of light reflected at the specular angle will be equal to the light reflected at all angles, giving a ratio of 1. For a highly specular surface such as a mirror, the ratio of specular to diffusely reflected light should be very high.

3 Experimental Procedures

PNNL conducted a series of experiments on cracked stainless steel samples to test the abilities of mechanical systems to image cracks and discriminate between cracks and innocuous surface features. Both the parametric study and the laboratory tests used a series of welded stainless steel samples built to mimic unoxidized BWR core shroud surface conditions.

3.1 Parametric Study

The parametric study was designed to test the effects of several variables on the ability of a mechanical system to image a crack on a metal surface. The parameters specifically examined in this study are the following:

- inspection-dependent parameters
    - camera resolution/magnification
    - lighting techniques
    - scanning speed
- sample-dependent parameters
    - crack opening displacement
    - surface specularity
    - surface features

3.2 Cameras and Lights

The parametric study experiments used three cameras. The largest part of the work was performed using a Lightwise ISG CMOS Firewire video camera with 1.3-megapixel resolution and a Navitar 12X automated zoom lens. Using a 1951 U.S. Air Force resolution target, the maximum resolution for the system with the standard lenses was 90.51 lines per millimeter. The camera was typically mounted on a peg-track scanner that allowed for very precise camera positioning and control. The system is shown in Figure 3.1. This camera was very useful in examining the influence of magnification, crack size, lighting style, and surface conditions.

The lights used in the parametric studies included incandescent and LED spotlights, an LED diffuse ring light, and a diffuse on-axis light™. The spotlights are standard spotlights used for different applications. The diffuse ring light is very similar to the ring lights used in microscopy or macro photography but with a layer of frosted glass in front of the lights. The diffuse on-axis light is designed to provide very flat diffuse lighting on a surface, allowing for good imaging of features on items with highly specular surfaces such as compact disks, glass, and polished metals. The various lights are shown in Figure 3.2. Figure 3.3 shows some of the capabilities of the camera, lens, and lighting systems on a familiar test subject. The diffuse axial provides the flattest and most even lighting on the subject. The diffuse ring light provides even illumination but with some glare. The spotlight produces a great deal of glare, and much of the dime is not well imaged.

Figure 3.1 Visual Testing Apparatus and Sample

Figure 3.2 Lights Used in Visual Testing Experiments. Diffuse on-axis light on the left, ring light in the middle, and spot lights on the right.

Figure 3.3 Dime Illuminated Using Three Lighting Techniques

The other cameras used for the parametric study were the two radiation-hardened cameras used in the laboratory studies and are detailed in the next section. They were useful in determining the effects of scanning speed and camera angle.

3.3 Specularity Measurements

Specularity measurements were made on two cracked samples. These measurements were taken to determine the effects of the different lighting techniques on surfaces with varying degrees of polish and shininess. The specularity measurements define the degree of shininess with objective measurements and allow for comparisons to materials with similar measured properties.

The measurements were made using a 12-in.-diameter integrating sphere and a helium neon laser (SpectraPhysics, Model 145-02, Class IIIb). The setup is shown in Figure 3.4.

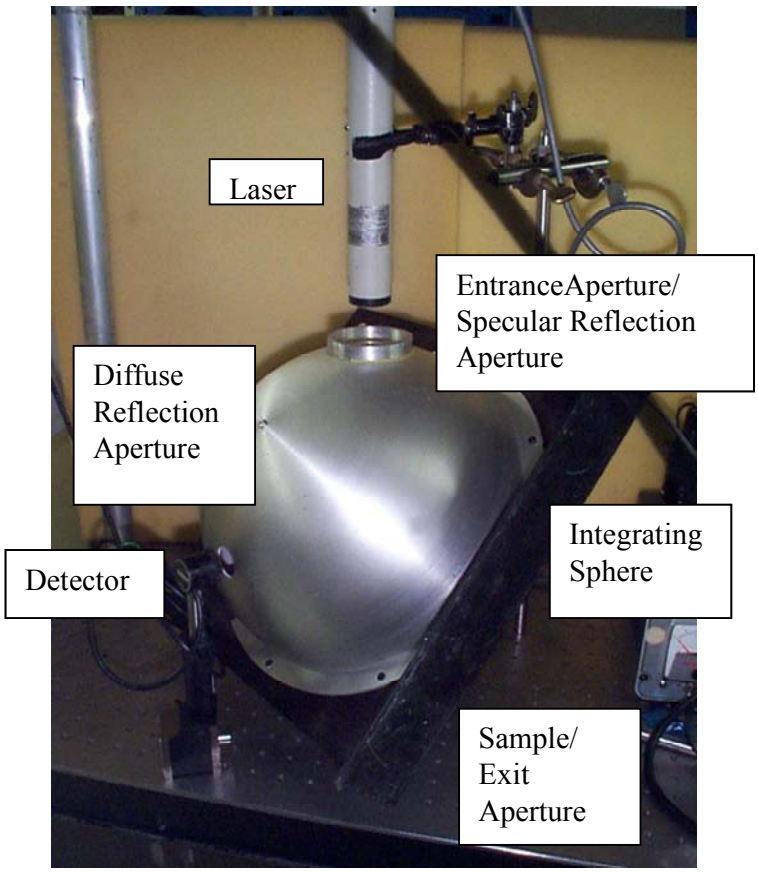

Figure 3.4 Experimental Setup for Specularity Measurements

3.4 Reactor Internals Samples

Reactor internals samples were used in both the parametric and laboratory tests. PNNL had acquired the welded stainless steel samples with implanted cracks and notches in 1997. These samples were made for and used in a parametric study and blind test to determine the effectiveness of ultrasonic techniques in finding cracks through welds in austenitic material. These samples were designed to simulate the materials, cracks, and surface conditions common to reactor internals components; i.e., to mock-up a BWR core shroud. The samples consist of approximately 250-mm by 450-mm, 50-mm-thick (10 × 18 × 2 in.) stainless steel slabs that have been cut into two pieces along the center and then welded back together again.

The surfaces of both sides of the samples were machined after welding and crack implantation to smooth them for ultrasonic examination. This machining has hidden all traces of the weld crown in most samples except where the weld crowns were left in the as-welded condition. The samples were machined using the end milling process after welding and crack implantation with a surface finish of roughly 1.6 μm RMS (63 micro-inches). Some samples have also been roughly ground near the weld line and have a surface roughness of at least 12.5 μm RMS (500 micro-inches). Two of the internals samples are shown in Figure 3.5.

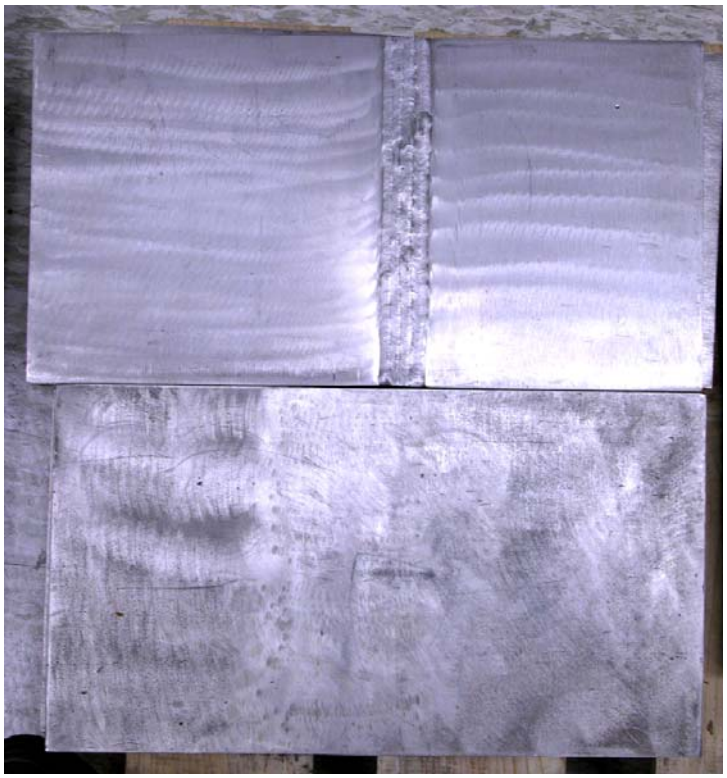

Figure 3.5 Reactor Internals Samples Used in Testing. Top shows weld crown present; bottom shows weld crown removed.

The flaws were implanted into the heat-affected zones of the welds. The flaws were generated by thermal cycling of a tension specimen to produce fatigue cracks of a specific size, removing the crack coupon from the tension bar, then in-situ fusing these coupons during the girth welding process. This technique allows the flaw face to be characterized via precise mechanical measurements and photographs prior to implantation and has been shown to produce cracks in the as-welded condition within ±1.0 mm (0.040 in.) of the specified length and height in the material. Also, this technique enables the vendor to produce various geometrical and welding conditions that simulate those found during field welding; for example, counterbore, inner diameter mismatch, weld root, fusion anomalies, and weld crown configurations.

Normally, cracks implanted in this fashion are not useful for visual testing, as the welding process often causes the two halves to shift in position slightly. This mismatch causes a vertical shift across the two halves of the crack. Odd circumstances can occur such as one lip of the crack jutting over the crack opening, completely covering the crack. Other issues involve the shadows and reflections, caused by lighting a vertically mismatched crack from different angles that are not representative of cracks in the field. Fortunately, the machining process applied to the samples after welding has evened out the surfaces, making the cracks much more representative of cracks expected in the field. It should be noted that effects of deposits or discoloration was not studied in these laboratory tests.

PNNL measured the widths of the cracks in the reactor internals samples using an optical micrometer. This micrometer has a magnification of 100X and a graduated reticule that gives measurements accurately to 12.7 μm (0.0005 in.). The cracks are in general very tight, but there is a good range of crack CODs. The CODs range from less than 5 μm to 125 μm (0.0002 to 0.005 in.) in size. The average COD is 60 μm, (0.0024 in.), with a median crack size of 25 μm (0.001 in.).

For the parametric study, the reactor internals samples were examined in the as-received condition, which contained machine marks and grinding marks, using the three lighting systems. Nine of the samples were then polished and re-examined using the three lighting systems. Scratches were made on the surfaces using 240-grit sandpaper perpendicular and parallel to the crack and were examined with the three lighting conditions at each step.

3.5 Laboratory Tests of Radiation-Hardened Cameras

Two cameras were used for the laboratory tests, a radiation-hardened fixed-focus video camera and a radiation-hardened zoom video camera. Both cameras were black and white only. The two cameras are shown in Figure 3.6.

The fixed-focus video camera has a focal length of 16 mm (0.63 in.) and provided 500 lines of TV resolution. This camera is very strongly radiation-hardened and can be used to inspect recently burned fuel pins in a reactor. The fixed focal length camera is typically used with a pair of spotlights mounted 180 degrees from each other on either side of the lens and can pass the standard 12-μm (0.0005-in.) wire test at a distance of 178 mm (7 in.) in air.

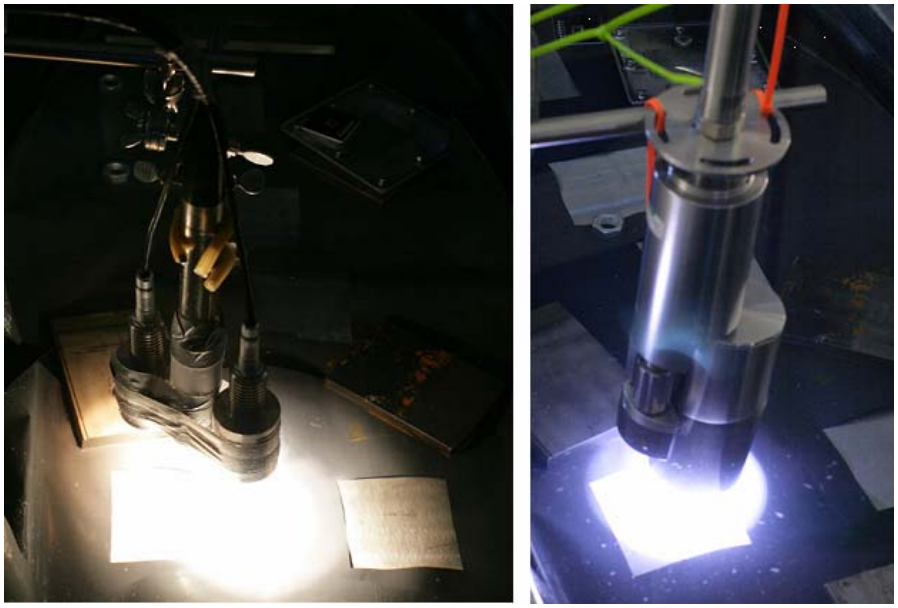

Figure 3.6 Cameras Used for Laboratory Tests. Left: fixed focal length camera with illumination provided by two spotlights. Right: pan/tilt/zoom camera illuminated by LED ring light.

The second camera used was a radiation-hardened video camera on a pan/tilt/zoom head. The pan/tilt/zoom camera uses a CCD imager instead of a video tube and has a zoom lens with a focal length ranging from 8–24 mm (0.31–0.94 in.). The pan/tilt/zoom camera has an integral ring light and provides an image with 470 TV lines. The cameras were mounted on a magnetic track scanner to allow for precise and stable camera movement.

Thirteen cracked and seven blank reactor internals specimens, described in Section 3.3, were placed in random order with random (0 degrees or 90 degrees) orientations inside four long water tanks. The samples were covered in plastic sheeting with thirty 100-mm by 100-mm (4 in. × 4 in.) square windows cut into the plastic. This arrangement provided 17 windows with cracks (some of the internals specimens have two cracks) and 13 windows as blanks. The tanks were filled with water approximately 200 mm (7.5 in.) above the surface of the samples to simulate some of the conditions for performing visual examinations underwater in the field. The test arrangement is shown in Figure 3.7. Photographs of each window are given in Appendix A.

Figure 3.7 Water Tanks with Specimens Prepared for Visual Inspection

Four inspectors were used for the test. Two of the inspectors were PNNL staff with visual testing training. One PNNL staff member is a current American Society of Nondestructive Testing (ASNT) Visual Testing Level III inspector, and the second was previously certified to ASNT Level II but is not currently certified. The other two inspectors were American Welding Society (AWS)-certified visual inspectors contracted through a local company.

The tests were invigilated by a PNNL staff member who had knowledge of the locations and appearances of the cracks used in the study. The PNNL member was able to determine if a call made by an inspector was correct or incorrect and this was noted as each call was made. While ideally such a test would be performed in a double blind fashion, it was decided that the person grading the test should be present during the inspection. This level of grading was needed, so when an inspector made a call the grader was able to ask the inspector to locate the crack on the screen. If the inspector pointed to the crack, the grader noted this as a hit. If the inspector was over a cracked window but indicated a scratch or some other non-crack, the grader noted this as a false call.

4 Parametric Study of Crack Detection Using Visual Testing

PNNL conducted a study on the effects of various parameters on the ability of a mechanical system to image cracks on a stainless steel surface. This section describes the results of the large parametric matrix experiment performed to explore the interaction of crack size, lighting conditions, and surface conditions. Six parameters—crack size, lighting conditions, scanning speed, camera resolution, surface specularity, and surface conditions—were classified according to those over which the inspector has control and those parameters that are sample-dependent. The results for each of these parameters are then described.

4.1 Parametric Matrix Results

The interplay between lighting technique, surface conditions, and crack CODs were explored in a matrix of 192 examinations. This matrix was constructed using nine samples with six CODs, four surface conditions, and six lighting conditions. Each sample was examined in the following conditions: as-received, polished, and with scratches perpendicular and parallel to the cracks. All examinations were performed at the same magnification and with the same resolution setting, 1.3 megapixels.

The most rigorous method of testing each of the inspections would be to have a series of inspectors make calls on the cracked surfaces for each inspection condition. This would be impractical for the number of conditions examined, however. A subjective evaluation was made by one inspector for each condition and the results tabulated. The inspector gave four levels of crack detectability—excellent, good, fair, and poor. This matrix is designed to show general trends for crack detection to help gain an understanding of the complexities of the interactions between and among crack size, surface conditions, and lighting technique.

The results for the subjective evaluation are given in Table 4.1. The results have been color-coded to make the table easier to read. Images of each sample are given in Appendix B. This matrix includes a mix of sample and inspection-dependent variables, and the results will be used throughout Section 4.

Table 4.1 Subjective Evaluation Results for Parametric Matrix for Samples 1-9

Sample 1 – COD 10 microns

Surface Conditions	Diffuse On-Axis	Diffuse Ring	Top Right Spotlighting	Top Left Spotlighting	Horizontal Lighting	Vertical Lighting
As-Received	good	good	poor	poor	poor	poor
Polished	excellent	poor	poor	poor	poor	poor
Parallel	poor	poor	poor	poor	poor	poor
Perpendicular	good	poor	fair	fair	good	good

Table 4.1 (continued)

Sample 2 – COD 10 microns

Surface Conditions	Diffuse On-Axis	Diffuse Ring	Top Right Spotlighting	Top Left Spotlighting	Horizontal Lighting	Vertical Lighting
As-Received	fair	poor	poor	poor	poor	poor
Polished	good	fair	poor	poor	poor	poor
Parallel	poor	poor	poor	poor	poor	poor
Perpendicular	fair	poor	poor	poor	good	poor

Sample 3 – COD 35 microns

Surface Conditions	Diffuse On-Axis	Diffuse Ring	Top Right Spotlighting	Top Left Spotlighting	Horizontal Lighting	Vertical Lighting
Polished	excellent	fair	excellent	excellent	excellent	fair
Parallel	fair	poor	excellent	fair	good	poor
Perpendicular	excellent	poor	good	good	fair	good

Sample 4 – COD 40 microns

Surface Conditions	Diffuse On-Axis	Diffuse Ring	Top Right Spotlighting	Top Left Spotlighting	Horizontal Lighting	Vertical Lighting
Polished	excellent	poor	excellent	good	good	poor
Parallel	poor	poor	good	fair	poor	poor
Perpendicular	fair	poor	excellent	excellent	good	good

Sample 5 – COD 40 microns

Surface Conditions	Diffuse On-Axis	Diffuse Ring	Top Right Spotlighting	Top Left Spotlighting	Horizontal Lighting	Vertical Lighting
Perpendicular	good	fair	poor	good	poor	poor
Perpendicular	excellent	poor	excellent	excellent	excellent	excellent

Sample 6 – COD 50 microns

Surface Conditions	Diffuse On-Axis	Diffuse Ring	Top Right Spotlighting	Top Left Spotlighting	Horizontal Lighting	Vertical Lighting
As-Received	fair	poor	poor	poor	poor	poor
Polished	excellent	excellent	fair	excellent	good	fair
Parallel	excellent	good	good	poor	good	poor
Perpendicular	excellent	excellent	good	poor	good	good

Sample 7 – COD 10-75 microns

Surface Conditions	Diffuse On-Axis	Diffuse Ring	Top Right Spotlighting	Top Left Spotlighting	Horizontal Lighting	Vertical Lighting
As-Received	good	good	fair	poor	poor	poor
Polished	excellent	excellent	poor	poor	poor	poor
Parallel	excellent	excellent	fair	poor	fair	fair
Perpendicular	excellent	fair	good	good	good	good

Table 4.1 (continued)

Sample 8 – COD 125 microns

Surface Conditions	Diffuse On-Axis	Diffuse Ring	Top Right Spotlighting	Top Left Spotlighting	Horizontal Lighting	Vertical Lighting
As-Received	fair	poor	poor	poor	poor	poor
Polished	excellent	excellent	excellent	excellent	excellent	good
Parallel	excellent	excellent	excellent	excellent	excellent	fair
Perpendicular	excellent	excellent	poor	good	excellent	fair

Sample 9 – COD 125 microns

Surface Conditions	Diffuse On-Axis	Diffuse Ring	Top Right Spotlighting	Top Left Spotlighting	Horizontal Lighting	Vertical Lighting
As-Received	fair	fair	poor	poor	poor	poor
Polished	excellent	excellent	good	excellent	excellent	excellent
Parallel	excellent	excellent	good	good	good	poor
Perpendicular	excellent	excellent	good	good	excellent	fair

4.2 Inspection-Dependent Parameters

The following parameters are ones over which an inspecting agency would have control. The choice of camera resolution and lighting style would be made at the time of camera purchase, and the scanning speed would be determined at the time of inspection.

4.2.1 Camera Resolution/Magnification

An important parameter in crack detection is the projected size of each pixel on the imaging chip or the projected width of each TV line in a video tube. Two factors determine the size of the pixel or video line—the number of pixels/lines and the area imaged by the lens. For example, a 640×480 video camera focused on a 75 mm by 50 mm (3 in. × 2 in.) area would have an average pixel size of 117 μm (0.0045 in.). When one may be inspecting for cracks on the order of 10–25 μm (0.0005–0.001 in.), it is clear that inspections are often done with crack sizes lower than or much lower than the size of each pixel. This reduces the contrast and sharpness of the image of the crack as it is averaged into the image of the surrounding metal surface. This situation can be improved either by increasing the magnification or using a higher resolution sensor.

Using high magnification can be very helpful but also carries some serious limitations. First and foremost, inspections carried out at very high magnifications take prohibitively long to conduct. If one wants to inspect an area with a 10-μm pixel size using a standard video camera, one will have to focus on an area 5 mm × 3 mm (0.2 in. × 0.12 in.) in size. Simply put, this is not practical. Second, inspections conducted at very high magnifications tend to rob the inspector of the context of the image. One does not see any fiduciaries in the image for a long time and the inspector can easily become disoriented with respect to location on the component or piece being inspected. High magnification may limit the number of a given crack's branches and bends being imaged on the screen, which may reduce the detectability of the crack.

High-resolution images provide improved contrast between a crack and the background while preserving the benefits of a larger field of view. The primary limitations of high-resolution images are technological. The highest-resolution radiation-hardened cameras have 640 × 480 pixels, and very few monitors have more than 1600 × 1200 pixels. There are six-megapixel video cameras available for machine-vision applications and five-megapixel medical display monitors, but none of this technology has been modified for use in the nuclear industry. It should be noted that viewing a high-megapixel video stream on a lower-resolution monitor can negate the benefit of the high-resolution video stream during a real-time visual inspection. The same crack illuminated under diffuse axial lighting at two resolutions is shown in Figures 4.1 and 4.2. Figure 4.1 shows the area imaged using 1.3 megapixels, and Figure 4.2 shows the same area imaged by the same camera using normal video resolution (640 × 480 pixels). The areas in the images have been cropped to allow the crack to be visible when reduced to fit the margins of this report and do not represent the entire image. The higher-resolution image clearly provides better contrast and detail and superior crack detection. The grayscale level difference between the crack and the background ranges from 10 to 60 levels in the high-resolution image and from only 0 to 20 levels in the low-resolution image. The low-contrast image in Figure 4.2 makes the crack challenging to detect if one does not know its exact location.

Resolution and magnification are secondary to lighting techniques in importance, however. A very high-resolution image with glare and poor contrast between indications of interest and the background is less useful than a lower-resolution image with even, diffuse lighting. The same crack and area imaged at high resolution using a bare-bulb spotlight is shown in Figure 4.3. The grayscale difference is essentially zero between the crack and the background, and while there is no signal from the crack present in the image, the scratches are highlighted very strongly.

4.2.2 Lighting Style

Lighting style can strongly affect all three factors in crack detection. Three lighting styles were used in the parametric study—bare-bulb LED and incandescent spotlights, a diffuse ring light, and a diffuse on-axis light. Examples of a crack illuminated with each technique using the Lightwise 1.3-megapixel video camera are given in Figure 4.4. In each figure, a 12-μm (0.0005-in.) COD crack is in the center of the image with a wire 25 μm (0.001 in.) wide stretched across the image. The metal surface was somewhat specular with some shallow scratches at roughly 45 degrees to the crack and some deeper scratches in line with the crack.

The results from the parametric matrix are shown in **Table** 4.2. The results show that the diffuse on-axis light provides the best lighting for crack detection. Surprisingly, the spotlighting was comparable to the diffuse ring lighting. While the ring light is somewhat better, spotlights from several directions is comparable. If one can get the spotlights parallel to the crack, one can get better illumination than with the ring light; but when the spotlighting is perpendicular to the crack, the lighting is relatively ineffective.

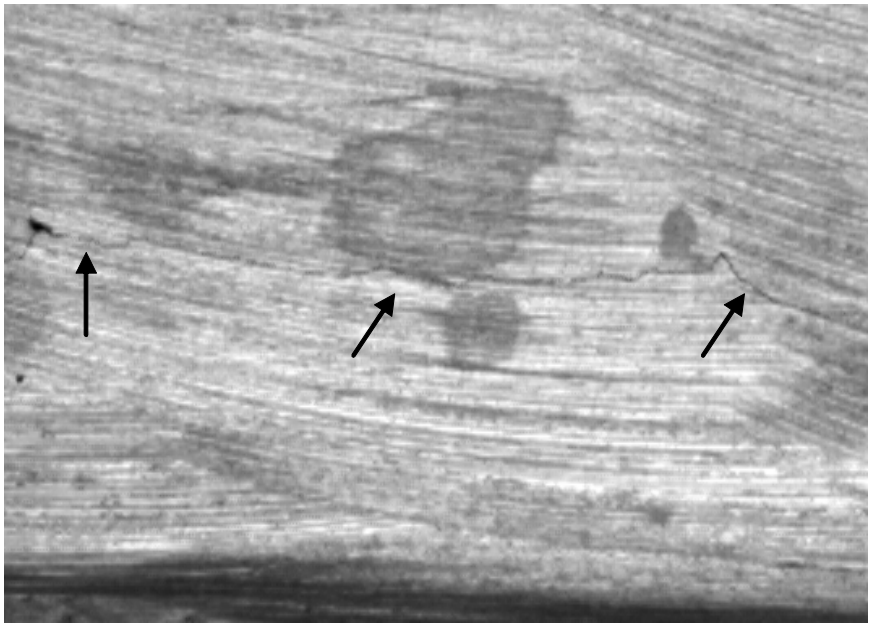

Figure 4.1 12-μm (0.0005-in.) COD Crack Illuminated with Diffuse On-Axis Lighting Imaged Using a 1.3-Megapixel Video Camera Set to Full Magnification. The crack is indicated with arrows.

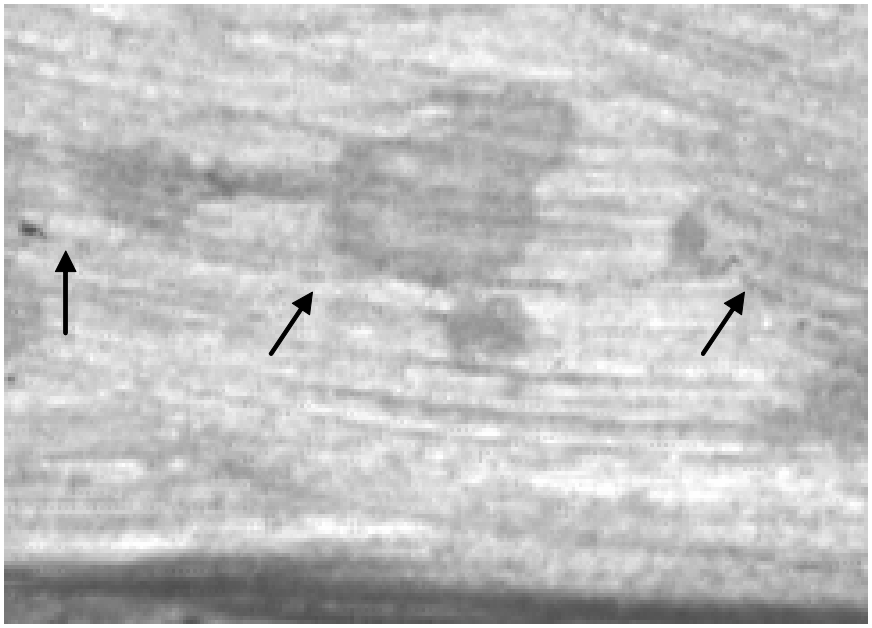

Figure 4.2 12-μm (0.0005-in.) COD Crack Illuminated with Diffuse On-Axis Lighting Imaged Using 640 × 480 Pixels of Resolution. The crack is indicated with arrows.

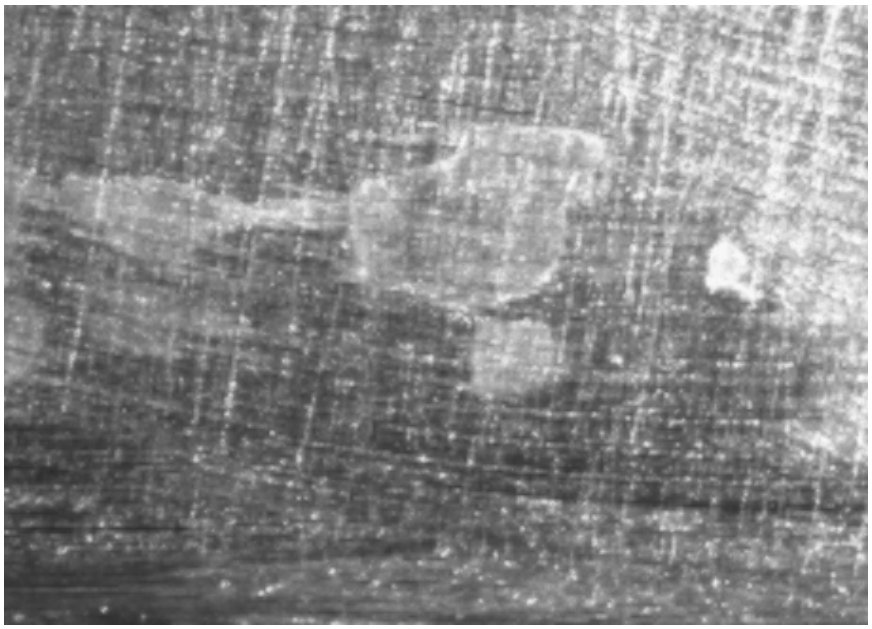

Figure 4.3 12-μm (0.0005-in.) COD Crack Illuminated with Spotlight Imaged Using 1.3-Megapixel Video Camera Set to Full Magnification. In this image, the spotlighting obscures the crack completely.

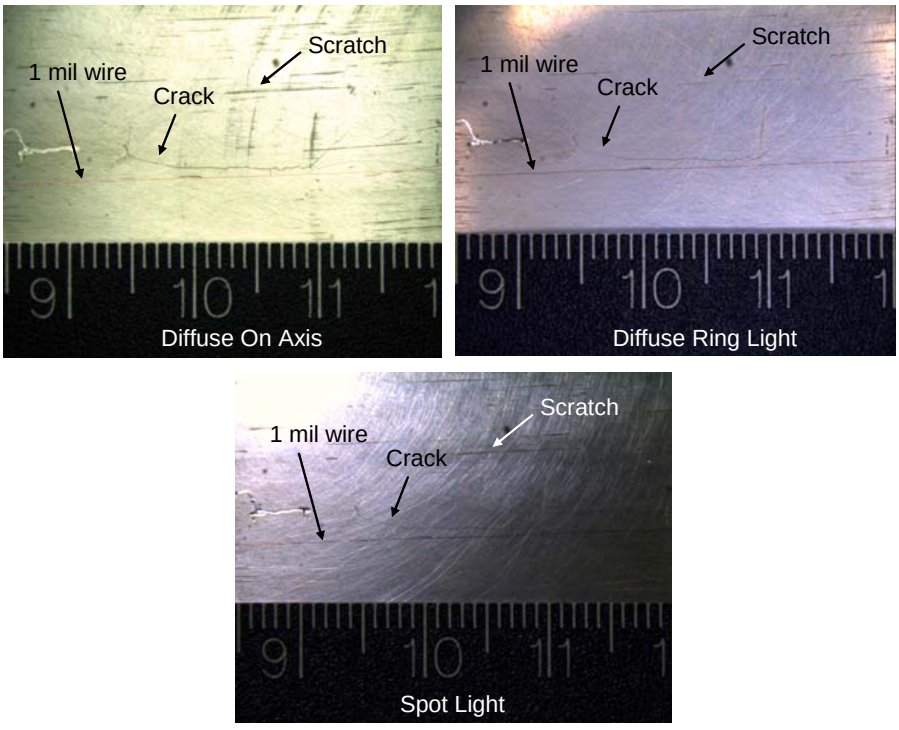

Figure 4.4 Images of Crack, Wire, and Scratches Taken Using Diffuse On-Axis Light, Diffuse Ring Light, and Bare-Bulb LED Spotlight

Table 4.2 Matrix Results for Lighting Techniques

Lighting Style	Excellent	Good	Fair	Poor
Diffuse Axis	56.7%	13.3%	23.3%	6.7%
Diffuse Ring	33.3%	6.7%	16.7%	43.3%
Spot Average	18.0%	25.8%	11.7%	44.5%
Parallel	21.9%	31.3%	6.3%	40.6%
Perpendicular	6.3%	18.8%	18.8%	56.3%
Diagonal Lighting	21.9%	23.4%	10.9%	43.8%

It was determined that spotlighting can be very hit or miss. If the spotlights are arranged perfectly, they can provide good illumination and allow for good crack detection. If the spotlights are aligned incorrectly, they can hide cracks and emphasize scratches and machine marks. Spotlights provided the most glare and most uneven lighting among the three techniques used in this study.

The ring light provides, on average, little glare and good contrast between cracks and the metal surface. The lighting is even across the imaged area, with some weak hot spots but nothing that obscures the image. Shallow scratches and machine marks are somewhat emphasized but are not as pronounced as in the spot-lit images.

The diffuse on-axis light produced a very strong contrast between the crack and the metal background and does not highlight the shallow scratches. The deeper scratches are visible but are clearly discernable as scratches and not cracks.

Poor lighting can cause a very strong drop in visual acuity, even with a very large crack. An example of a large crack (125 μm or 0.005 in.) imaged first using a ring light and then with two spotlights is shown in Figure 4.5. In the image lit by the ring light, the crack is clearly visible as a dark indication. In the spotlight-lit image, the spotlights are perpendicular to the crack, and this lighting does a very effective job of hiding the crack.

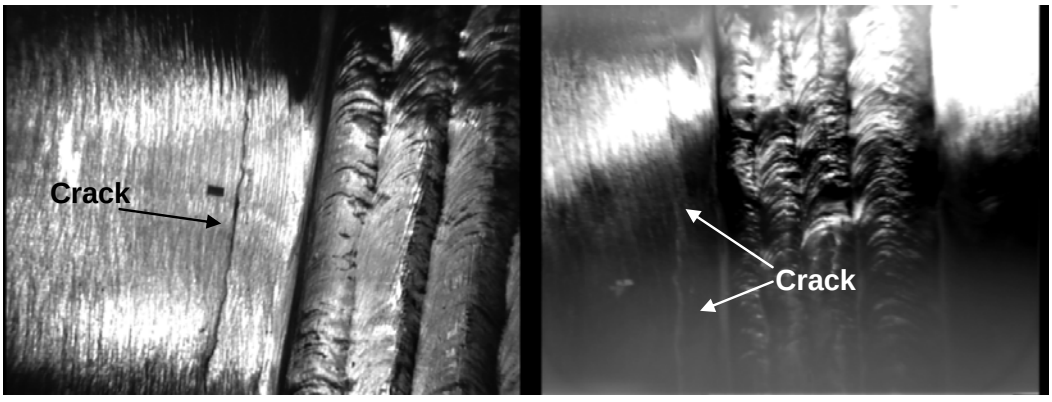

Figure 4.5 125-μm COD Crack Imaged Using Ring Light (left image) and Two Spotlights (right image)

4.2.3 Scanning Speed

The effects of scanning need to be quantified for the actual inspection conditions. Every camera is different, and how a given camera will respond to scanning speed is very strongly dependent on several factors.

When describing camera motion, defining the camera speed is complex. The effects of camera motion on image sharpness are a function of the camera speed, the distance between the camera and the subject, the focal length of the lens, and the exposure time used to take the image. When one is taking images from a moving automobile, objects close to the car can be very blurred while objects very far away would remain sharp. For a digital camera, the ultimate arbiter of the effect of camera motion is the distance a pixel is scanned over the course of the exposure.

Scanning over a surface can have effects on both the contrast and the resolution of the image captured by a camera. The loss of contrast and resolution are caused by the pixel imaging a larger area than it would in a stationary image. The area imaged by each pixel, and the resulting loss in contrast and resolution, increase as the scanning speed and exposure time increases. A specialized system using short-duration flashes and extremely short exposure times can make high-contrast, high-resolution images of a bullet in flight. A video camera in low light produces noticeable loss of acuity when moved even at slow speeds.

The Lightwise video camera was not a good instrument for this test. The refresh rates were very long under typical lighting conditions using the Navitar lens, and any movement tended to completely blur the image. The scanning speed tests were conducted using the pan/tilt/zoom, radiation-hardened video camera used in the laboratory tests.

The radiation-hardened pan/tilt/zoom camera was scanned at speeds ranging from 6 mm/s to 76 mm/s (0.24 to 3.0 in./s) over a 125-μm (0.005 in.) COD crack, and the resulting images were examined. Example images from this experiment are given in Figure 4.6. Slow scanning appeared to cause little distortion in the image, while scanning at 76 mm/s caused gross distortion in the image. The grayscale level contrast between the crack and the background was determined for each scanning speed and compared to a still image of the crack taken using the same camera. The results of the grayscale level calculations are given in Figure 4.7. This experiment shows that at slow speeds the contrast drops slightly, and at higher scanning speeds the contrast drops to less than half of the value of a still camera.

For the resolution tests, the camera was scanned over a 1951 Air Force resolution target, and the camera resolution was recorded for each pass. The smallest resolvable group and element number were recorded, as well as the corresponding number of lines per millimeter. The theoretical maximum resolution for the magnification was 4.7 lp/mm, which is close to the 4 lp/mm that was obtained on a stationary target. Sample images from the scanning speed experiment are given in Figure 4.8. A graph of the results of the scanning speed versus resolution experiment is given in Figure 4.9. It must be stressed that these results are for a given radiation-hardened camera under one set of conditions, but the results for another camera under other conditions may be different.

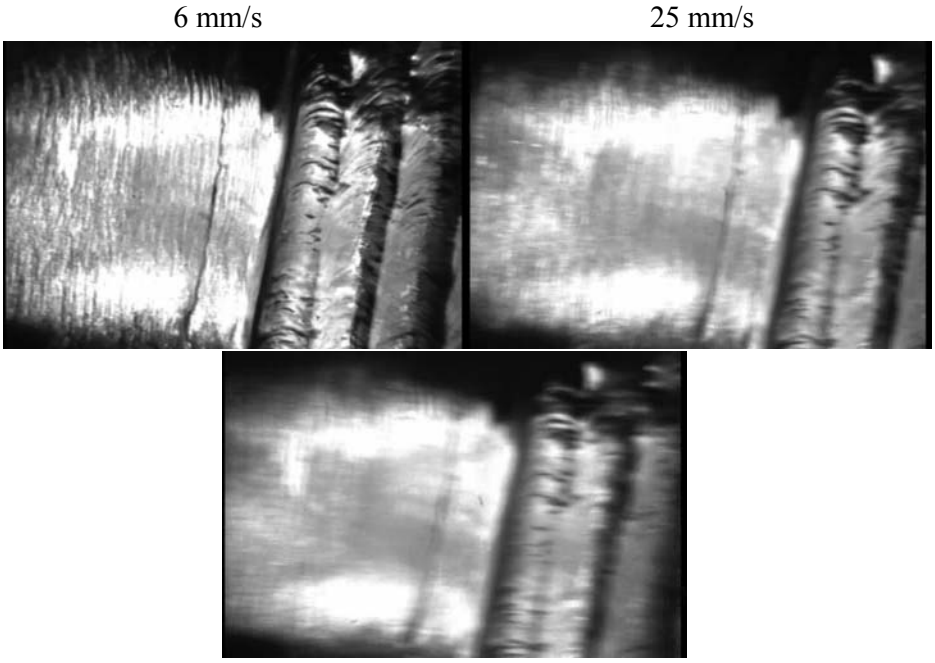

Figure 4.6 Sample Images of a 125-mm COD Crack Imaged at Three Scanning Speeds

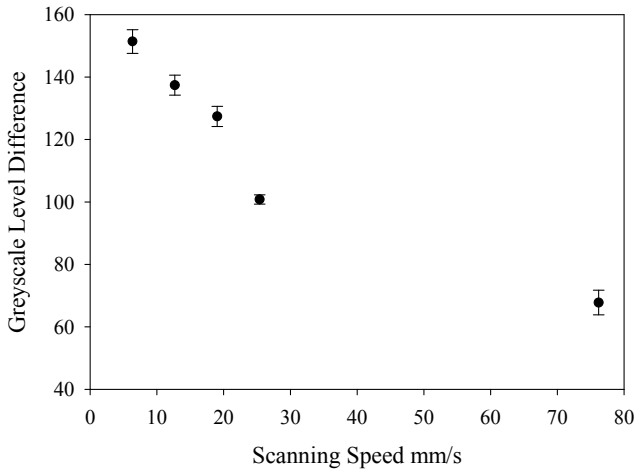

Figure 4.7 Effect of Scanning Speed on Grayscale Level Contrast Between Crack and Background

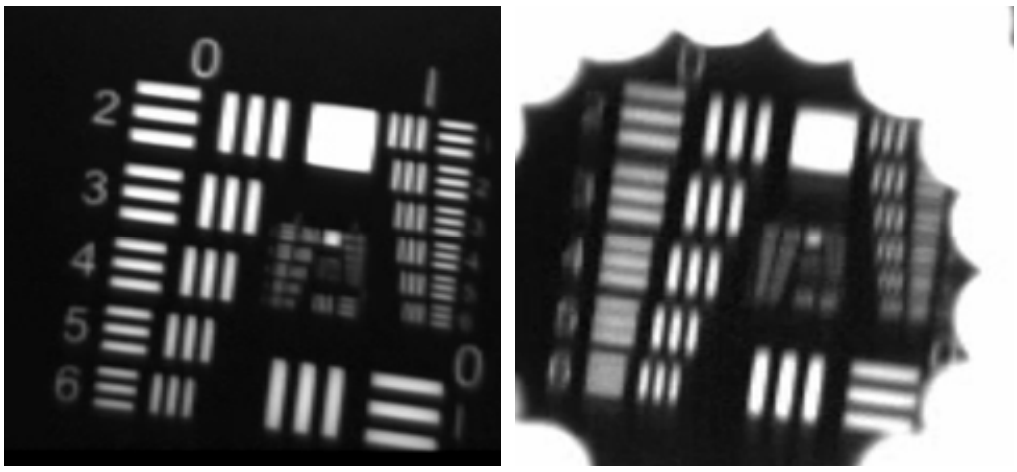

Stationary 51 mm/s

Figure 4.8 1951 Air Force Resolution Target Imaged at Two Scan Speeds

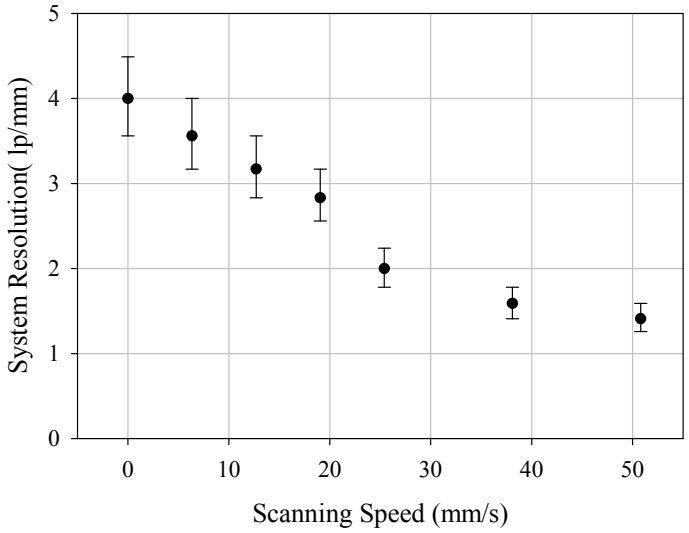

Figure 4.9 Effects of Scanning Speed on Resolution of Radiation-Hardened Camera

The scanning experiment shows that the resolution loss at slow speeds such as 6 mm/s (0.24 in.) do not greatly reduce the resolution of the system, while scanning at higher speeds reduces the resolution to less than half the acuity of a stationary camera.

A factor more difficult to quantify but noted during the test of the effects of scanning was that slow scanning seemed to help the inspectors find cracks. The inspectors reported that the slow scanning gave them the opportunity to view the area of interest from different angles as the camera scanned across and past the area.

As slow scanning (less than 6 mm/s) degrades image quality only slightly and may actually help slightly in crack detection, scanning at these speeds is unlikely to harm the inspection. However, scanning at greater than 25 mm/s (1 in./s) severely degrades the image quality.

4.3 Subject-Dependent Parameters

Although an inspector has a great deal of control over a visual inspection, there are many sample-dependent factors. These factors will be different for each individual component in a reactor. The three subject-dependent parameters examined include the crack COD, the degree of surface scratching, and the surface specularity.

4.3.1 Crack Opening Displacement/Crack Size

As the COD increases, all three main parameters, contrast, recognition, and discrimination between the crack and innocuous features, are improved. The COD affects primarily the contrast between the crack and the background when one is using brightfield lighting. In almost all cases, the contrast between the crack and the background increases as the crack COD increases. Also, the crack becomes more easily recognized as a crack as it gets larger. Crack tortuosity and possible branching are often easier to recognize. Finally, the crack is much more easily discriminated compared to the surface conditions, such as scratches and machining marks, as the COD increases. When a crack COD is larger than the size of the scratches or geometrical effects, it is less likely to be confused for an innocuous feature.

As crack length increases, the crack becomes easier to detect as the inspector has more length over which to recognize the crack. The contrast between the crack and the background is *not* improved by crack length, however. A short crack with a large COD (<100 μm or <0.004 in.) is easier to detect than a long crack with a very small COD (<20 μm or 0.0008 in.).

The parametric matrix results show a strong effect of the COD on crack detectability, as shown in Table 4.3. Cracks larger than 100 μm (0.004 in.) are usually detectable, while cracks less than 20 μm (0.0008 in.) are usually very difficult to detect. The detectability of the middle range of 20- to 100-μm COD cracks depends strongly on the lighting and surface conditions and does not show any clear trend.

A long crack with a wide COD (≥100 μm) can usually be detected on a bad surface with a low-resolution camera under poor lighting conditions. The only time when such a crack becomes difficult to detect is when one is panning the camera quickly over the cracked area.

Table 4.3 Effects of Crack COD on Crack Detectability

COD (μm)	Excellent	Good	Fair	Poor
<20	2.1%	14.6%	10.4%	72.9%
20–40	31.3%	22.9%	16.7%	29.2%
40–100	22.9%	27.1%	16.7%	33.3%
100+	47.9%	16.7%	12.5%	22.9%

4.3.2 Surface Scratching and Machine Marks

The surface of the inspected material has a strong influence on the ability to detect cracks. A mirror-smooth surface can allow for the detection of very tight cracks while a deeply scratched surface or an irregular surface can make crack detection much more difficult. An improperly lit shiny surface can be next to impossible to properly inspect, while a dull matte-finish surface can be quite easy to inspect. For examples of the effect of surface conditions on crack detectability, Figure 4.10 shows cracks of the same width lit using a diffuse axial light on three very different surfaces.

How strongly the surface conditions affect the inspection is greatly dependent on the lighting style. If one used very flat diffuse lighting, then the surface effects can be greatly mitigated. A crack appears as a dark image on a neutral background, even in the presence of scratches and other features such as weld beads.

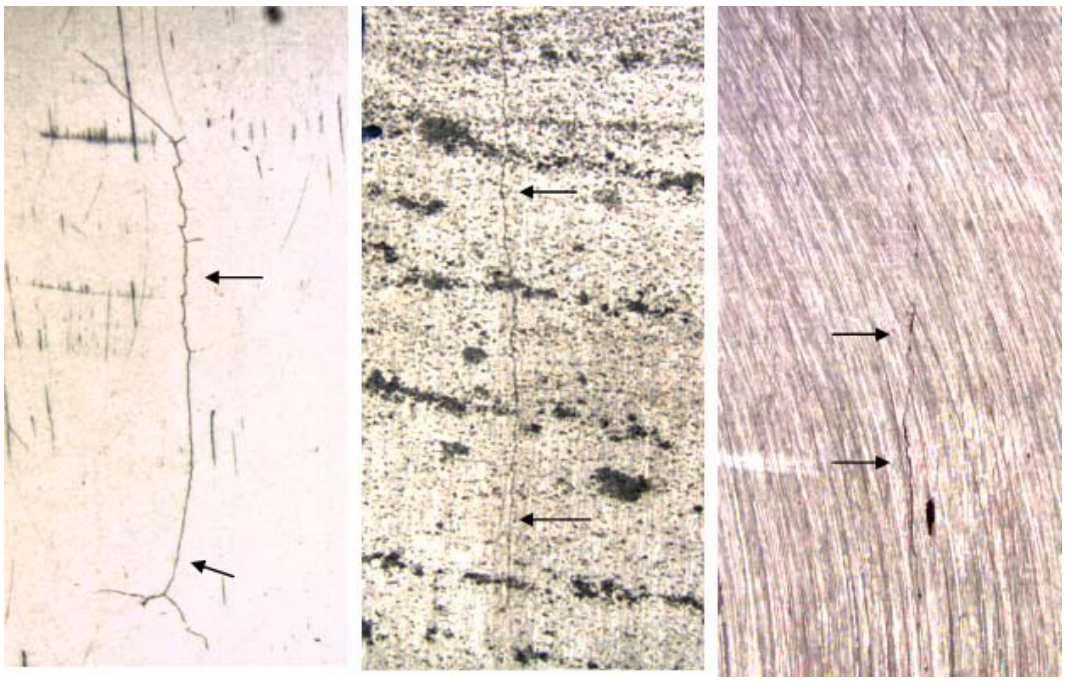

Figure 4.10 Sample Images of Three 12-μm COD Cracks

Poor surface conditions can magnify the effects of poor lighting. A surface with many scratches can become very hard to inspect when one uses spotlighting, for example. As shown in Figure 4.3, poor lighting can greatly emphasize scratches and other marks and obscure otherwise visible cracks.

The matrix results for the effects of surface conditions on crack detection are given in Table 4.4. These show that a very rough surface makes crack detection very difficult. Sample root-mean-square roughness for the samples ranged from 0.0016 to 0.0635 mm (63-250 microinches). A smooth, polished surface yields the best results; when scratching is present, it helps if the scratches are perpendicular to the crack.

Table 4.4 Effects of Surface Conditions on Crack Detectability

Surface Conditions	Excellent	Good	Fair	Poor
Unpolished	0.0%	11.1%	19.4%	69.4%
Polished	45.8%	12.5%	10.4%	31.3%
Parallel	20.4%	18.5%	14.8%	46.3%
Perpendicular	31.5%	35.2%	16.7%	16.7%

4.3.3 Surface Specularity

On the very specular surface of sample 1, the diffuse on-axis light provided the highest contrast between the crack and the background. This light evened out the illumination the most effectively and had negligible glare. The crack appears as a high-contrast dark indication on a bright background. The diffuse ring light provided low glare on the surface, but there were some mixed brightfield and darkfield responses, making the crack image lower contrast than in the diffuse on-axis image. The spotlight provided a darkfield response and is visible against the perpendicular machining marks on the surface. The three images are shown in Figure 4.11.

For a sample with low specularity, the diffuse on-axis light and the ring light provided very similar results, while the spotlight performed very poorly. The crack appeared as a dark indication against a light background in the images made using the diffuse on-axis and ring lights. For the diffuse on-axis light, the contrast between the crack and the background ranges between 20 and 40 levels. For the ring light, the grayscale levels between the crack and the background ranges from 10 to 40. In the image made using the spotlight, the crack is essentially not visible. For most of the crack length, the grayscale level between the crack and the background are the same. At the very top of the sample where the glare is brightest, the grayscale level difference between the crack and the background ranges from 0 to 50. One can find the dark indication against the background if the image is enlarged, but the crack has a much lower contrast than in the other two images. A crack imaged on a low-specularity sample is shown in Figure 4.12.

To ensure that the low-contrast image resulting from the use of the spotlight in Figure 4.3 was not an artifact of using only one lighting angle, the same crack was imaged with the spotlight shining from four angles—from the top, bottom, left, and right of the crack. The results are shown in Figure 4.13. In all images, there is low contrast between the crack and the background. The best contrast is provided by shining light from the right of the crack, which gives a low-contrast darkfield response.

The imaging results for the different surfaces are useful in guiding lighting styles for inspections. If one wishes to inspect a smooth and highly specular surface, one needs to use a diffuse axial light for brightfield imaging or properly angled spotlighting to provide darkfield imaging. For a somewhat specular surface, the ring light and the diffuse axial light perform well, while the spotlight is not especially effective at imaging cracks, even when illuminating from several angles.

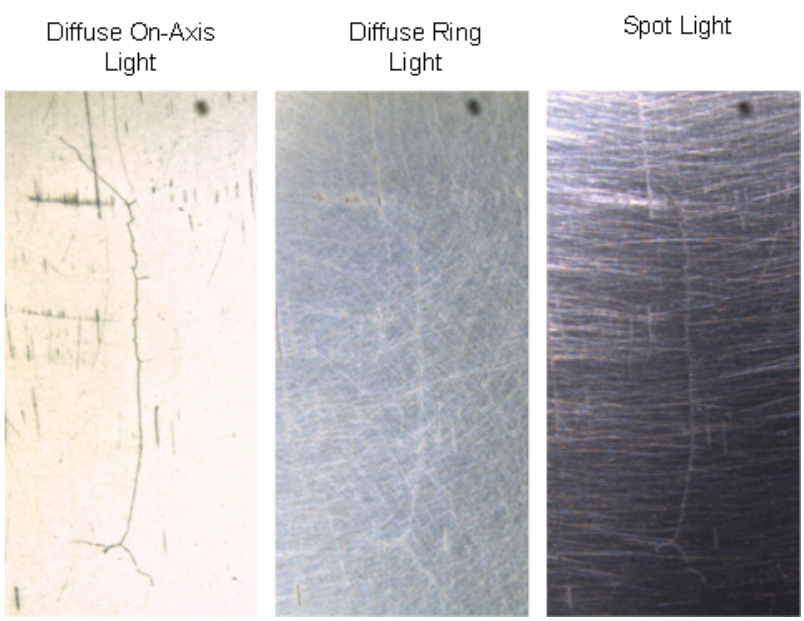

Figure 4.11 Influence of Lighting Style on Crack Detectability on Highly Specular Surface (S/D ratio of 49.86)

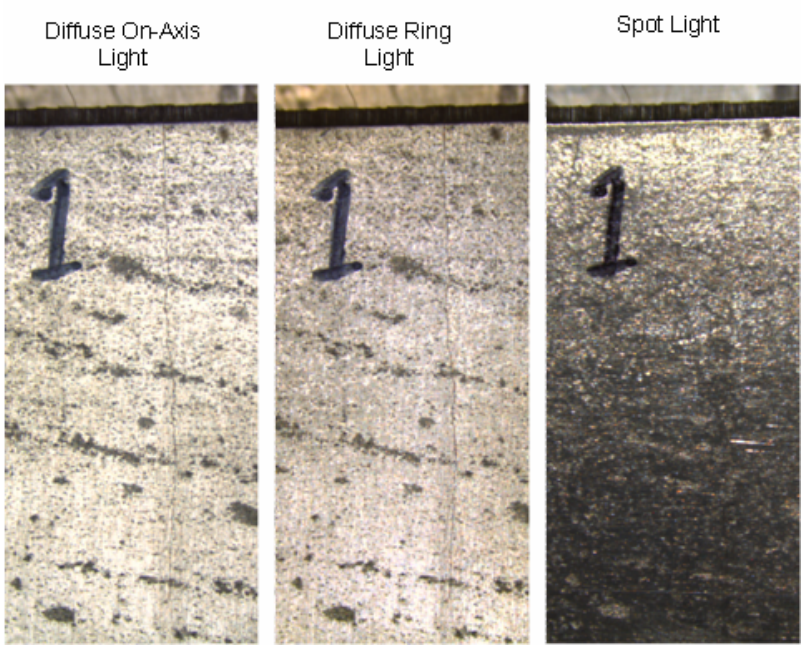

Figure 4.12 Influence of Lighting Style on Crack Detectability on Somewhat Specular Surface (S/D ratio of 4.32)

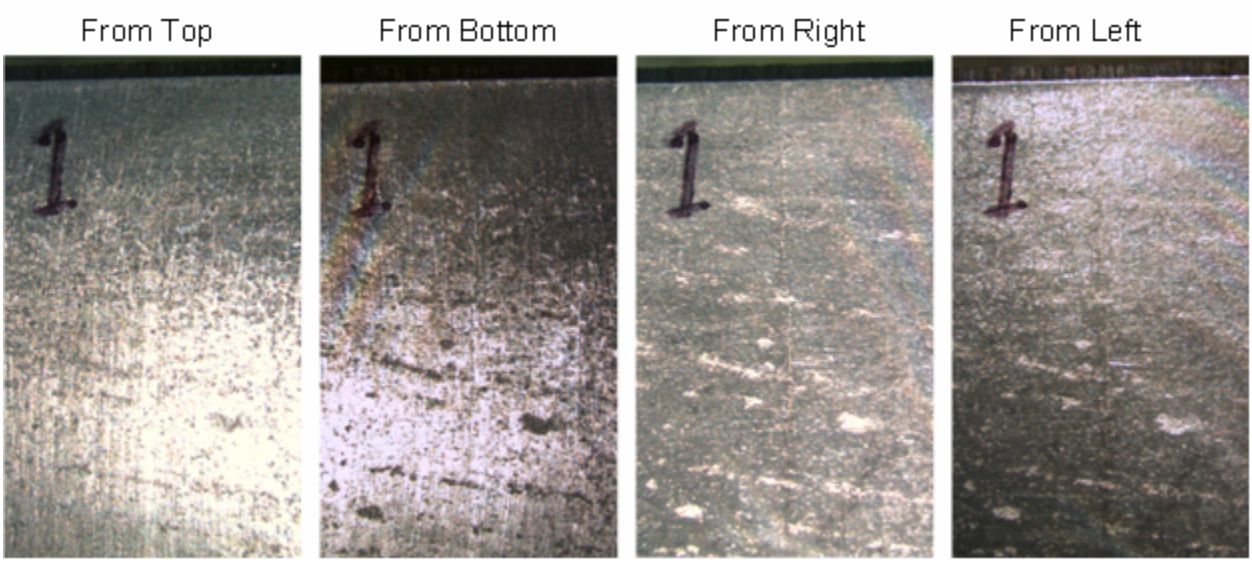

Figure 4.13 Influence of Spotlighting Angle on Crack Detectability on Somewhat Specular Surface (S/D ratio of 4.32)

5 Laboratory Test Results

In October 2005, PNNL conducted a limited laboratory test. Four inspectors examined thirty regions of the reactor internals samples to determine the ability of radiation-hardened cameras to detect cracks on stainless steel components. The camera vendors (IST imaging) had representatives on hand to assure that the cameras were operated correctly and were used at the optimum levels of performance.

5.1 Fixed-Focus Camera Test Results

For the tests, the fixed-focus camera was set 145 mm (5.7 in.) from the surface of the samples, focusing on an area 70 mm wide by 47 mm long (2.75 in. × 1.8 in.). The camera was moved over the sample surface using a mechanical scanner. The fixed focus camera was able to image two crossed 12-μm (0.0005-in.) wires at this distance using the spotlights. A 12-μm (0.0005-in.) wire test was performed prior to each test of a camera, and a resolution test using a 1951 Air Force resolution target was performed at the conclusion of a camera test. The inspectors were allowed to call detected indications as definite cracks or as areas of interest (AOI).

In the most lenient case, it was assumed that all indications noted as areas of interest were called correctly; that is, all cracks that were noted were counted as a hit, and all scratches that were called areas of interest were left blank. The strict method of grading counted only definite hits on actual cracks. As this study is focused on crack detectability using these cameras and not on the overall reliability of visual testing, the inspectors were not penalized for false calls. Also, given the areas they were scanning and that the grader knew exactly where the flaws were and what they looked like, it was next to impossible for a false call to be counted as a hit. The results of the tests are shown in Table 5.1.

Table 5.1 Probability of Detection by Inspector Using Fixed-Focal Length Camera

Fixed Focus Camera	**Strict**	**Lenient**	**False Calls**	**Time taken**
PNNL Inspector 1	29%	53%	9	4 hr
PNNL Inspector 2	29%	29%	11	4.5 hr
Contractor 1	18%	35%	1	2.5 hr
Contractor 2	29%	53%	1	2.5 hr

The false call rates for the PNNL staff were very high. The high level of vigilance, extra time taken on the test, and propensity to make false calls did *not* help the PNNL staff to find more cracks than the outside contractors, as their hit rates were roughly equivalent. Also, two of the four testers took 2.5 hours to complete the test, while one took 4.5 hours. The extra time did not allow this tester to score better than one who took 2.5 hours.

The crack detection results were added and averaged. To determine the effects of COD on crack detectability, the crack CODs were characterized in four categories—less than 20 μm (less than 0.0008 in.), 20–40 μm (0.0008–0.0016 in.), 40–100 μm (0.0016–0.004 in.), and greater than 100 μm (0.004 in.), and the hit rates were determined. The results are summarized in Table 5.2.

Table 5.2 Probability of Detection Versus Crack COD Results Using Fixed-Focal Length Camera

	Probability of Detection	
Crack Size	**Lenient**	**Strict**
<20 μm	6 ± 6%	0 ± 6%
20–40 μm	37 ± 11%	11 ± 7%
40–100 μm	42 ± 11%	32 ± 11%
100–150 μm	92 ± 8%	92 ± 8%

In summary, the very tight cracks were not reliably detected, the large cracks were easily detected, and the medium cracks were difficult but possible to detect.

5.2 Pan/Tilt/Zoom Camera Results

For the pan/tilt/zoom camera tests, the camera was situated 65 mm (2.6 in.) above the samples. The inspector was free to scan the areas using the pan/tilt/zoom features of the camera. The imaged area ranged from 75 mm by 50 mm (3 × 2 in.) at the minimum magnification and 25 mm by 17 mm (1 × 0.67 in.) at the maximum magnification. Again, each test was preceded and concluded with the 12-μm (0.0005-in.) wire test and a resolution test using a 1951 Air Force resolution target. The samples were examined by three of the four inspectors. The results from the inspections are provided in Table 5.3.

Table 5.3 Probability of Detection Versus Crack COD Results Using the Pan/Tilt/Zoom Camera

	Strict	Lenient	False Calls	Time taken
PNNL Inspector 1	70%	76%	5	4.5 hr
Contractor 1	35%	35%	0	2 hr
Contractor 2	29%	29%	0	2 hr

For this test, the statistics do not tell the entire story. The outside contractors hired to perform the tests each completed the test in slightly less than 2 hours, and each of the contractors found only the largest of cracks. Virtually all cracks smaller than 100 μm (0.004 in.) were missed by both inspectors, and their hit rate is more a function of the crack size distribution in the test than any other effect. The PNNL staff member took 4.5 hours to complete the test but was able to find all cracks greater than 20 μm (0.0008 in.) in width. It was clear that the test was not testing the abilities of the camera but of how much time and vigilance was being put into the test. When set to maximum magnification, the pan/tilt/zoom camera itself was able to get good images of all cracks over 20 μm in COD.

The zoom capabilities of the camera allowed for much more confidence in each call, resulting in only one crack being called an area of interest and fewer false calls on scratches and pores. The PNNL inspector who made 11 false calls using the fixed focal length camera made only five using the pan/tilt/zoom camera. Five false calls are still far too many, but it is a large improvement over 11. The two outside

contractors were able to get through the test making no false calls at all. The pan/tilt/zoom camera provided the inspectors with much more control than the fixed focal length camera, allowing them to have greater confidence in their calls.

6 Conditions in Commercial Reactors

The U.S. nuclear industry has proposed replacing current volumetric and/or surface examinations of certain components in commercial nuclear power plants with VT methods. Remote VT is presently used to examine BWR vessel internal components. This section focuses on these components.

The visual tests performed in the field are generally not performed on clean, flat samples. The welds are often in as-welded conditions with weld beads and weld toe intact. The surfaces are not polished smooth and have a variety of scratches, grinding marks, and machining marks. Some cladding styles leave ripples along the surfaces. Also, the surfaces are usually oxidized and covered in oxide material. While this section is far from comprehensive, it gives some descriptions and images of some of the surface conditions and oxides found in reactor internals.

6.1 Oxide Deposits in Reactors

The stainless steel reactor internals in operating BWRs and PWRs usually are covered by a surface layer of deposits. This layer of deposits is made up of colloidal corrosion products from the primary water. These corrosion products are a mix of oxides, consisting of Fe_2O_3, Fe_3O_4, Fe_2CoO_4, Fe_2NiO_4, and other metal oxides. BWRs have highly oxidizing conditions in the primary system and the deposits tend to consist primarily of Fe_2O_3 (hematite). The deposits in PWRs tend to be primarily M_3O_4, with M being made up of Fe, Ni, and Co (Kim 2003).

BWRs primarily have red hematite-based deposits on all internal components. In PWRs, which have magnetite-based deposits, one sees dark grey or black deposits on internals components. Examples of each are shown in Figure 6.1. The image on the left was taken during an EVT-1 inspection in a BWR during a scheduled outage and shows a component prior to any cleaning. The surface is highly diffuse and dull red. The image on the right shows the wetted side surface of a control rod drive mechanism (CRDM) that had been removed from service and sent to PNNL for examination. The CRDM has been decontaminated using a wide variety of techniques, and the surface is somewhat specular. Prior to the decontamination, the CRDM wetted surface was also very diffusely reflecting. The bottom surface in a PWR is shown in Figure 6.2. Also shown at the left of the image are a resolution target and a bottom-mounted instrument penetration. The white section of the resolution target was used to white-balance the image. The bottom of the PWR appears to be dark brown, suggesting a mix of oxides.

The deposits usually accumulate in two layers, an adherent layer on the metal surface and a loose layer on top of the adherent layer. The loose layer can usually be removed with a brush or water jet, while the adherent layer requires aggressive methods such as wire brushing or acid etching to remove it. For practical purposes during visual testing in a reactor, soft brushing or hydrolasing is convenient to remove the loose layer and leave the adherent layer. Also, as virtually all visual testing is performed using spot lighting, removing the adherent layer and exposing a highly specular surface would severely degrade the inspectability of the cleaned components. An example of a component in a BWR before and after light brushing is shown in Figure 6.3. The image on the left shows a cracked component before cleaning, with the loose and adherent layers present. The image on the right shows the same area after the loose

Figure 6.1 Examples of Deposit Layers from BWR (left) and PWR (right)

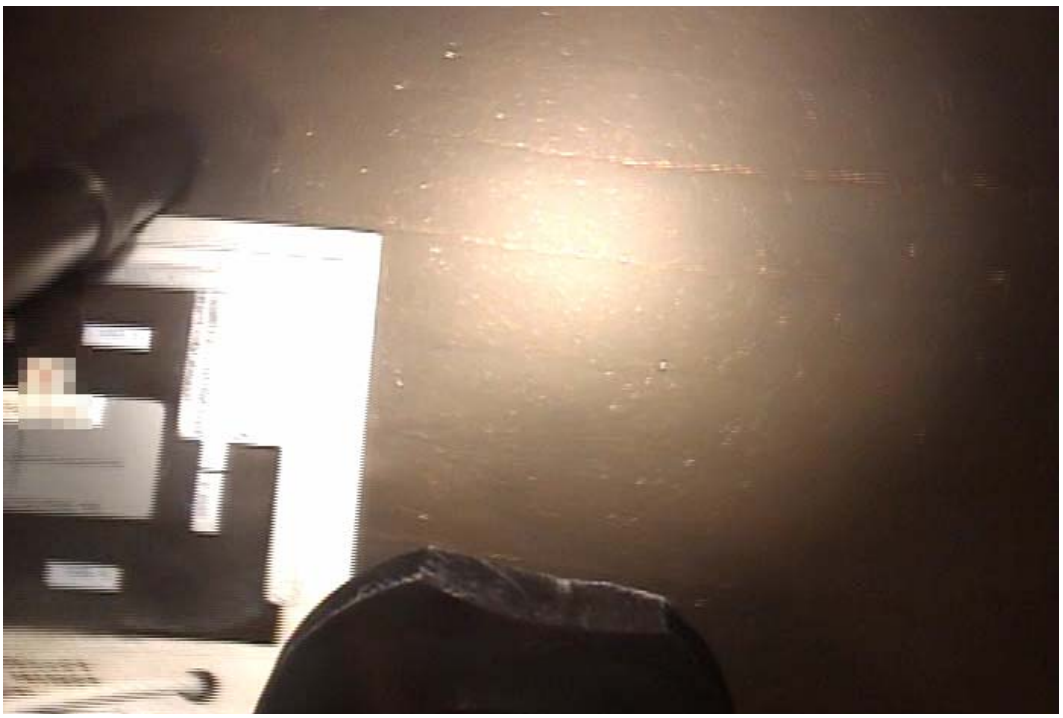

Figure 6.2 Bottom of PWR Pressure Vessel

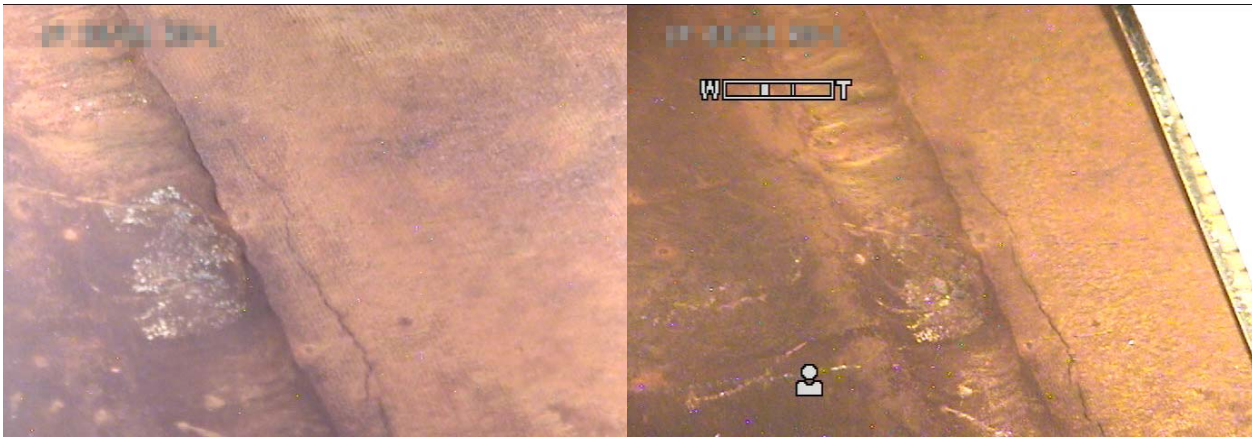

Figure 6.3 A Crack Before (left image) and After (right image) Cleaning Loose Oxide Layer from Surface

deposits have been brushed off, as well as part of a tape measure that has been lowered to facilitate measuring the length of the crack. The image of the area before brushing shows the layers to be almost entirely diffuse, and the spotlights provide very even illumination with no signs of glare. The cleaned image shows the adherent layer to be somewhat specular with slight glare but still less specular than the tape measure, which shows significant glare.

6.2 Effects of Oxide Layer on Crack Detectability

It should be noted that for the purposes of this study, PNNL focused on analyzing under laboratory conditions pertinent issues associated with the reliability of VT. In the course of the study, some limited information was found regarding field conditions. For example, VT practitioners have indicated that the oxide layer may sometimes be helpful in finding cracks. There is anecdotal evidence of the oxide patina being discolored around cracks, making the cracks easier to find. It was learned that a recent examination of a BWR provided two cases in which crack detection was assisted by markings and discolorations in the oxide layer. Both cracks were mechanical fatigue cracks. In the first case, the crack was very long, had a large COD, and would have been found even without the discoloration. This crack is shown in Figure 6.4. The discoloration is near the end of the crack, where it is the tightest. For the second crack, the oxide layer was disturbed near the crack, greatly enhancing the crack visibility. This crack is shown in Figure 6.5, both before and after the loose oxide layer was brushed off. The crack was, in fact, more visible before the loose oxide layer was removed.

Another example of a crack that was made more visible by oxides is shown in Figure 6.6. In this case, the component had stainless steel cladding over carbon steel. When the stainless cladding cracked through, the carbon steel oxidized, and the resulting oxide bled through the crack, decorating the surface of the stainless steel. This oxide decoration draws attention to the cracked region. While the crack is faintly visible without the oxide, the oxide decoration does help in crack detection.

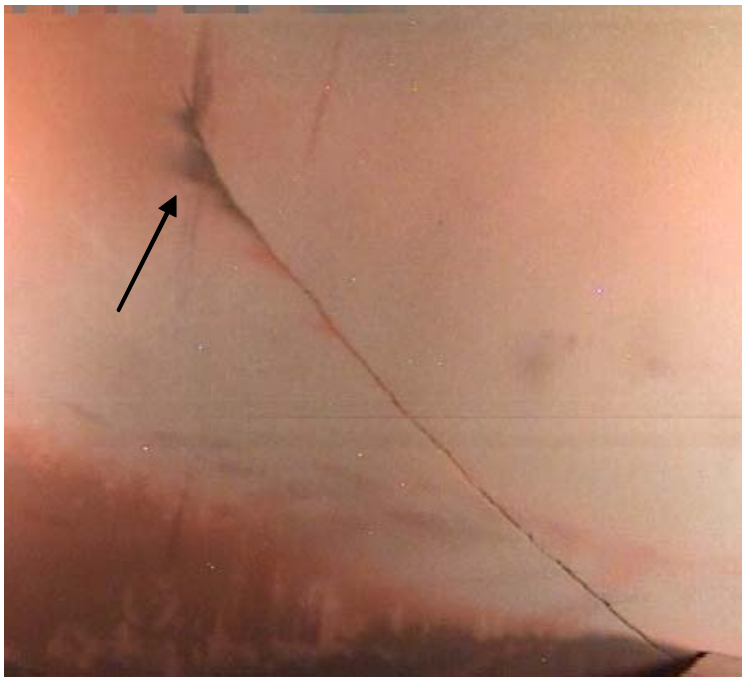

Figure 6.4 Mechanical Fatigue Crack with Black Oxide Decorating One End of Crack

Figure 6.5 Mechanical Fatigue Crack Made Visible by Disturbance in Loose Oxide Layer

One important question not researched in this study is "are deposits hiding cracks." Some types or sizes of cracks would be expected to cause decorations and disturbances in the oxide layer. Conversely, some types or sizes of cracks are more likely to be hidden by deposits. The VT of reactor internals is predicated on the fact that most of these components have been demonstrated to be crack tolerant, and large cracks would be detected before structural integrity was threatened.

One way to explore the numbers and types of cracks that are hidden by the oxide layer is to perform a nondestructive test such as ultrasound on reactor components and then perform VT on the areas shown to be cracked.

Figure 6.6 Stress Corrosion Crack Through Stainless Steel Made More Visible by Oxide Decoration

One difficulty that can be caused is uneven layer distribution. Uneven layer distribution may result in a mottled surface on a component. When one is examining a region with light and dark regions, imaging a crack is challenging. If one sets the lighting and exposure to optimize crack visibility on the lighter areas, the crack will be invisible in the dark regions; and if one sets the lighting and exposure for the darker regions, the image will be overexposed in the lighter regions. Also, a mottled distribution can result in very different specularity levels across the imaged area. Parts covered will be dull, and any bare metal may be highly specular. A weld region removed from a PWR with a mottled and uneven buildup is shown in Figure 6.7.

6.3 Surface Features and Geometry

In addition to being covered in oxides, reactor components are often not flat plates and have a variety of textures and configurations. Figure 6.8 shows a pipe coming out of a larger component, and one can see pipe, ground weld, clad plate, and the transition regions clearly. The deposits have not accumulated evenly over these surfaces, and there is more than one place for a crack to hide on such a surface. There are two linear indications that were not called as cracks shown in Figure 6.8. The transition between the pipe and the plate shows an oddly colored deposit region that could potentially hide a crack along the boundary. There is also a mottled region of deposits that presents a challenge to crack detection. All these features occur close to welds, which put them in regions that should be highly scrutinized.

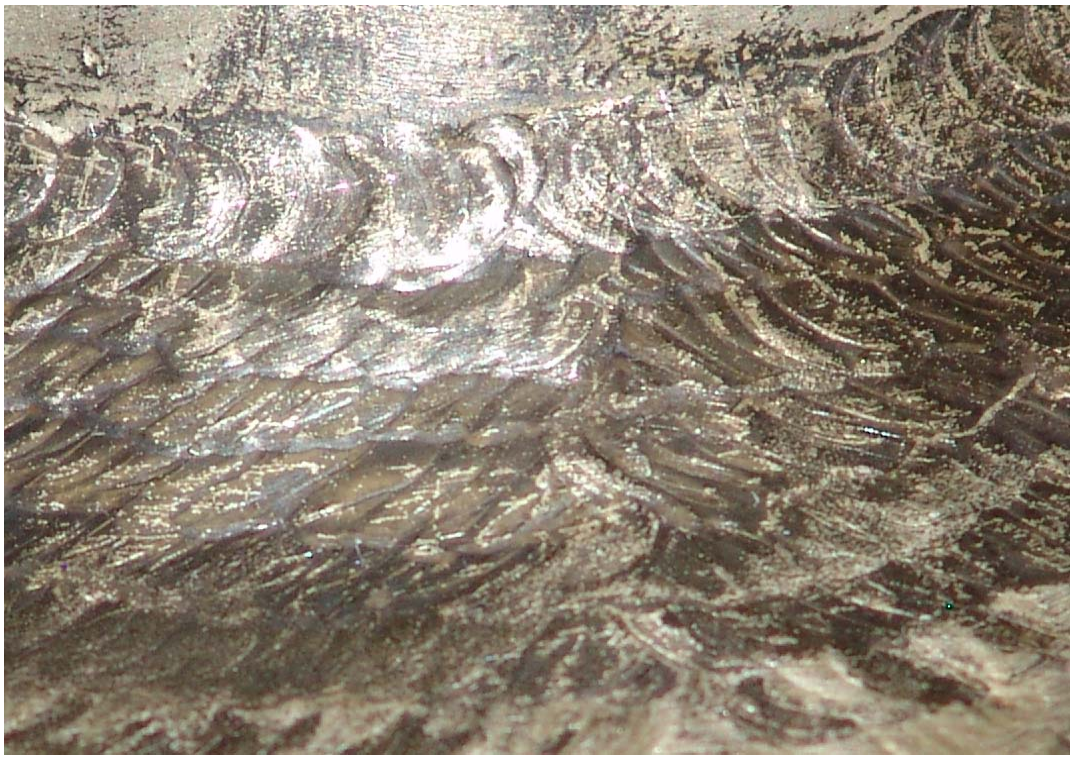

Figure 6.7 Mottled Surface with Varying Color and Specularity Across Surface

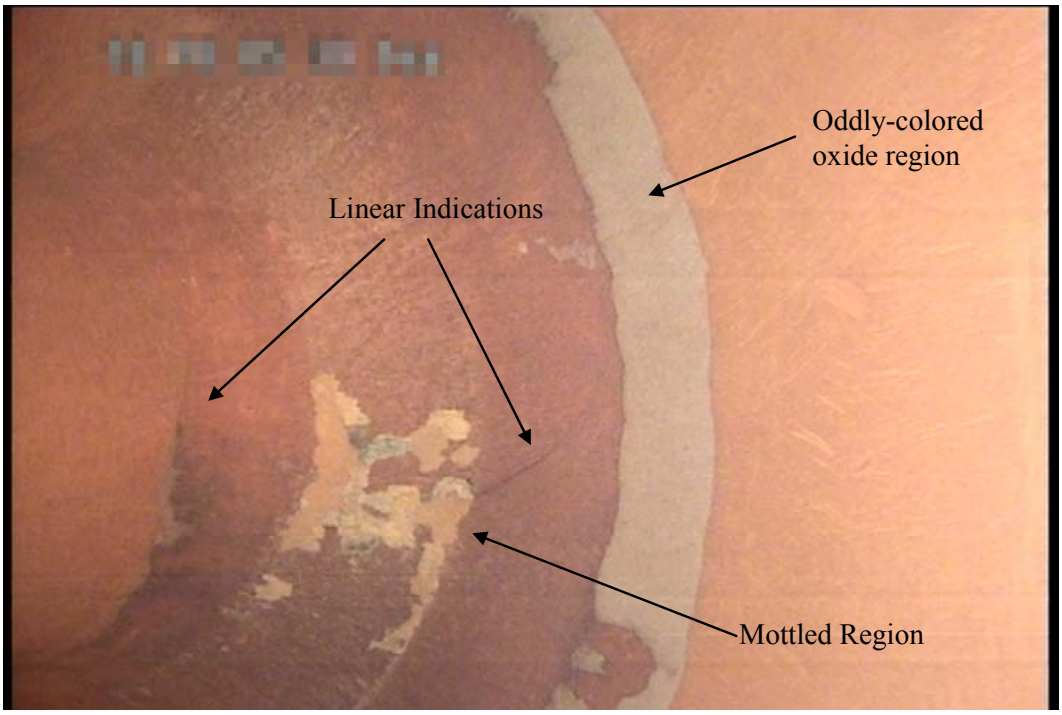

Figure 6.8 Complex Surface Geometry and Deposit Layering on BWR Component

Weld root and crown conditions provide several challenges. As many cracks, especially IGSCC, tend to occur along welds, visual inspections often occur on and near weld roots and crowns. Weld roots and crowns can affect the flow of the colloidal deposits and thus create different thicknesses and color patterns of the deposits around the weld. An example of this is shown in Figure 6.9. Notice the dark linear mark along the bottom right portion of the weld. High magnification and resolution would be needed to discern such deposits from a small crack.

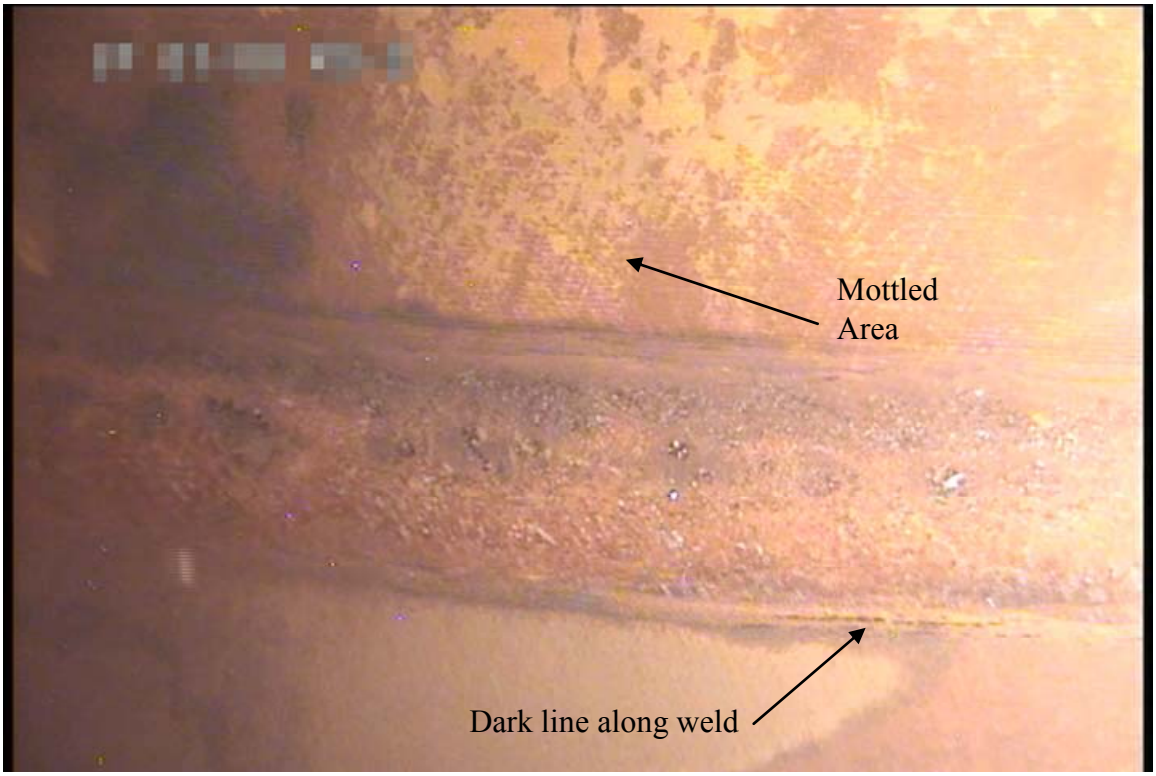

Figure 6.9 Complex Surface Deposit Layering On and Near BWR Weld

7 Discussion

The parametric study and limited laboratory test demonstrate that performing adequate visual testing is complicated — many of the factors involved in the quality of visual testing are interrelated and often very subjective. Developing a coherent understanding of the issues is challenging. Some clear trends emerged, and these issues and trends are discussed in this section.

7.1 Parametric Study

The parameter that appeared to have the largest effect on detection reliability is the crack COD. The matrix results and the other examinations showed that cracks with CODs above 100 μm (0.004 in.) are usually detectable unless the inspection parameters and surface conditions are very unfavorable. Cracks with CODs less than 20 μm (0.0008 in.) were difficult to detect under all but the most favorable conditions.

Between these two extremes in crack COD, results become more difficult to quantify. When the other parameters are considered, the matrix study showed little difference in the reliability in detecting cracks between 20–40 μm (0.0008–0.0016 in.) and 40–100 μm (0.0016–0.004 in.). How well one can detect these cracks appears to be very dependent on the other factors in the test.

The parametric study pointed to the factors that most affect the quality of the inspections. The most important factor is scanning speed. Higher scanning speeds severely limit crack detection capability with the result that only large cracks can be reliably detected. The parametric study suggests that reliable inspections should be limited to the use of stationary or very slowly moving cameras (6 mm/s in our tests). While very slow scanning does not appear to greatly reduce the resolving power of the camera and contrast of indications, higher scanning speeds can severely lower the quality of an inspection.

The second most important factor is lighting. Current practice is to use one or two fixed spotlights. This may lead to missed cracks. When spotlights are misaligned relative to the crack orientation, they can effectively hide even larger cracks. Properly aligned spotlights can be as effective as a diffuse ring light, but unfortunately one does not know the orientation of the cracks ahead of time. The parametric study shows that diffuse on-axis light produced by far the best results. The diffuse on-axis light is not very practical for use in a reactor environment, but some engineering work may lead to development of a system that is equally as effective.

The following factors would have less impact on visual testing than those discussed above, but are important nonetheless. A higher-resolution radiation-hardened camera would greatly help in detecting small cracks, as the greater pixel count would allow for a higher contrast between the crack and the metal surface and would enhance discrimination between cracks and innocuous surface features such as scratches and machining marks. In addition, the current CCTV resolution standard of 400–500 lines vertical can almost certainly be improved.

7.2 Laboratory Tests

The results of the limited laboratory test and the previous studies performed in Sweden and Finland (Enkvist 2003) are supportive of certain positions on visual testing.

In the study, cracks with CODs larger than 100-μm (0.004-in.) wide were readily detected. This was largely independent of the lighting and magnifications used in the tests. No system was able to reliably detect cracks with CODs smaller than 20 μm (0.0008 in.) in width. This included the PNNL use of the pan/tilt/zoom camera system and a very vigilant inspector under nearly ideal conditions.

The quality of the examinations and camera systems was of great importance in the reliability of detecting cracks with CODs between 20–100 μm (0.0008–0.004 in.). Careful inspections using good lighting and stationary cameras allowed good detection of the smaller cracks, while quick scanning resulted in very poor crack detection in this range of crack sizes. The higher magnification used in the Swedish study is one reason why better results for crack detection in this range were found when compared to the PNNL study using the fixed-focus camera.

7.3 Conditions in Reactor Components

In the course of this study, some information was gathered relative to deposits on nuclear power plant components. The net effects of deposits on crack detectability have not been studied. The deposits cover all components in different thicknesses and have different characteristic in PWRs and BWRs. The deposits have some positive and some negative impacts on remote VT inspection effectiveness. Some of the effects are described below.

7.3.1 Reduced Specularity

The deposit layer reduces the specularity of stainless steel and inconel surfaces. This reduced specularity makes the surfaces easier to light and reduces glare, and makes the spotlights commonly used in remote VT less problematic than if there were no deposits. This reduced specularity is a large help in finding cracks under all but the most diffuse lighting conditions or well-prepared darkfield imaging.

7.3.2 Discoloration

The red discoloration in a BWR possibly does not have a strong effect on crack detectability. The dark grey/black discoloration in a PWR could make crack detection more difficult, however. The dark color of the oxide in a PWR can be at least partially overcome with more lights and longer exposures. The largest problem encountered in remote VT on reactor components was caused by mottled surfaces. When a tight crack passes through regions that are both light and dark, finding and sizing the crack can be very difficult.

7.3.3 Crack Decoration

The oxide layer can help in crack detection with the periodic decoration of the outside of the crack. This phenomenon has been observed several times, and some photographs of this are shown in Section 6.3. The cause of this decoration and the probability of it occurring are as yet unknown.

7.3.4 Crack Masking

One issue that has not yet been studied is deposit thickness, i.e., could a crack large enough to affect structural integrity be hidden? Fracture mechanics analyses of critical flaw size for reactors internals have been performed. The analyses show that for most of the reactors internals, cracks must be relatively large to affect component structural integrity. Industry personnel indicate that these large cracks would be easily detected by present visual testing practices. This conclusion appears to be supported by industry operating experience.

There have been a few unanticipated failures of components, however, where the critical crack size is much smaller. For example, there have been failures of the jet pump hold down beam in BWRs. As a result of the failure analysis, new guidelines were adopted by the BWRs. Any flaw detected is considered rejectable, and the jet pump hold down beam is subsequently replaced. Thus, for this component, the potential for deposits to mask cracks becomes germane. The potential for crack masking was not addressed in the laboratory tests conducted to date but is under consideration for future research.

7.4 Integrated Results

Both the parametric study and the limited laboratory test showed that cracks with large CODs are easy to find, very tight cracks are extremely difficult to find, and cracks between can be found. Further, the reliability of finding these mid-sized COD cracks depends on the inspection variables.

There is good agreement among results of the parametric study, the limited round-robin, the Swedish human factors study, and the Finish camera test—all agree that large cracks can be defined as cracks with a COD larger than 100 μm (0.004 in.), tight cracks can be defined as cracks with a COD smaller than 20 μm (0.0008 in.), and the mid-range cracks fall in between these values.

This mid range of 20 μm to 100 μm (0.0008 in. to 0.004 in.) is problematic, as many types of cracks have a median crack COD on the order of 16–30 μm (0.0006–0.0012 in.). This suggests that a significant fraction of potential cracks in nuclear reactors approach the low end of what the current equipment and procedures are capable of finding under ideal conditions. Careful inspections using good lighting and stationary cameras allowed good detection of the tight cracks, while quick scanning resulted in very poor crack detection in this range of crack COD sizes. The higher magnification used in the Swedish study was one reason why it may have found higher performance for crack detection in this range when compared to the PNNL study using the fixed-focus camera.

8 Conclusions

Based on the results achieved in both the parametric and laboratory studies, the following conclusions can be drawn:

- The current radiation-hardened video cameras being used in the field can be expected to reliably find cracks with CODs greater than 100 μm (0.004 in.), provided surface conditions are not overly unfavorable, adequate lighting is achieved, and sufficiently slow scan rates are applied.

- The current radiation-hardened video cameras being used in the field are not capable of effectively detecting cracks with CODs smaller than 20 μm (0.0008 in.).

- The reliability of detecting cracks with CODs between 20 and 100 μm (0.0008 and 0.004 in.) using current radiation-hardened video cameras is strongly dependent on the camera magnification, lighting, inspector training, and inspector vigilance.

- The scanning rate of a video camera over a surface strongly affects the visual acuity of the camera. At low speeds, the camera suffers little loss of visual acuity, but at high rates, the image becomes severely degraded.

- Diffuse lighting helps to increase the contrast between a crack and the metal surface while decreasing the contrast from scratches and machining marks in the metal surface.

- Reliable detection of tight cracks in nuclear components may require higher-resolution cameras.

- Although the oxide layer in reactors can aid in crack detection, the overall effects of the oxide layer are not known and need to be understood regarding influence on crack detectability.

9 References

Allgaier MW, S Ness, P McIntire and PO Moore. 1993. *Nondestructive Testing Handbook, Volume 8, Visual and Optical Testing*. 2nd ed. American Society for Nondestructive Testing, Columbus, Ohio.

Chen DL, B Weiss and R Stickler. 1996. "A Model for Crack Closure." *Engineering and Fracture Mechanics* **53**(4):493–509.

Cumblidge SE, MT Anderson and SR Doctor. 2004. *An Assessment of Visual Testing*. NUREG/CR-6860, U.S. Nuclear Regulatory Commission, Washington, D.C. Available at http://www.nrc.gov/reading-rm/doc-collections/nuregs/contract/cr6860/index.html (September 2006).

De Petris C and C Macro. 2000. "Verification of the resolution capability for equipment used for visual testing." In *Proceedings of the 15th World Congress on Non-Destructive Testing*. AIPnD — the Italian Society for Non-Destructive Testing and Monitoring Diagnostics, Brescia, Italy. Available at http://www.ndt.net/article/wcndt00/papers/idn300/idn300.htm (September 2006).

Efsing P, J-Å Berglund, C Sandelin and A Werner. 2001. "Visual inspection of brackets for emergency core cooling system in Barsebäck Unit 2." In *Proceedings of the 3rd International Conference on NDE in Relation to Structural Integrity for Nuclear and Pressurized Components*, pp. C 25–32. November 14–16, 2001, Seville, Spain. Tecnatom s.a., Seville.

Ekström P and J Wåle. 1995. *Crack Characterization for In-Service Inspection Planning*. SKI Report 95:70, Swedish Nuclear Power Inspectorate, Stockholm, Sweden.

Electric Power Research Institute. 2005. *BWRVIP-03 Revision 8: BWR Vessel and Internals Project – Reactor Vessel Pressure Vessel and Internals Examination Guidelines*. TR-105696-R8, Palo Alto, California.

Electric Power Research Institute. 2003. *BWRVIP-41-A: BWR Vessel and Internals Project – BWR Jet Pump Assembly Inspection and Flaw Evaluation Guidelines*. Palo Alto, California.

Enkvist J. 2003. "A study of operator performance in a visual NDT inspection task by remote video camera." *Insight* **45**(4):252–257.

García C, F Martin, P De Tiedra, JA Heredero and ML Aparicio. 2001. "Effects of prior cold work and sensitization heat treatment on chloride stress corrosion cracking in type 304 stainless steels." *Corrosion Science* **43**(8):1591–1599.

Kim K, H-J Lee, D-W Kanga and S Inoue. 2003. "Synthesis of simulated cruds for development of decontaminating agents." *Nuclear Engineering and Design* **223**:329–337.

Sine Patterns. 2004. "Standard Charts." Sine Patterns LLC, Pittsford, New York. Available at http://www.sinepatterns.com/i_Stdrds.htm (September 2006).irkkunen I., M. Kemppainen, R. Paussu, P. Seppälä, D.S. Dybal, and A.A. Nikitin. 2004. *Cracked samples for visual testing*. 286AER002,

Trueflaw Ltd., Espoo, Finland. Available at
http://www.trueflaw.com/Publications/SamplesForVisual.pdf (September 2006).

Wåle J. 2006. *Crack Characterisation for In-service Inspection Planning – An Update*. SKI Report 2006:24, Swedish Nuclear Power Inspectorate, Stockholm, Sweden.

Xaio QZ and BL Karihaloo. 2002. "Approximate Green's functions for singular and higher order terms of an edge crack in a finite plate." *Engineering Fracture Mechanics* **69**(8):959–981.

Yoneyama H, M Senoo, J Miharada and N Uesugi. 2000. "Comparison Test of Echo Heights Between Fatigue Crack and EDM Notch." In *Proceedings of the 2nd International Conference on NDE in Relation to Structural Integrity for Nuclear and Pressurized Components.* May 24–26, 2000, New Orleans, Louisiana. Electric Power Research Institute, Palo Alto, California.

Appendix A

Surface Conditions for Each Window Used in the Limited Round Robin Test

Each window is roughly 100 mm × 100 mm (4 in. × 4 in.)

Figure A.1 Window 1

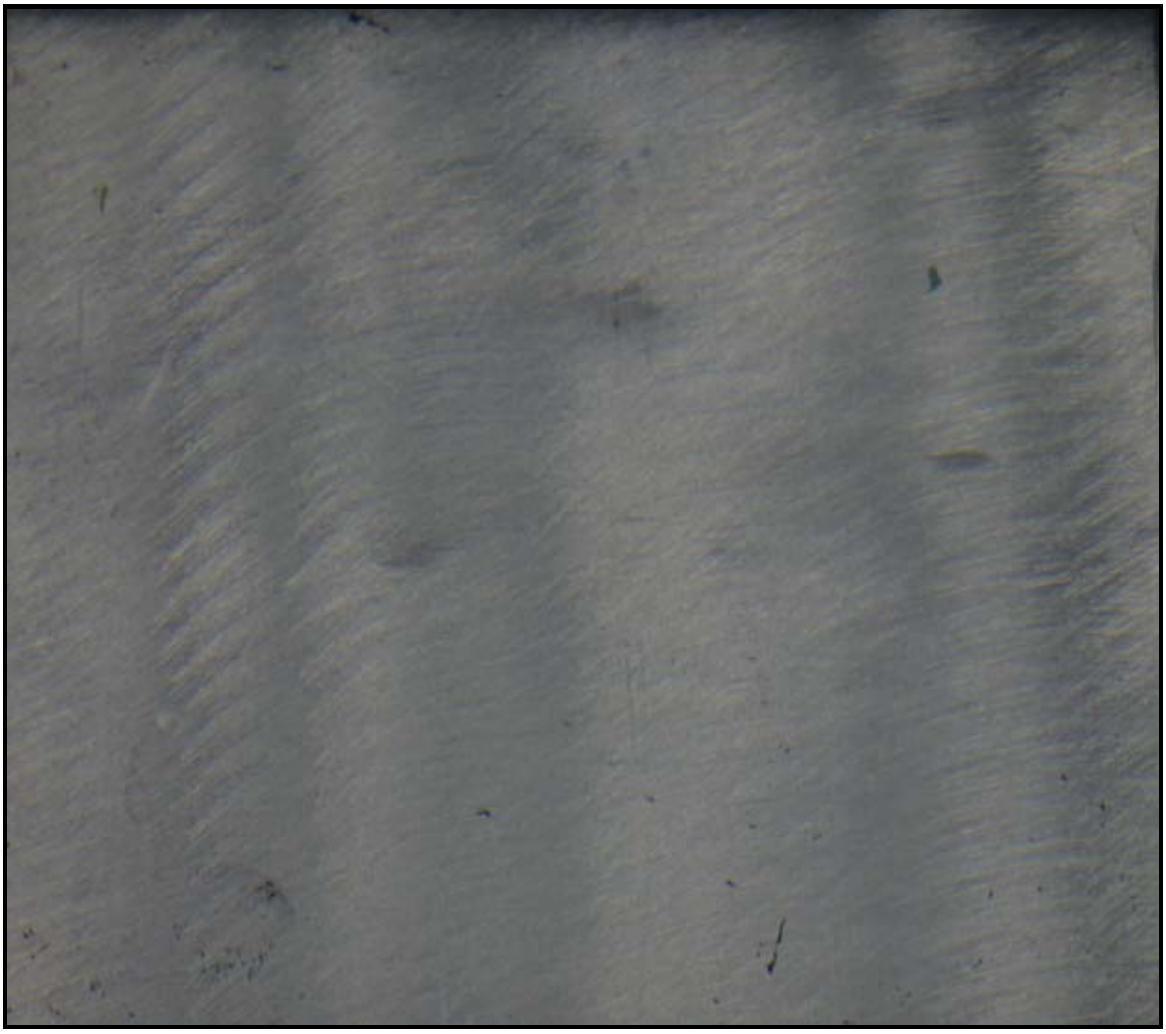

Figure A.2 Window 2

Figure A.3 Window 3

Figure A.4 Window 4

Figure A.5 Window 5

Figure A.6 Window 6

Figure A.7 Window 7

Figure A.8 Window 8

Figure A.9 Window 9

Figure A.10 Window 10

Figure A.11 Window 11

Figure A.12 Window 12

Figure A.13 Window 13

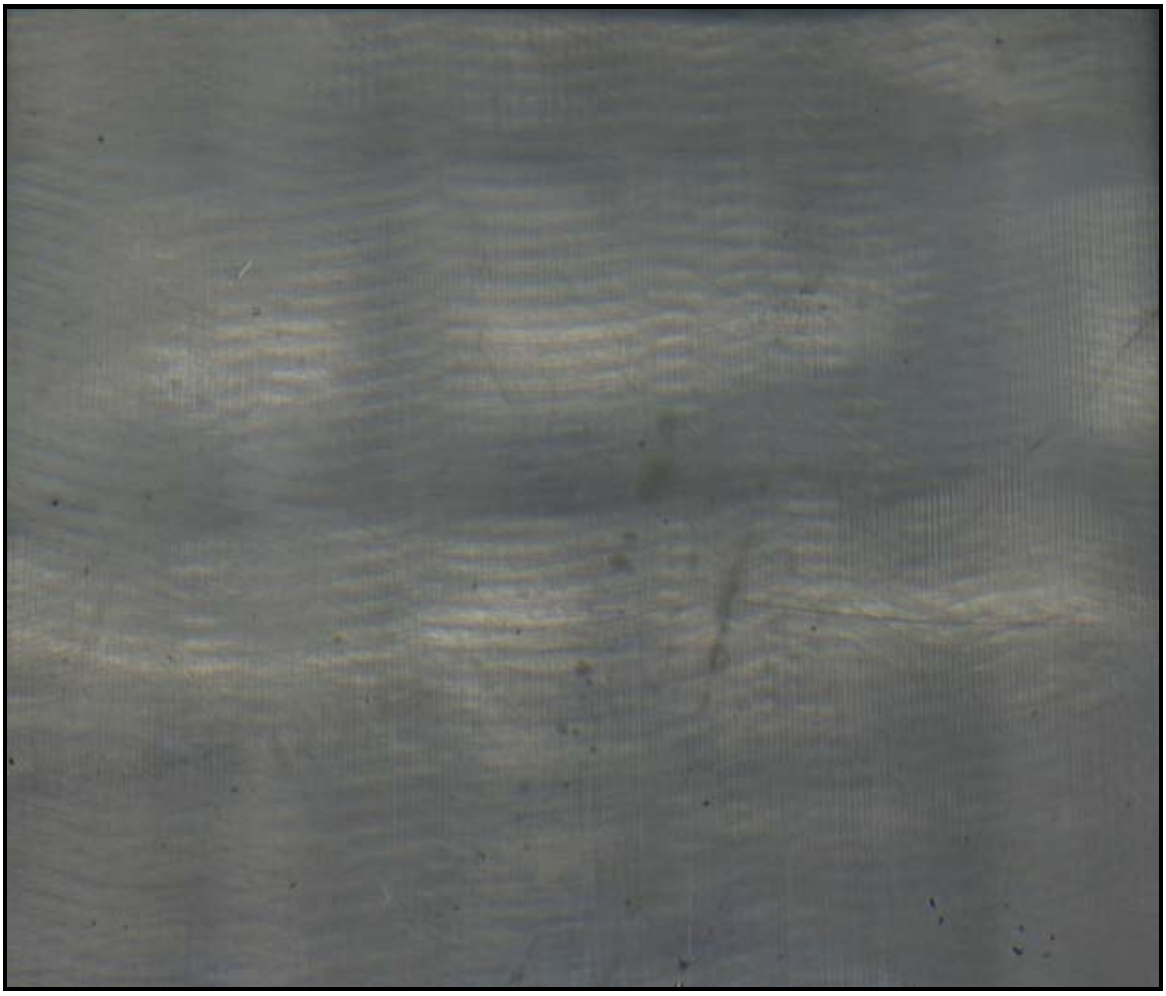

Figure A.14 Window 14

Figure A.15 Window 15

Figure A.16 Window 16

Figure A.17 Window 17

Figure A.18 Window 18

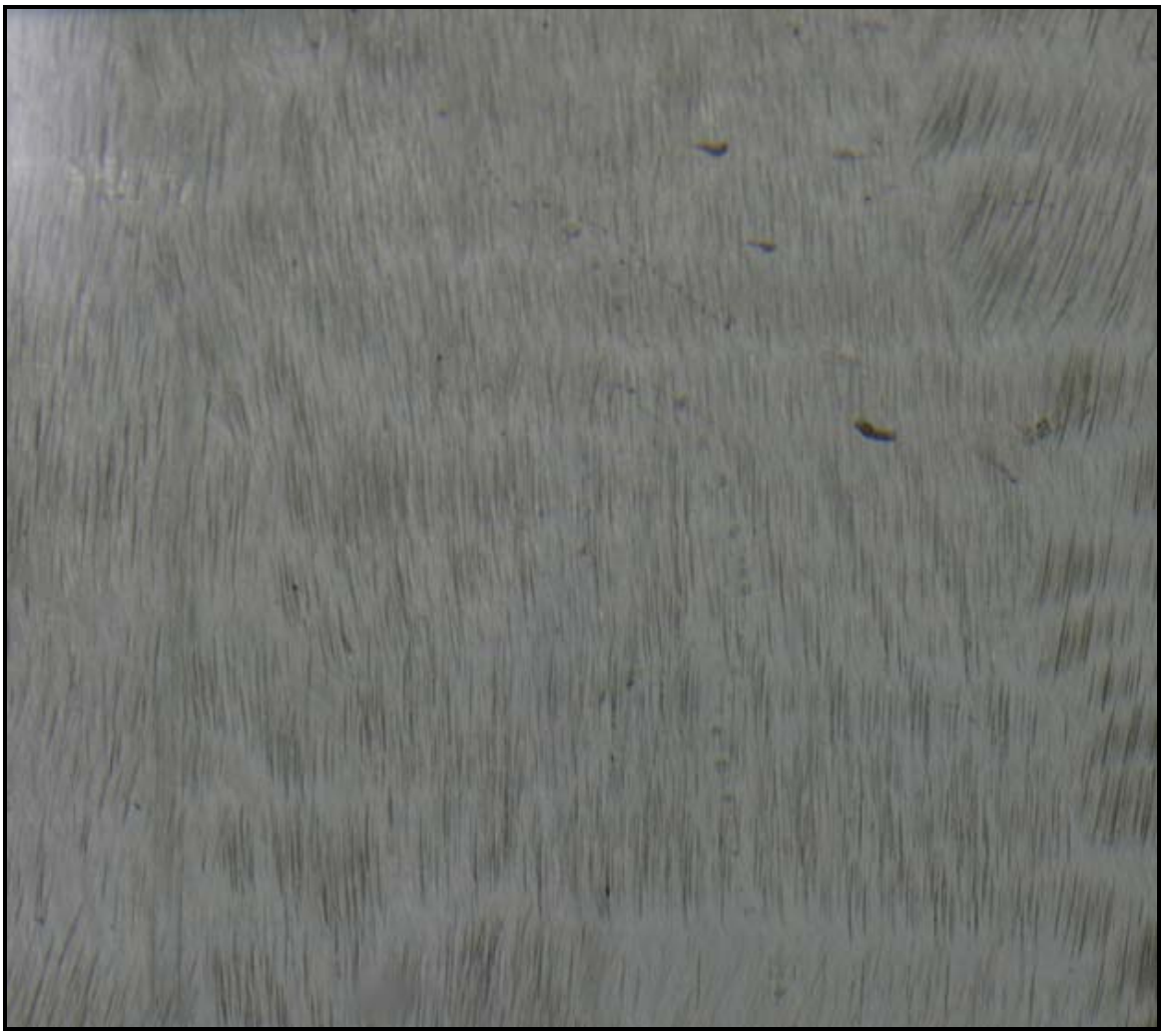

Figure A.19 Window 19

Figure A.20 Window 20

Figure A.21 Window 21

Figure A.22 Window 22

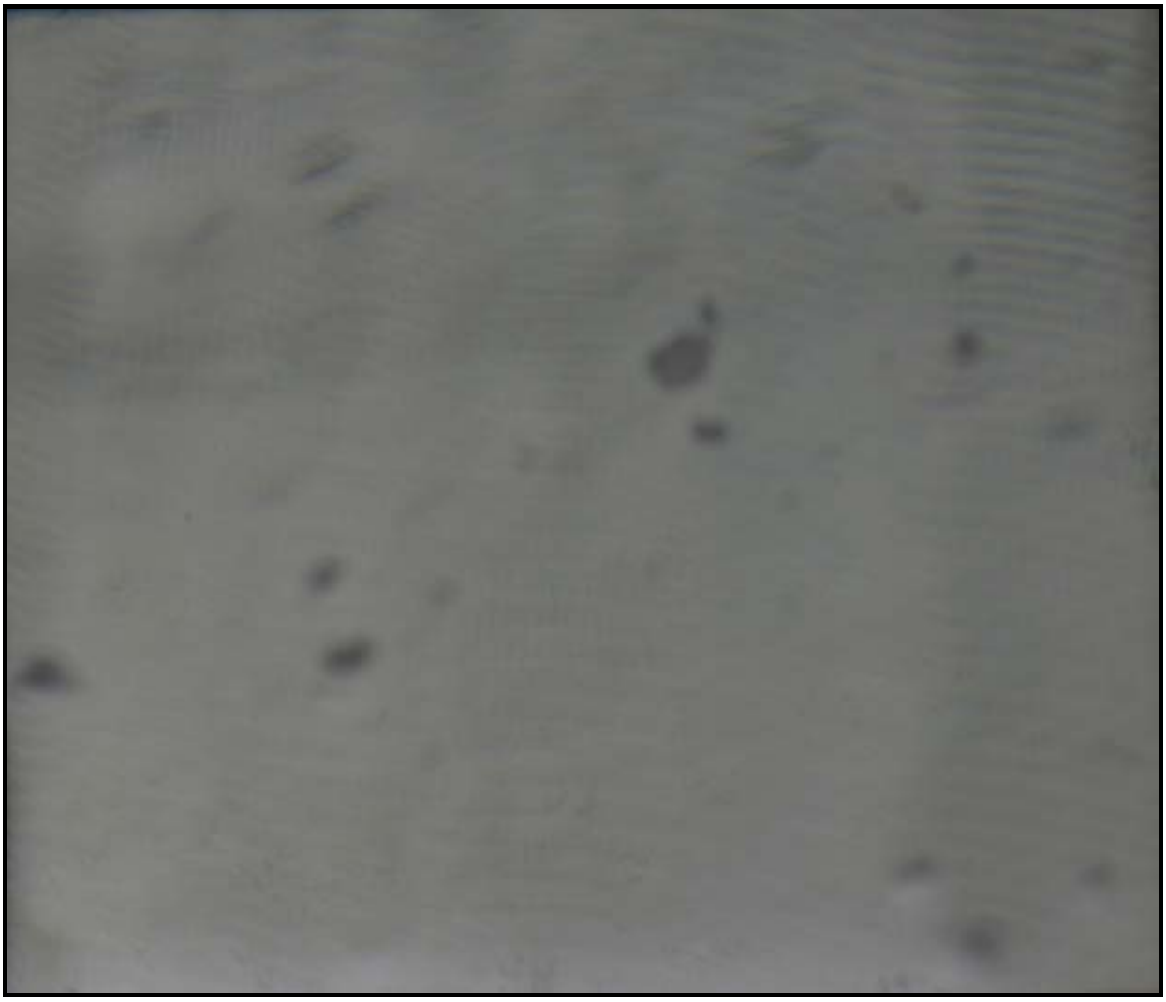

Figure A.23 Window 23

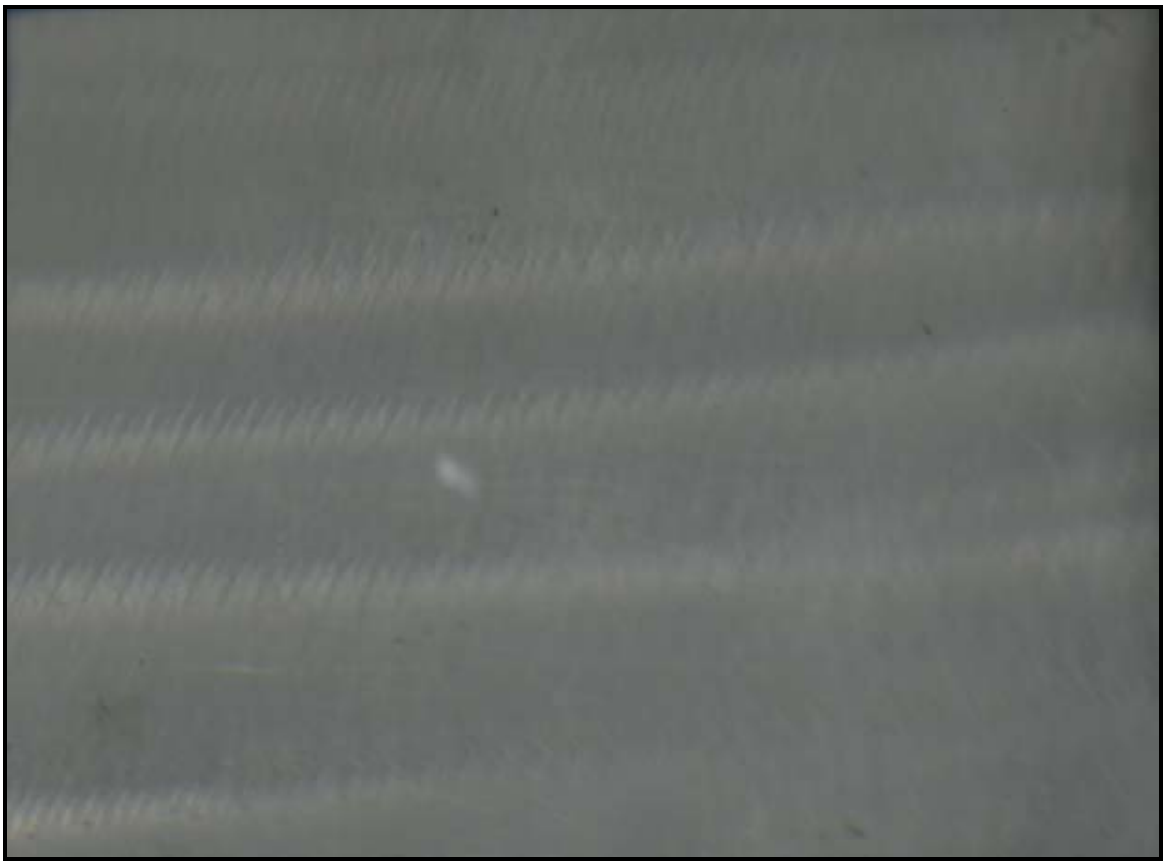

Figure A.24 Window 24

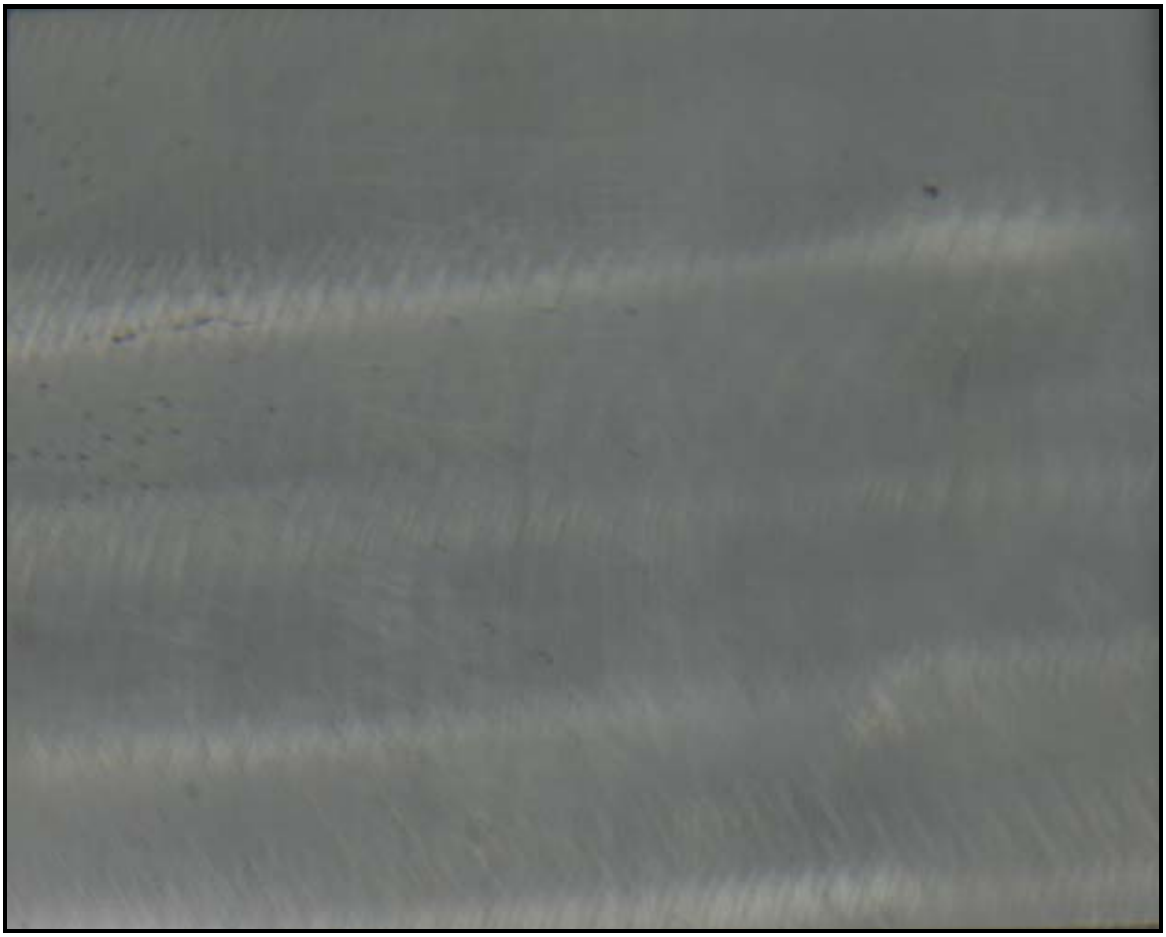

Figure A.25 Window 25

Figure A.26 Window 26

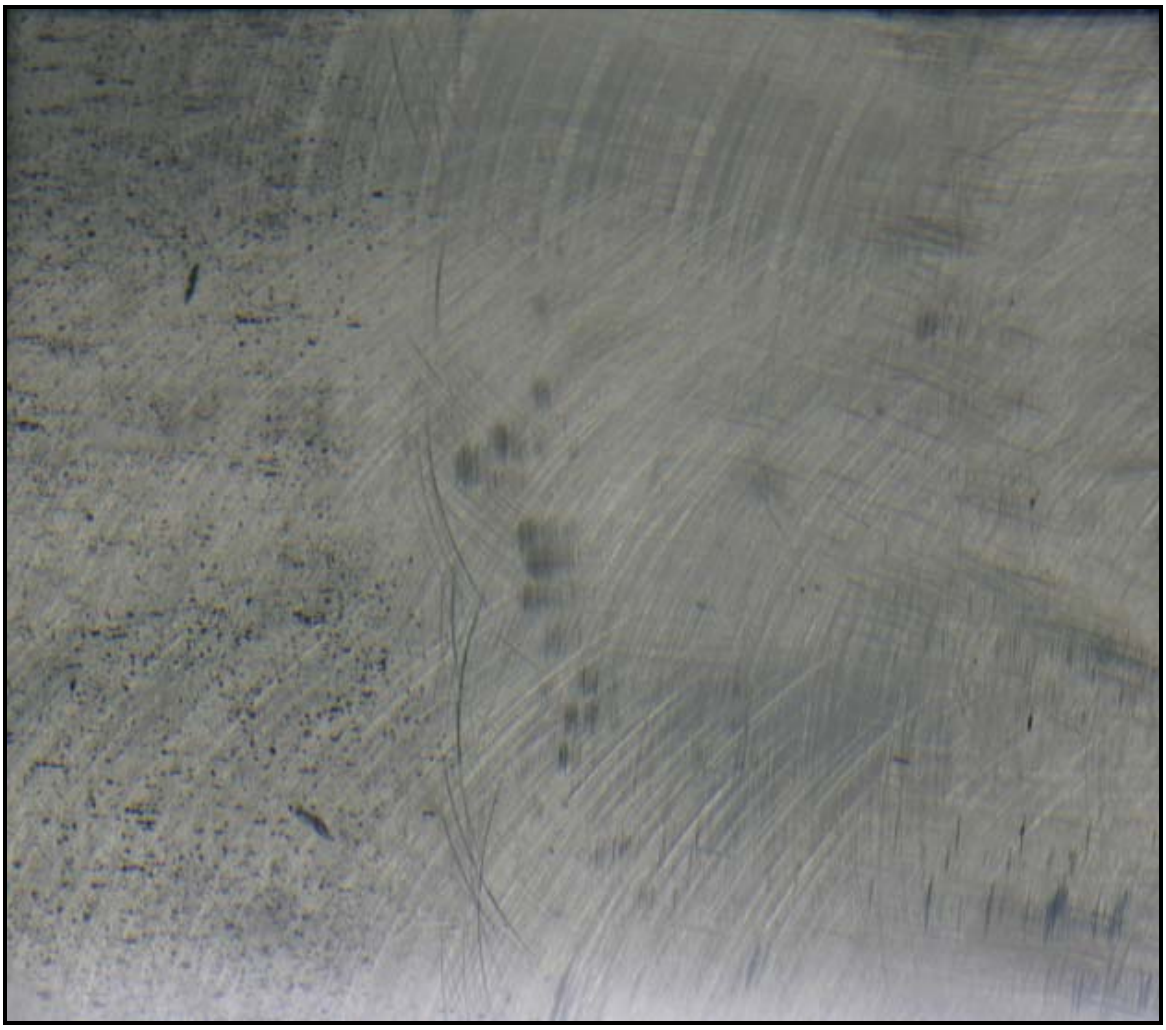

Figure A.27 Window 27

Figure A.28 Window 28

Figure A.29 Window 29

Figure A.30 Window 30

Appendix B

Images from the Parametric Test Matrix

Each window is roughly 36 mm × 24 mm (1.5 in. × 1 in.)

Sample 1 – Unpolished – 10-µm Crack Opening Dimension

Figure B.1 - Sample 1
Diffuse On-Axis Lighting

Figure B.2 - Sample 1
Diffuse Ring Lighting

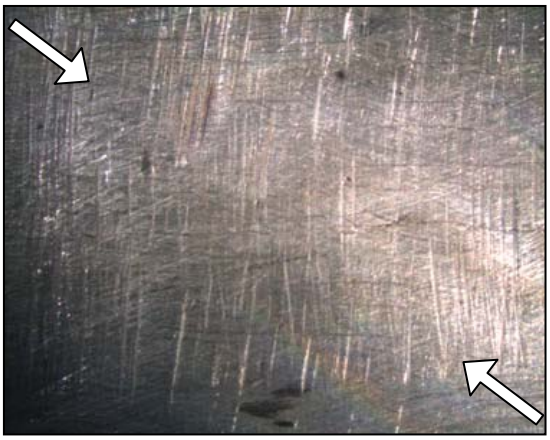

Figure B.3 - Sample 1
Spotlighting from Indicated Directions

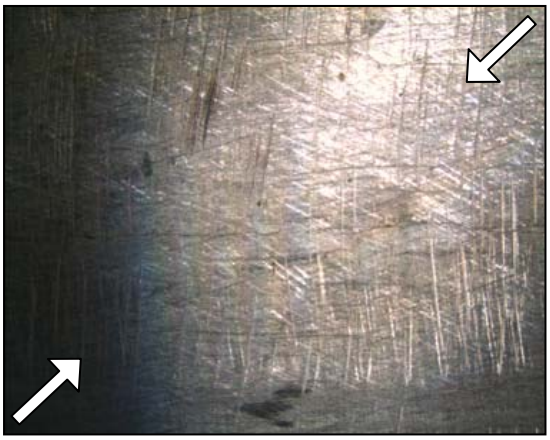

Figure B.4 - Sample 1
Spotlighting from Indicated Directions

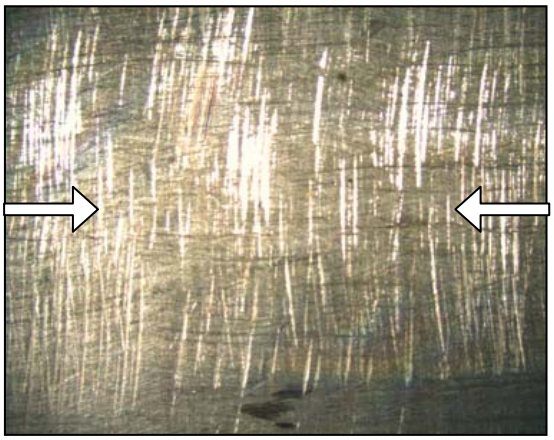

Figure B.5 - Sample 1
Spotlighting from Indicated Direction

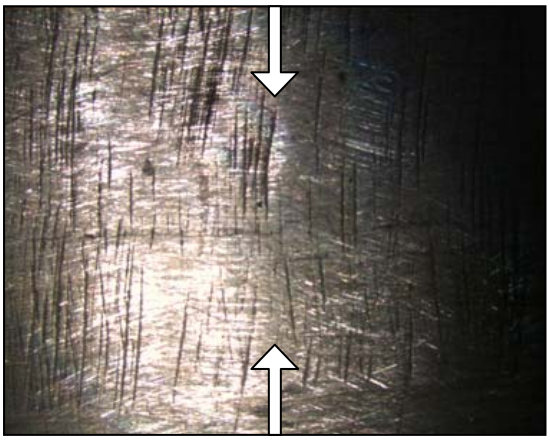

Figure B.6 - Sample 1
Spotlighting from Indicated Direction

Sample 1 – Polished – 10-µm Crack Opening Dimension

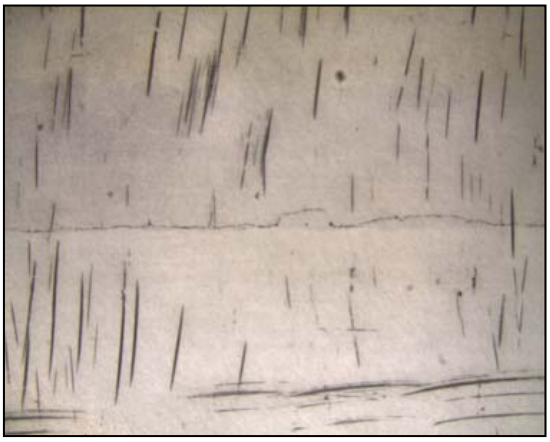

Figure B.7 - Sample 1
Diffuse On-Axis Lighting

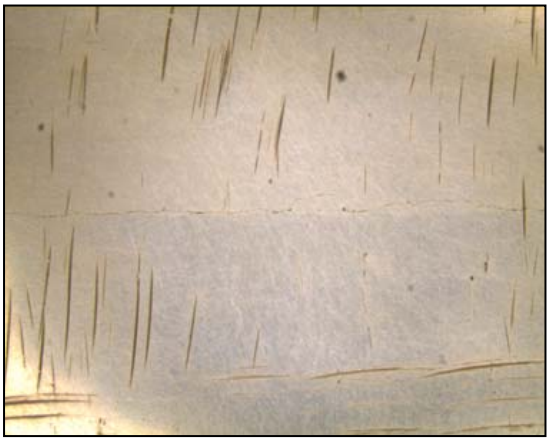

Figure B.8 - Sample 1
Diffuse Ring Lighting

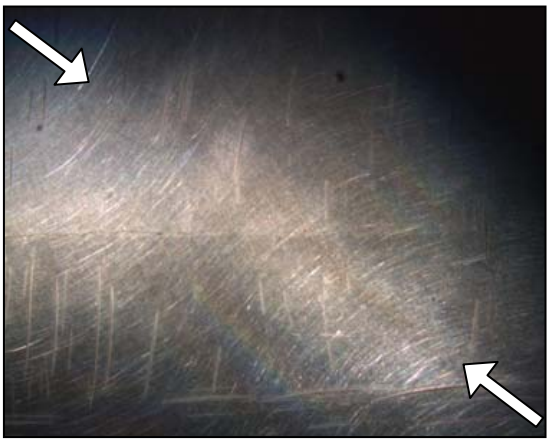

Figure B.9 - Sample 1
Spotlighting from Indicated Directions

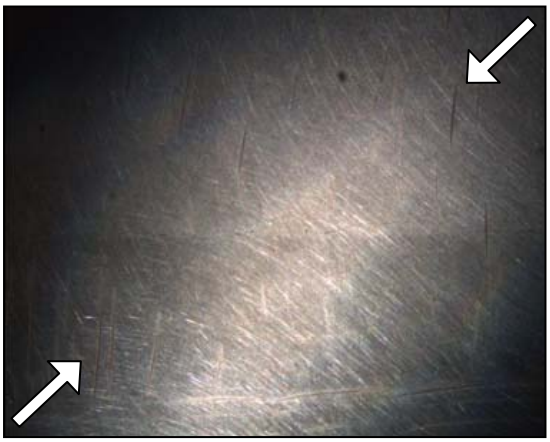

Figure B.10 - Sample 1
Spotlighting from Indicated Directions

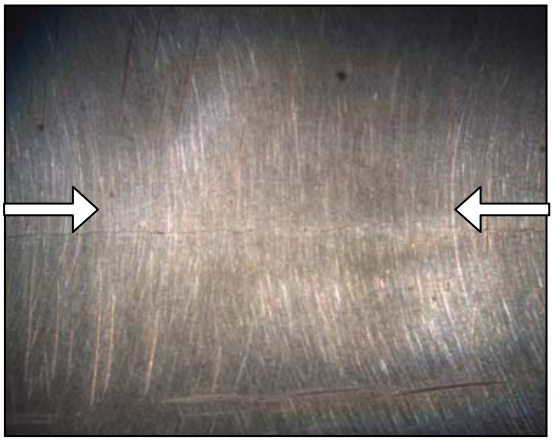

Figure B.11 - Sample 1
Spotlighting from Indicated Direction

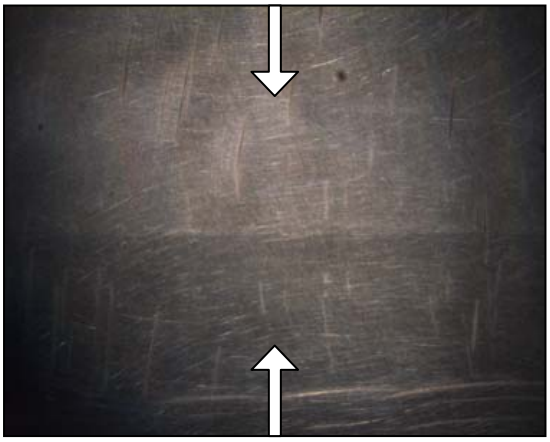

Figure B.12 - Sample 1
Spotlighting from Indicated Direction

Sample 1 – Horizontal Scratching – 10-μm Crack Opening Dimension

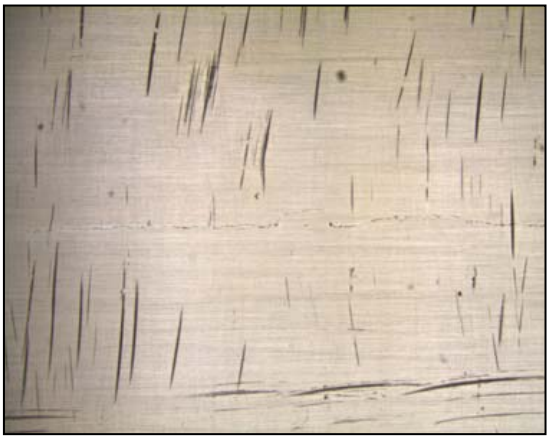

Figure B.13 - Sample 1
Diffuse On-Axis Lighting

Figure B.14 - Sample 1
Diffuse Ring Lighting

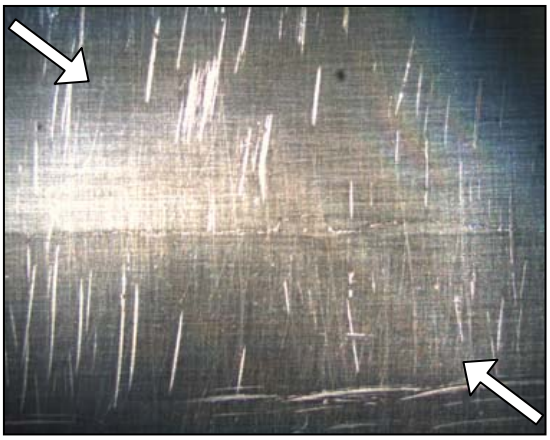

Figure B.15 - Sample 1
Spotlighting from Indicated Directions

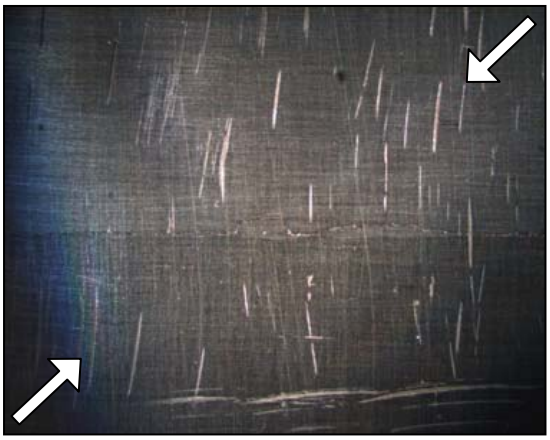

Figure B.16 - Sample 1
Spotlighting from Indicated Directions

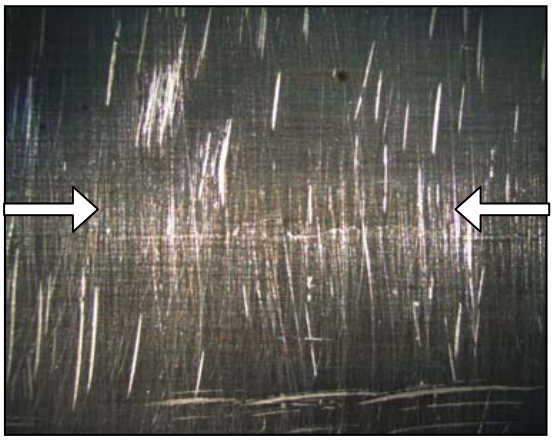

Figure B.17 - Sample 1
Spotlighting from Indicated Direction

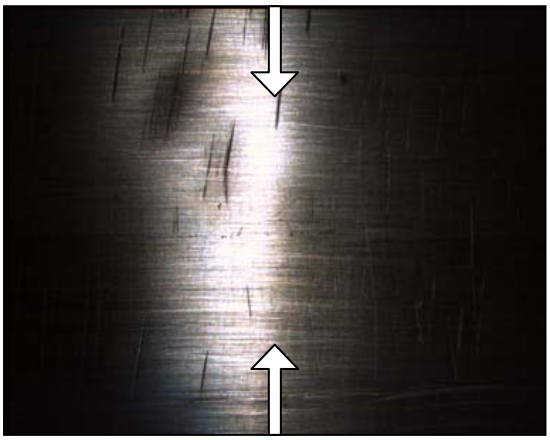

Figure B.18 - Sample 1
Spotlighting from Indicated Direction

Sample 1 – Vertical Scratching – 10-µm Crack Opening Dimension

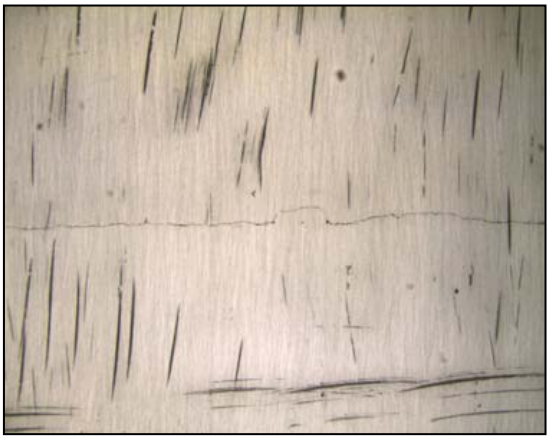

Figure B.19 - Sample 1
Diffuse On-Axis Lighting

Figure B.20 - Sample 1
Diffuse Ring Lighting

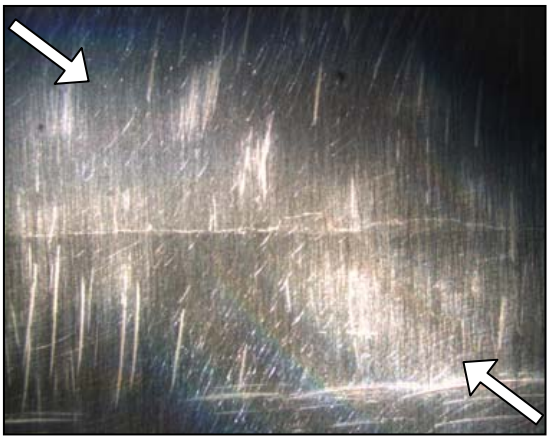

Figure B.21 - Sample 1
Spotlighting from Indicated Directions

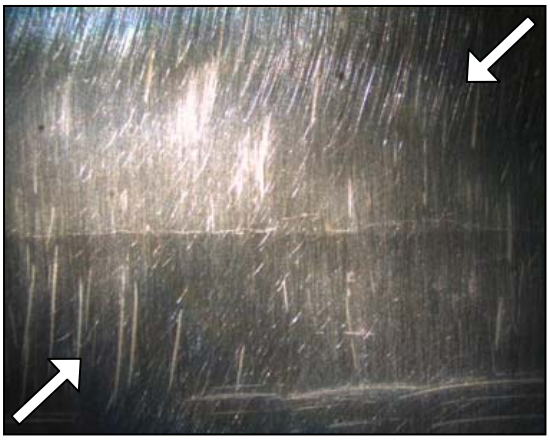

Figure B.22 - Sample 1
Spotlighting from Indicated Directions

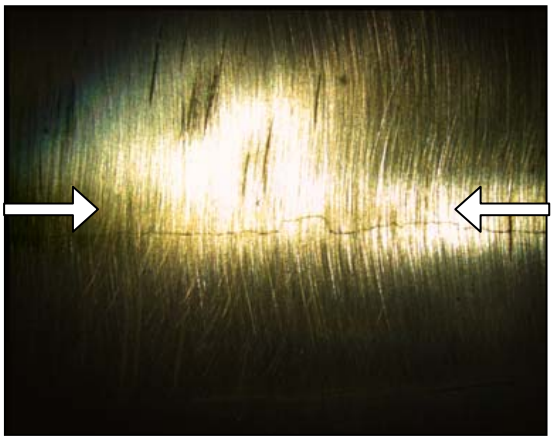

Figure B.23 - Sample 1
Spotlighting from Indicated Direction

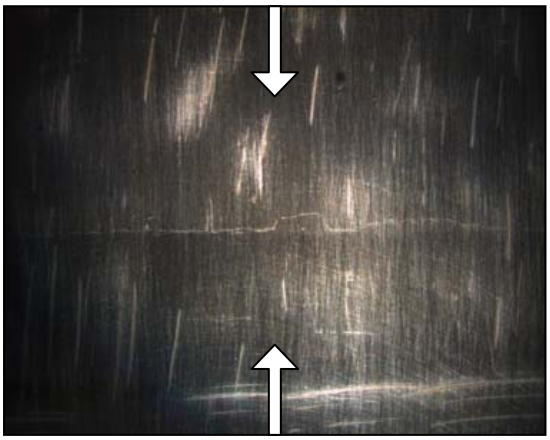

Figure B.24 - Sample 1
Spotlighting from Indicated Direction

Sample 2 – Unpolished – 10-µm Crack Opening Dimension

Figure B.25 - Sample 2
Diffuse On-Axis Lighting

Figure B.26 - Sample 2
Diffuse Ring Lighting

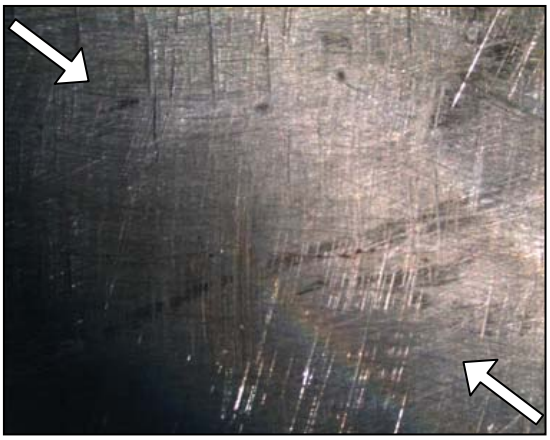

Figure B.27 - Sample 2
Spotlighting from Indicated Directions

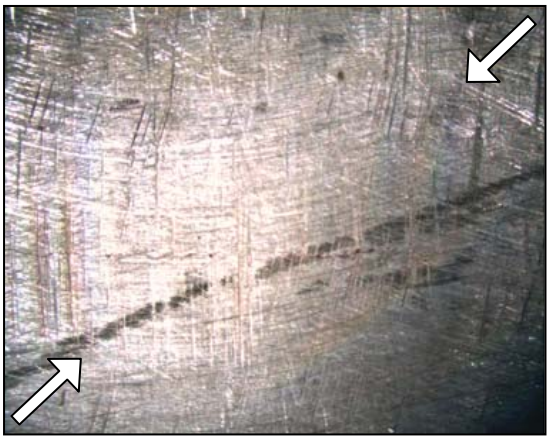

Figure B.28 - Sample 2
Spotlighting from Indicated Directions

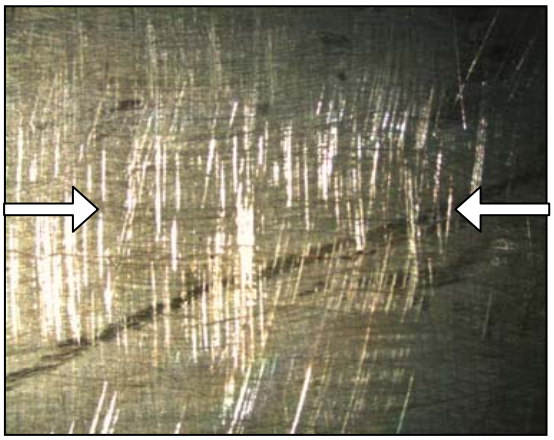

Figure B.29 - Sample 2
Spotlighting from Indicated Direction

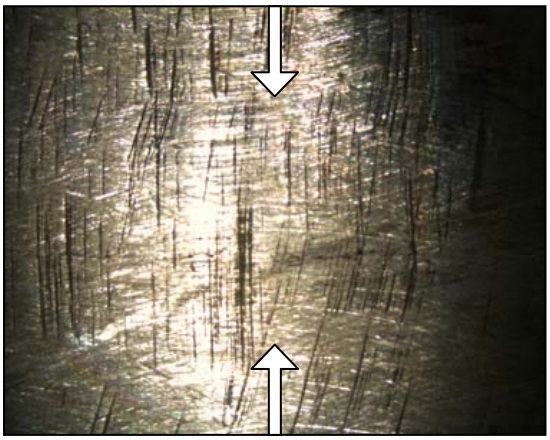

Figure B.30 - Sample 2
Spotlighting from Indicated Direction

Sample 2 – Polished – 10-µm Crack Opening Dimension

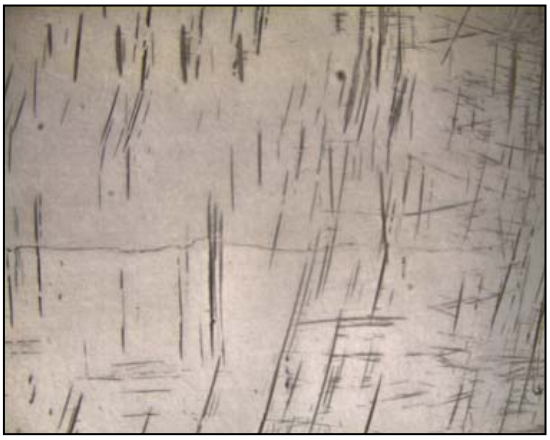

Figure B.31 - Sample 2
Diffuse On-Axis Lighting

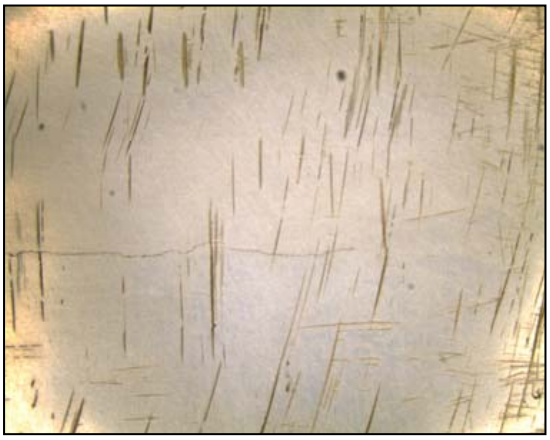

Figure B.32 - Sample 2
Diffuse Ring Lighting

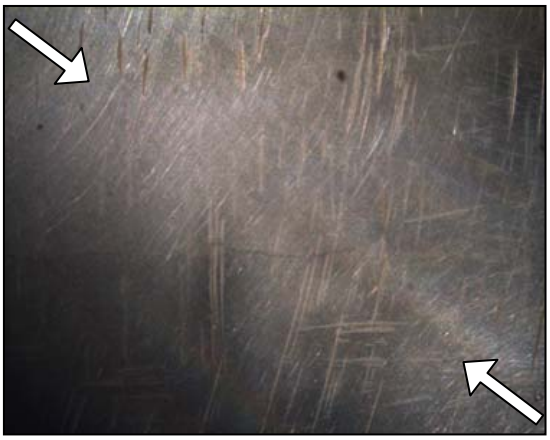

Figure B.33 - Sample 2
Spotlighting from Indicated Directions

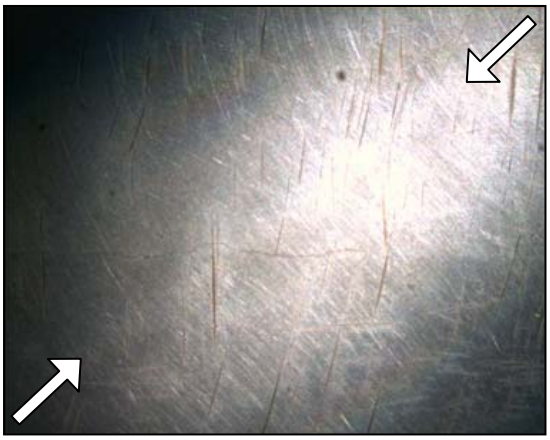

Figure B.34 - Sample 2
Spotlighting from Indicated Directions

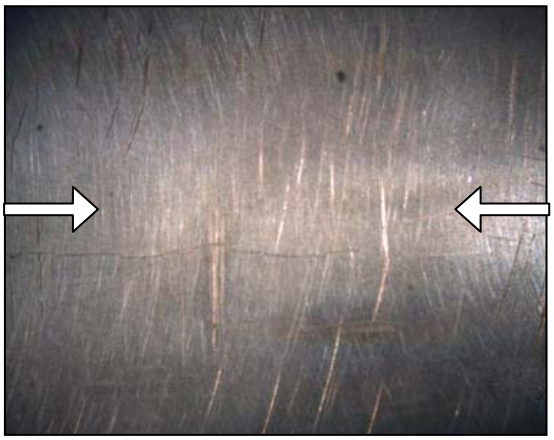

Figure B.35 - Sample 2
Spotlighting from Indicated Direction

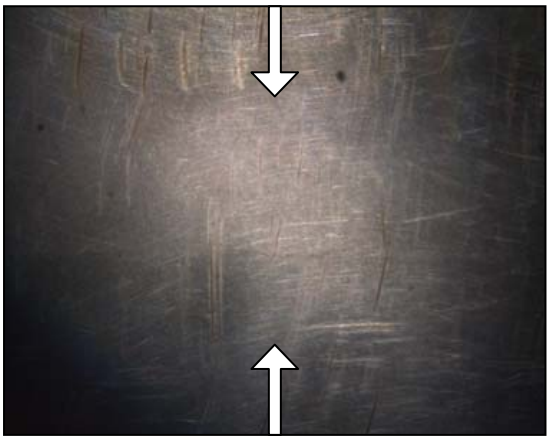

Figure B.36 - Sample 2
Spotlighting from Indicated Direction

Sample 2 – Horizontal Scratching – 10-μm Crack Opening Dimension

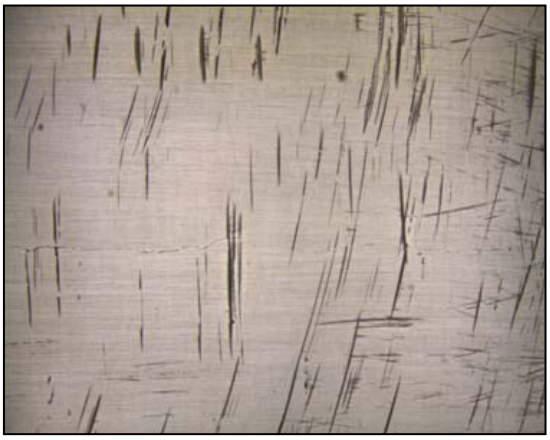

Figure B.37 - Sample 2
Diffuse On-Axis Lighting

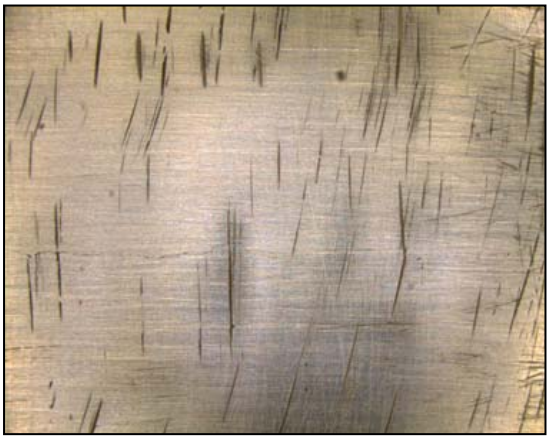

Figure B.38 - Sample 2
Diffuse Ring Lighting

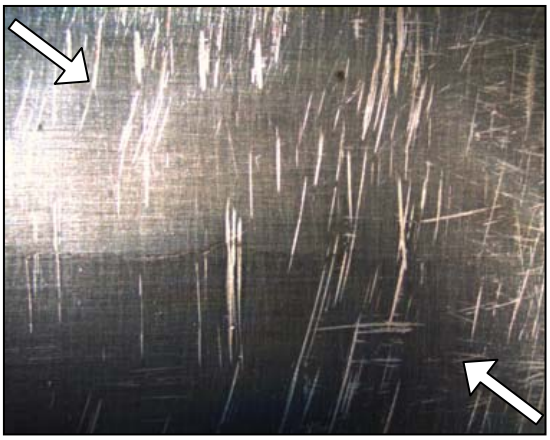

Figure B.39 - Sample 2
Spotlighting from Indicated Directions

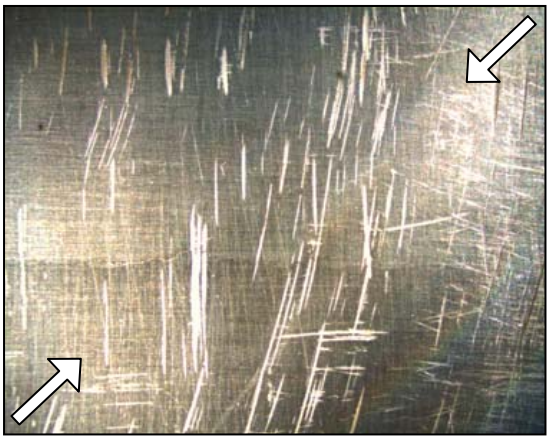

Figure B.40 - Sample 2
Spotlighting from Indicated Directions

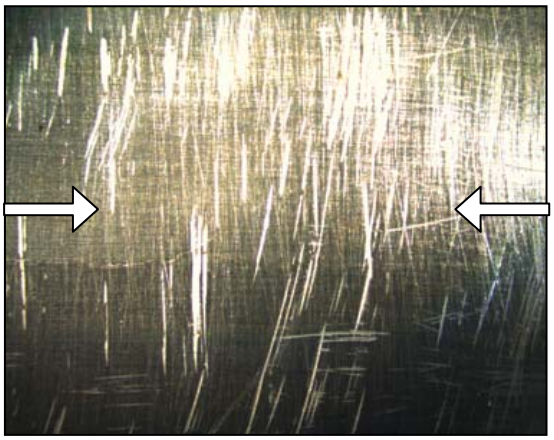

Figure B.41 - Sample 2
Spotlighting from Indicated Direction

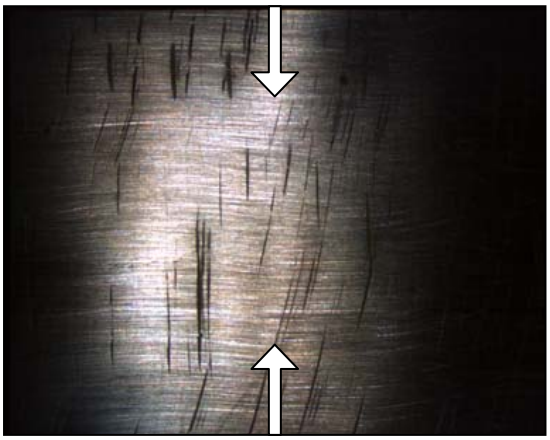

Figure B.42 - Sample 2
Spotlighting from Indicated Direction

Sample 2 – Vertical Scratching – 10-µm Crack Opening Dimension

Figure B.43 - Sample 2
Diffuse On-Axis Lighting

Figure B.44 - Sample 2
Diffuse Ring Lighting

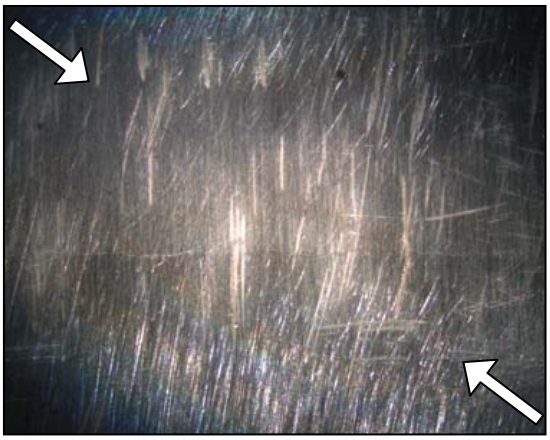

Figure B.45 - Sample 2
Spotlighting from Indicated Directions

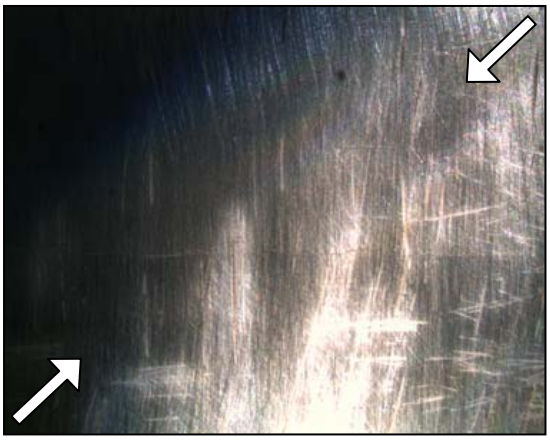

Figure B.46 - Sample 2
Spotlighting from Indicated Directions

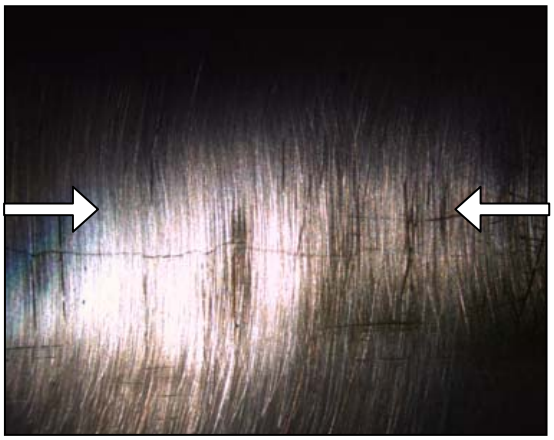

Figure B.47 - Sample 2
Spotlighting from Indicated Direction

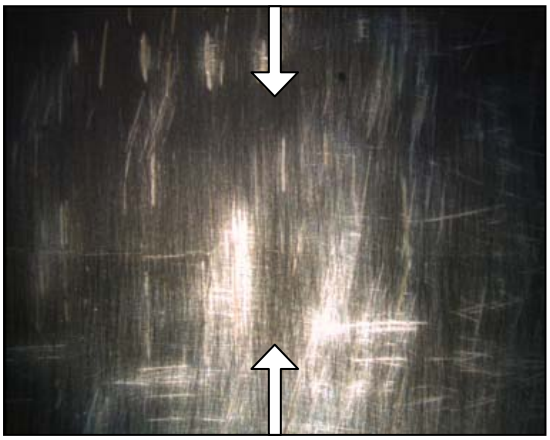

Figure B.48 - Sample 2
Spotlighting from Indicated Direction

Sample 3 – Polished – 35-µm Crack Opening Dimension

Figure B.49 - Sample 3
Diffuse On-Axis Lighting

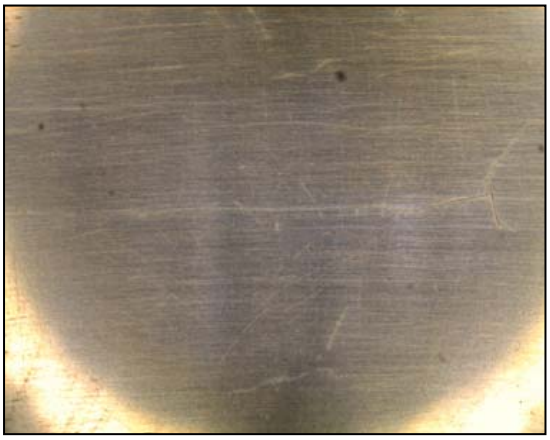

Figure B.50 - Sample 3
Diffuse Ring Lighting

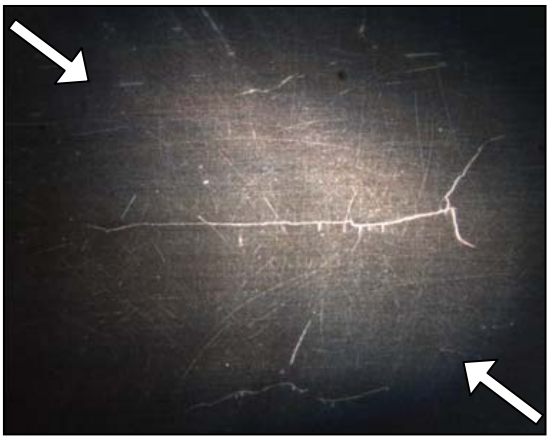

Figure B.51 - Sample 3
Spotlighting from Indicated Directions

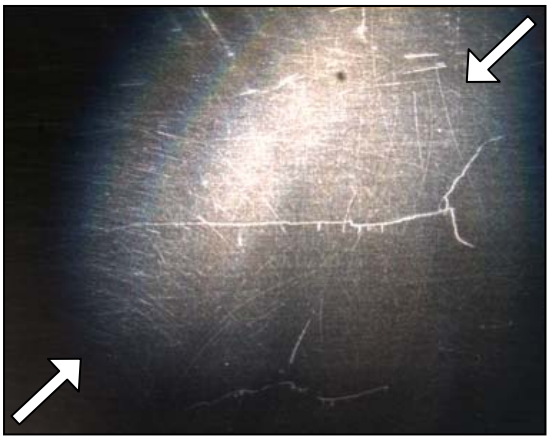

Figure B.52 - Sample 3
Spotlighting from indicated Directions

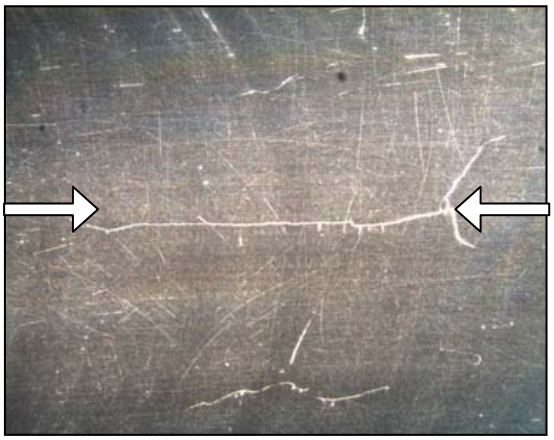

Figure B.53 - Sample 3
Spotlighting from Indicated Direction

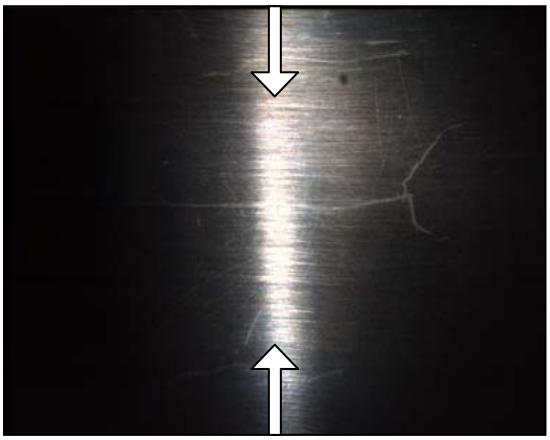

Figure B.54 - Sample 3
Spotlighting from Indicated Direction

Sample 3 – Horizontal Scratching – 35-µm Crack Opening Dimension

Figure B.55 - Sample 3
Diffuse On-Axis Lighting

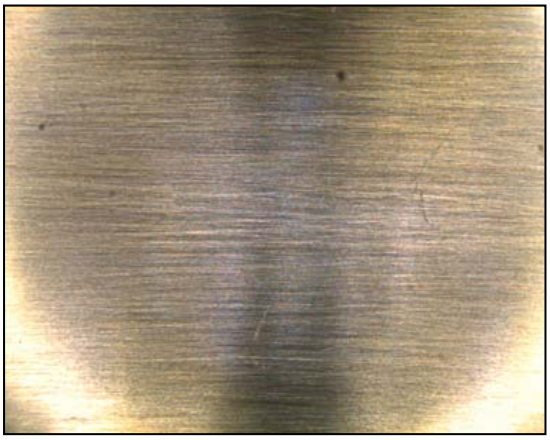

Figure B.56 - Sample 3
Diffuse Ring Lighting

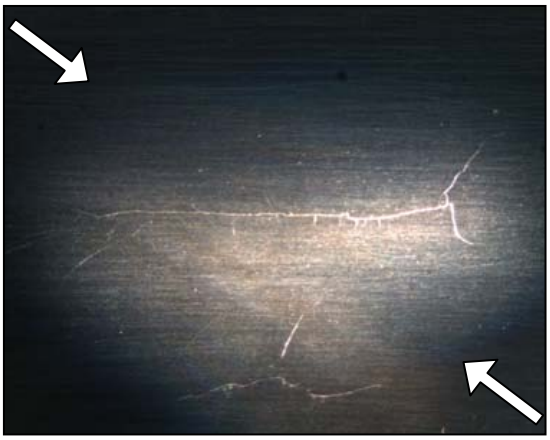

Figure B.57 - Sample 3
Spotlighting from Indicated Directions

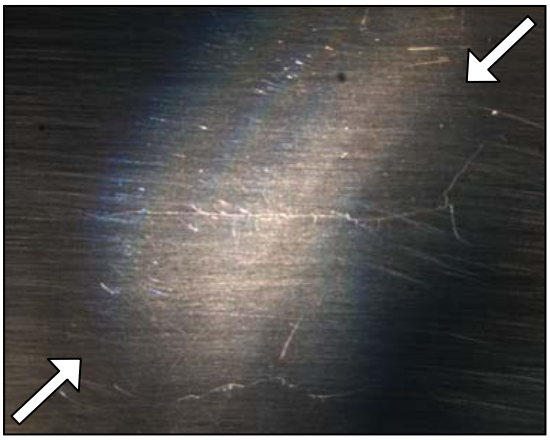

Figure B.58 - Sample 3
Spotlighting from Indicated Directions

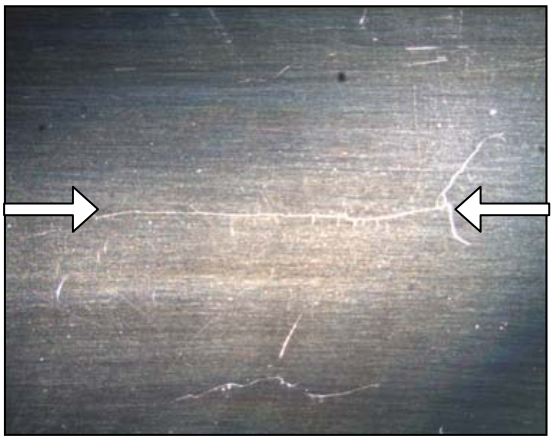

Figure B.59 - Sample 3
Spotlighting from Indicated Direction

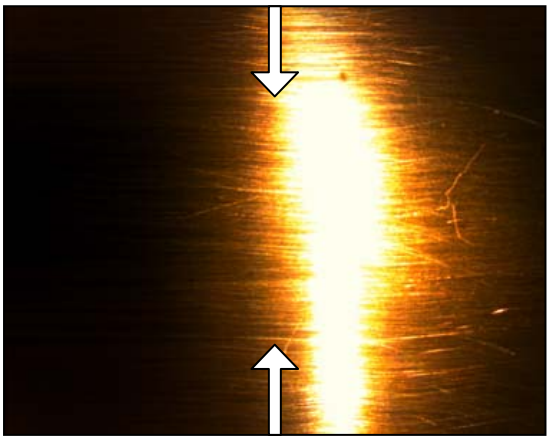

Figure B.60 - Sample 3
Spotlighting from Indicated Direction

Sample 3 – Vertical Scratching – 35-µm Crack Opening Dimension

Figure B.61 - Sample 3
Diffuse On-Axis Lighting

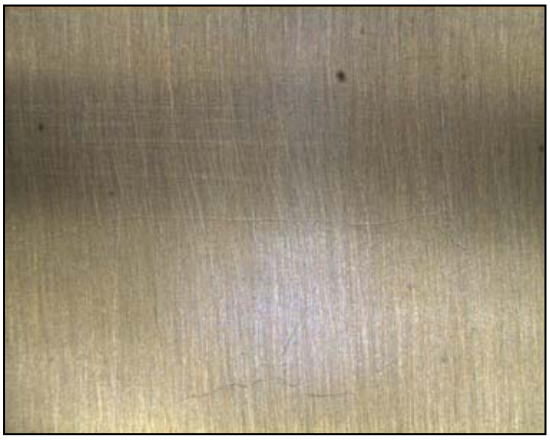

Figure B.62 - Sample 3
Diffuse Ring Lighting

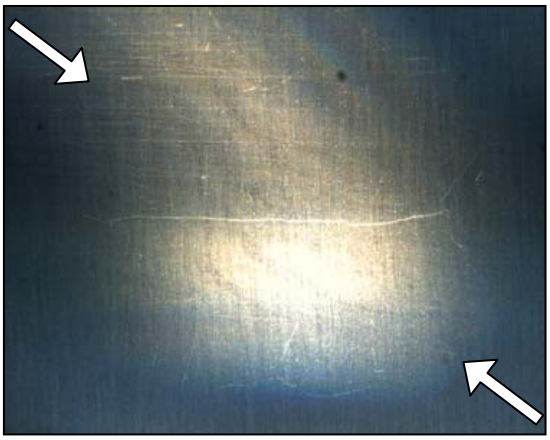

Figure B.63 - Sample 3
Spotlighting from Indicated Directions

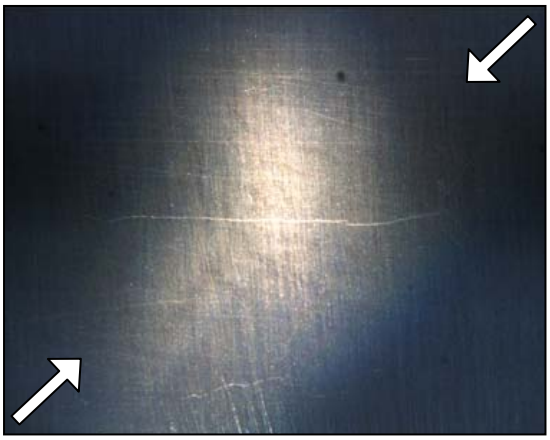

Figure B.64 - Sample 3
Spotlighting from Indicated Directions

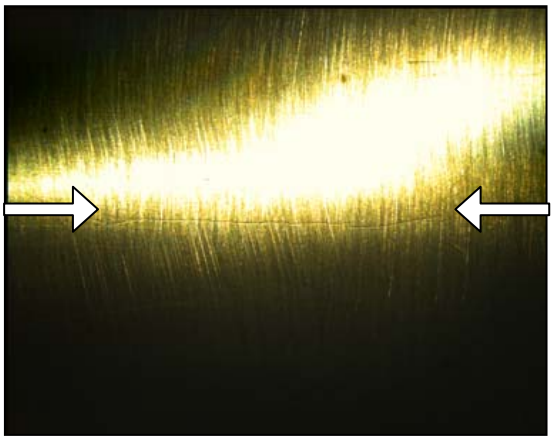

Figure B.65 - Sample 3
Spotlighting from Indicated Direction

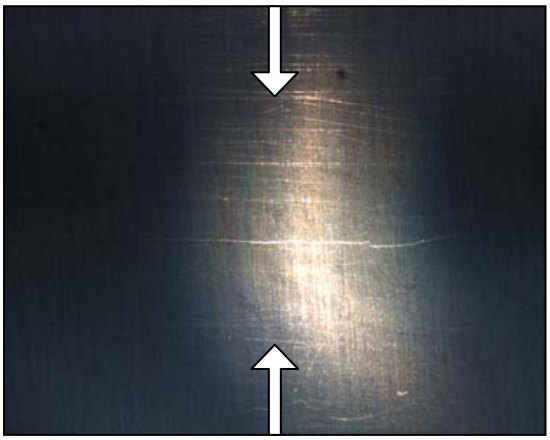

Figure B.66 - Sample 3
Spotlighting from Indicated Direction

Sample 4 – Polished – 40-µm Crack Opening Dimension

Figure B.67 - Sample 4
Diffuse On-Axis Lighting

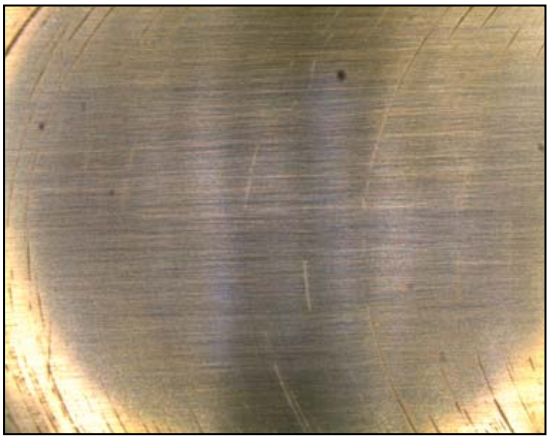

Figure B.68 - Sample 4
Diffuse Ring Lighting

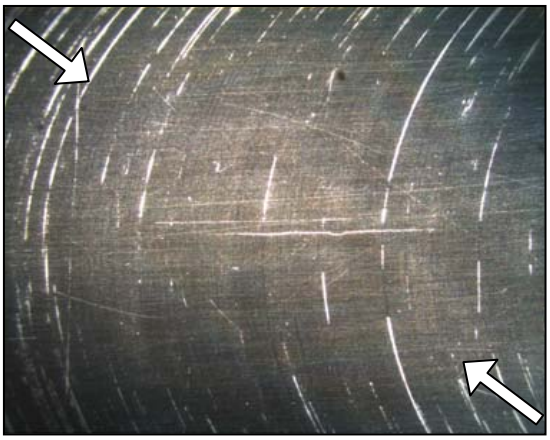

Figure B.69 - Sample 4
Spotlighting from Indicated Directions

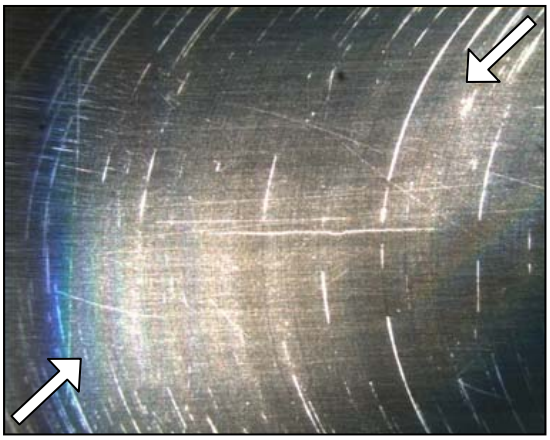

Figure B.70 - Sample 4
Spotlighting from Indicated Directions

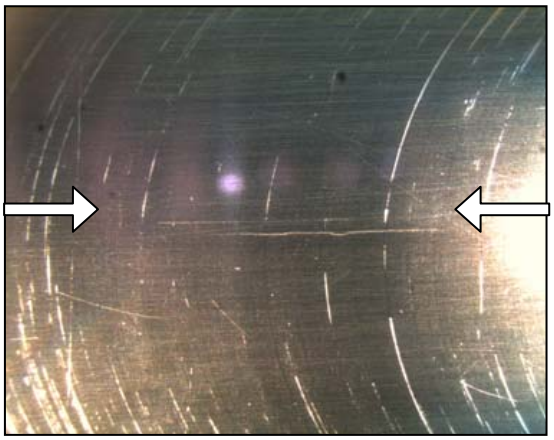

Figure B.71 - Sample 4
Spotlighting from Indicated Direction

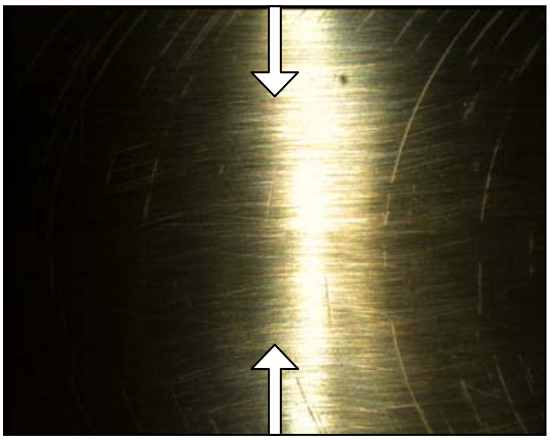

Figure B.72 - Sample 4
Spotlighting from Indicated Direction

Sample 4 – Horizontal Scratching – 40-μm Crack Opening Dimension

Figure B.73 - Sample 4
Diffuse On-Axis Lighting

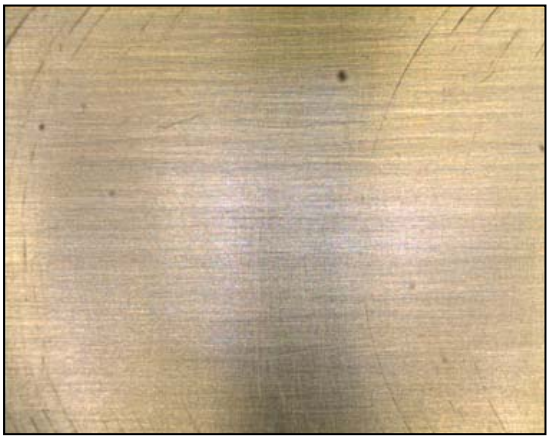

Figure B.74 - Sample 4
Diffuse Ring Lighting

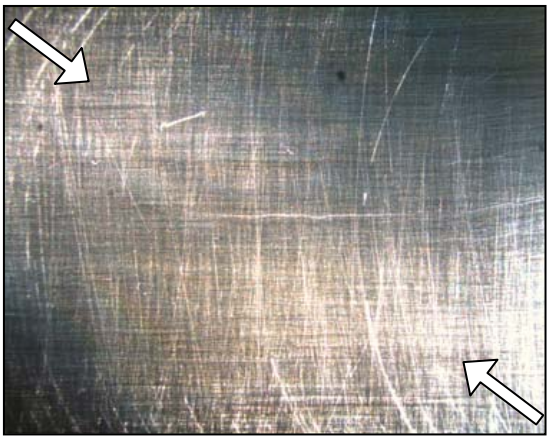

Figure B.75 - Sample 4
Spotlighting from Indicated Directions

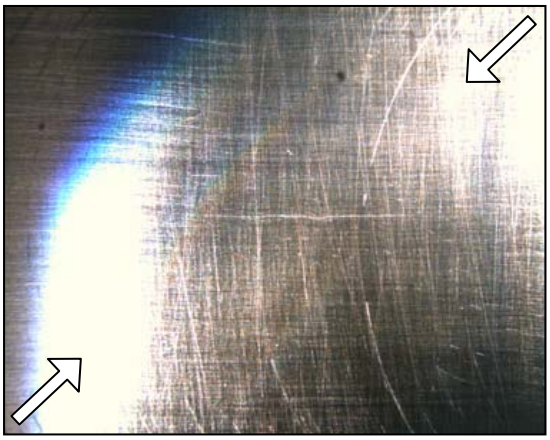

Figure B.76 - Sample 4
Spotlighting from Indicated Directions

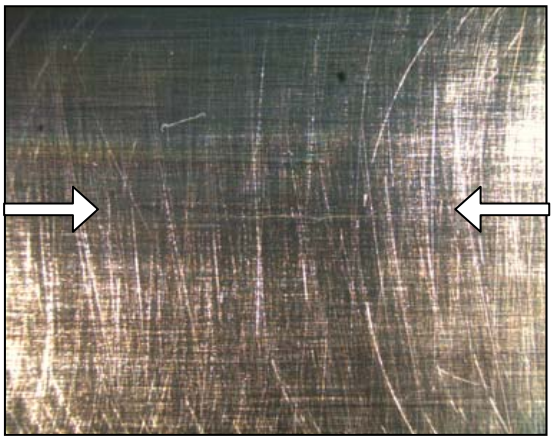

Figure B.77 - Sample 4
Spotlighting from Indicated Direction

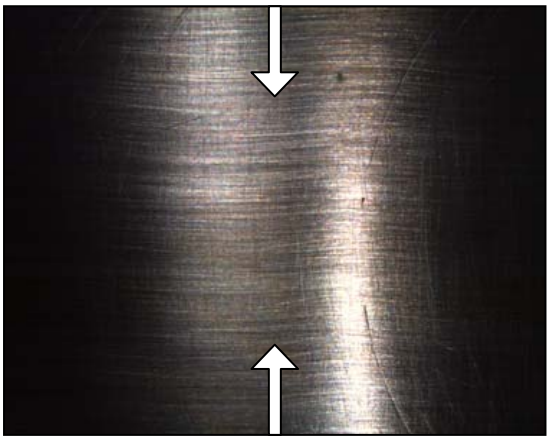

Figure B.78 - Sample 4
Spotlighting from Indicated Direction

Sample 4 – Vertical Scratching – 40-µm Crack Opening Dimension

Figure B.79 - Sample 4
Diffuse On-Axis Lighting

Figure B.80 - Sample 4
Diffuse Ring Lighting

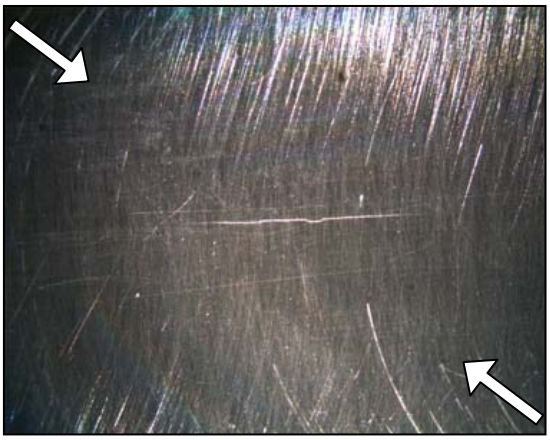

Figure B.81 - Sample 4
Spotlighting from Indicated Directions

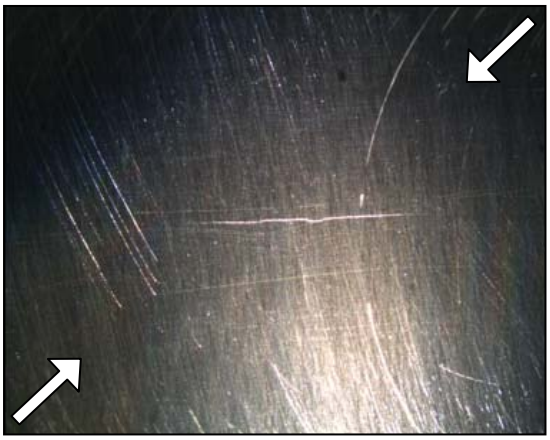

Figure B.82 - Sample 4
Spotlighting from Indicated Directions

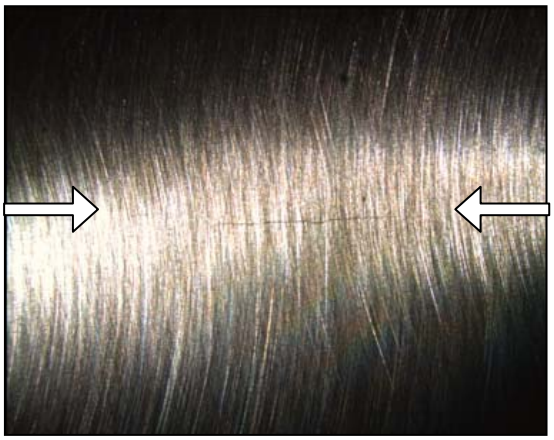

Figure B.83 - Sample 4
Spotlighting from Indicated Direction

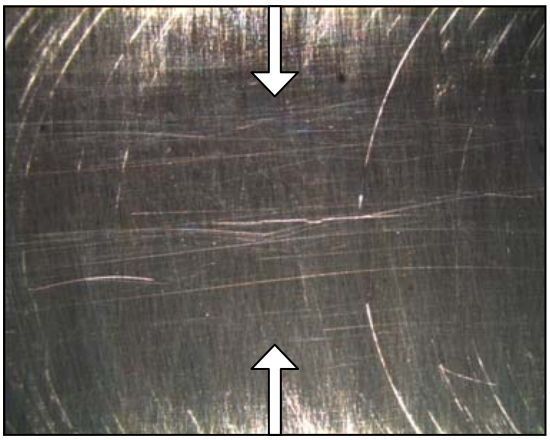

Figure B.84 - Sample 4
Spotlighting from Indicated Direction

Sample 5 – Horizontal Scratching – 40-μm Crack Opening Dimension

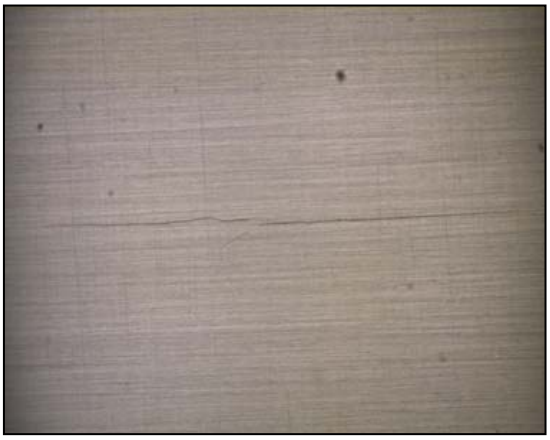

Figure B.85 - Sample 5
Diffuse On-Axis Lighting

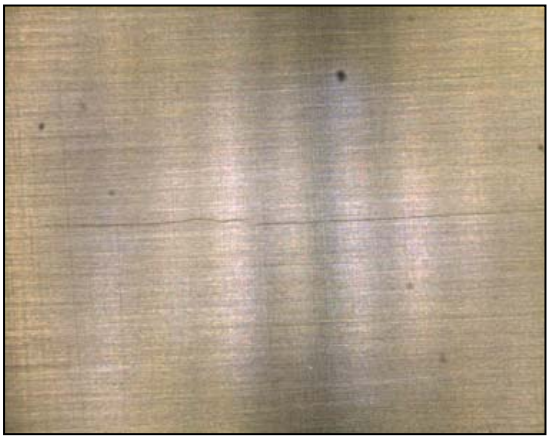

Figure B.86 - Sample 5
Diffuse Ring Lighting

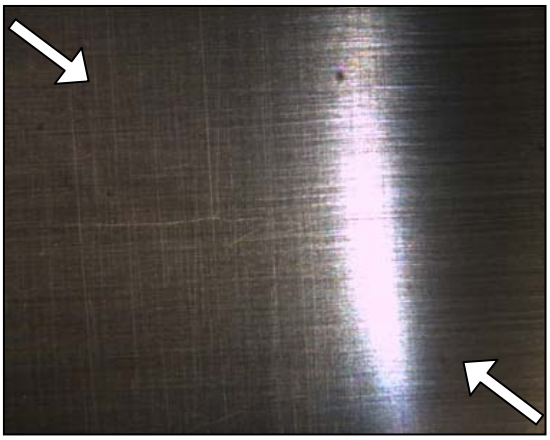

Figure B.87 - Sample 5
Spotlighting from Indicated Directions

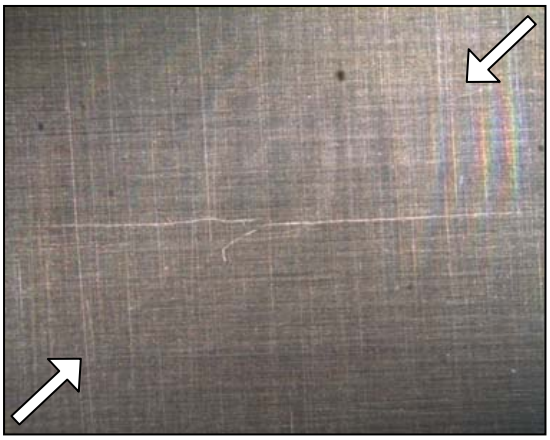

Figure B.88 - Sample 5
Spotlighting from Indicated Directions

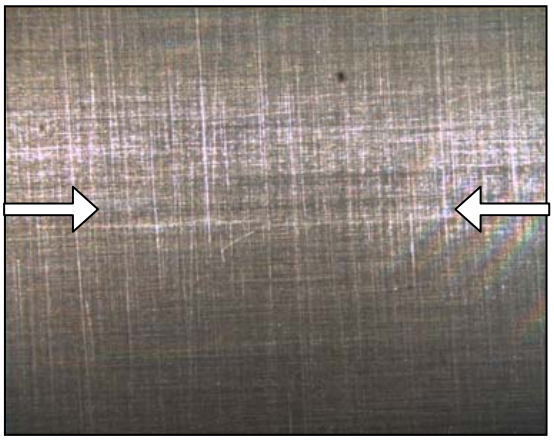

Figure B.89 - Sample 5
Spotlighting from Indicated Direction

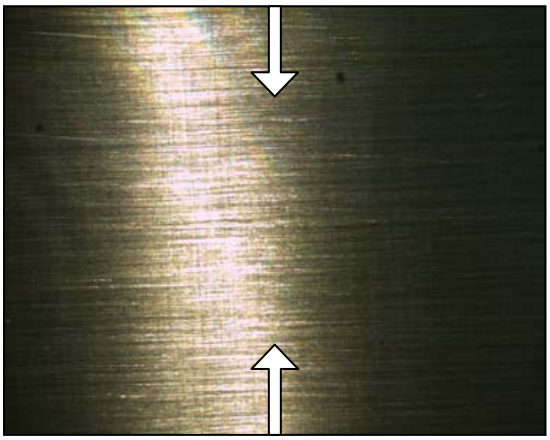

Figure B.90 - Sample 5
Spotlighting from Indicated Direction

Sample 5 – Vertical Scratching – 40-µm Crack Opening Dimension

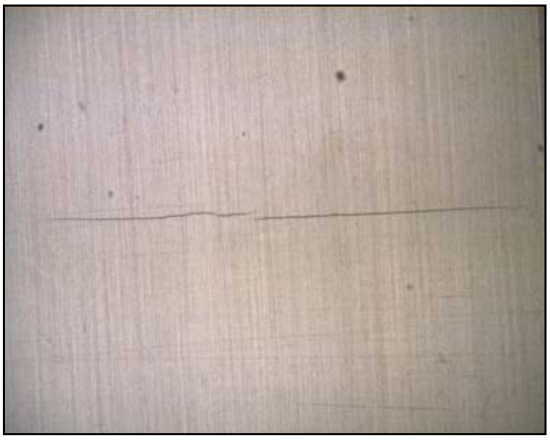

Figure B.91 - Sample 5
Diffuse On-Axis Lighting

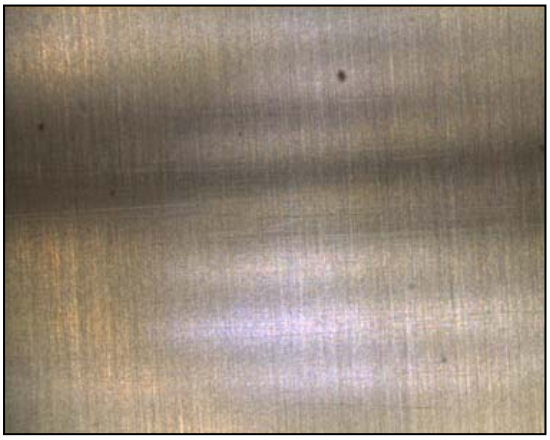

Figure B.92 - Sample 5
Diffuse Ring Lighting

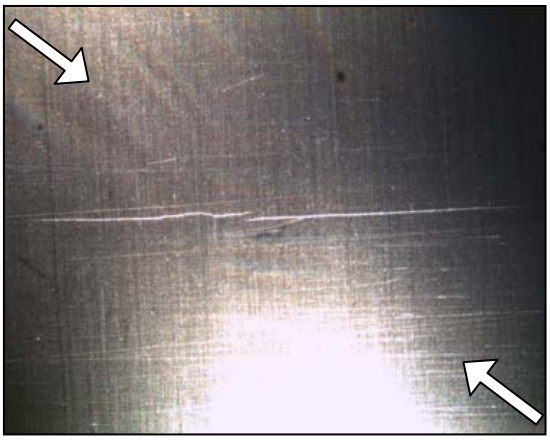

Figure B.93 - Sample 5
Spotlighting from Indicated Directions

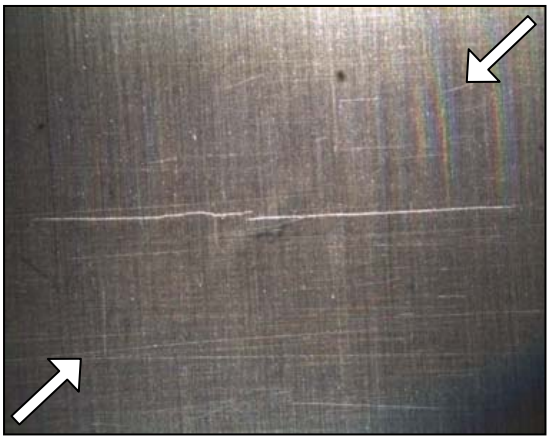

Figure B.94 - Sample 5
Spotlighting from Indicated Directions

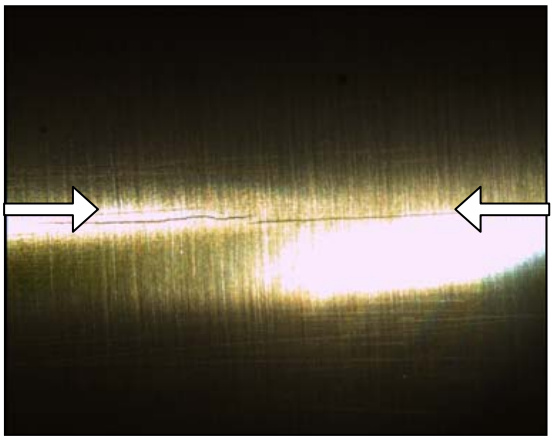

Figure B.95 - Sample 5
Spotlighting from Indicated Direction

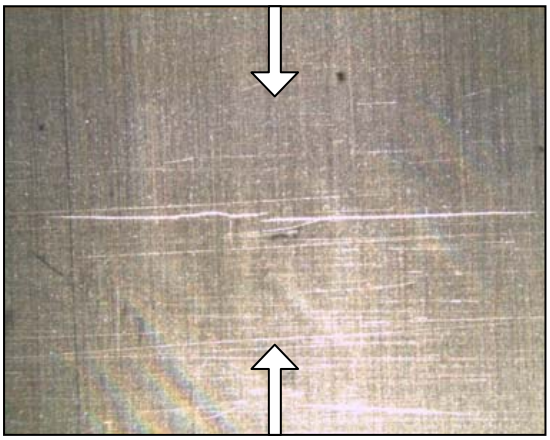

Figure B.96 - Sample 5
Spotlighting from Indicated Direction

Sample 6 – Unpolished – 50-µm Crack Opening Dimension

Figure B.97 - Sample 6
Diffuse On-Axis Lighting

Figure B.98 - Sample 6
Diffuse Ring Lighting

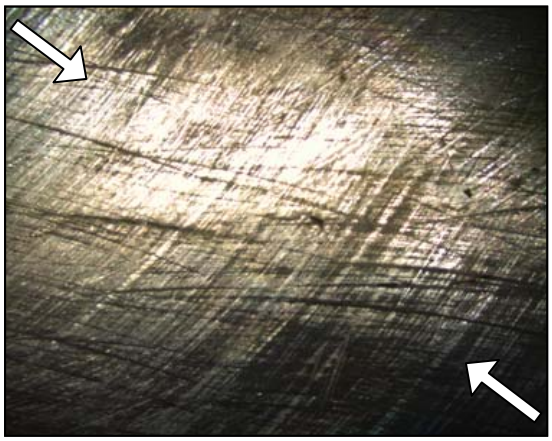

Figure B.99 - Sample 6
Spotlighting from Indicated Directions

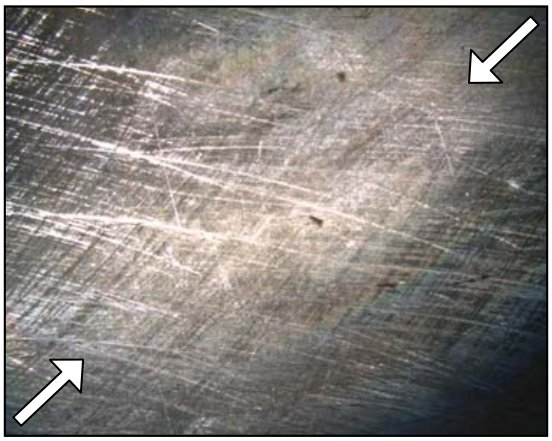

Figure B.100 - Sample 6
Spotlighting from Indicated Directions

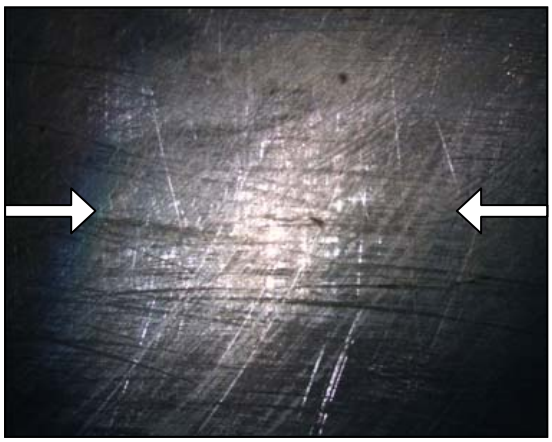

Figure B.101 - Sample 6
Spotlighting from Indicated Direction

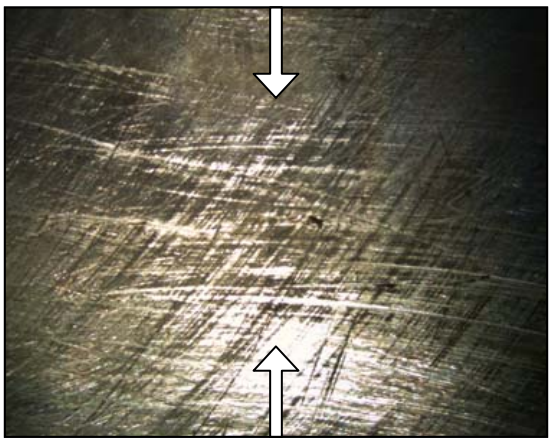

Figure B.102 - Sample 6
Spotlighting from Indicated Direction

Sample 6 – Polished – 50-µm Crack Opening Dimension

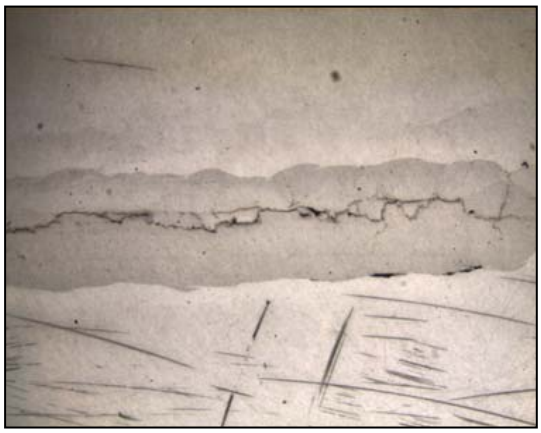

Figure B.103 - Sample 6
Diffuse On-Axis Lighting

Figure B.104 - Sample 6
Diffuse Ring Lighting

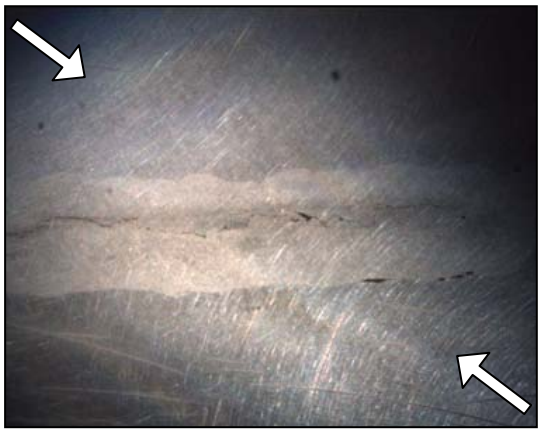

Figure B.105 - Sample 6
Spotlighting from Indicated Directions

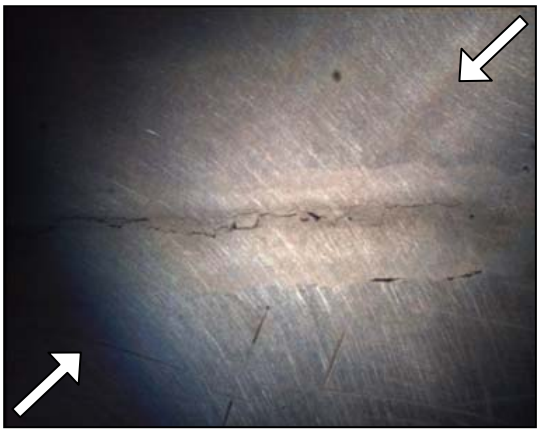

Figure B.106 - Sample 6
Spotlighting from Indicated Directions

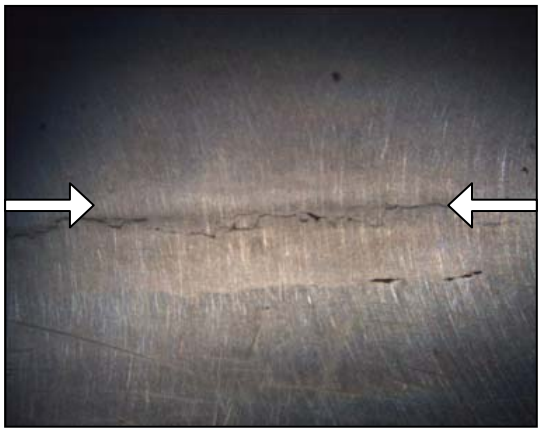

Figure B.107 - Sample 6
Spotlighting from Indicated Direction

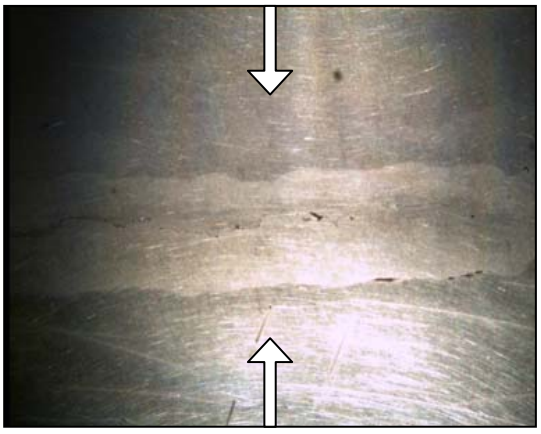

Figure B.108 - Sample 6
Spotlighting from Indicated Direction

Sample 6 – Horizontal Scratching – 50-µm Crack Opening Dimension

Figure B.109 - Sample 6
Diffuse On-Axis Lighting

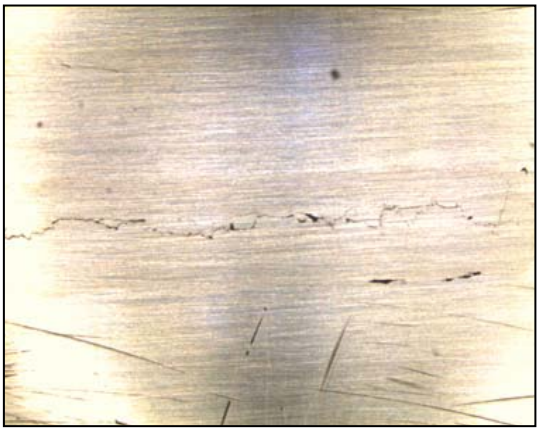

Figure B.110 - Sample 6
Diffuse Ring Lighting

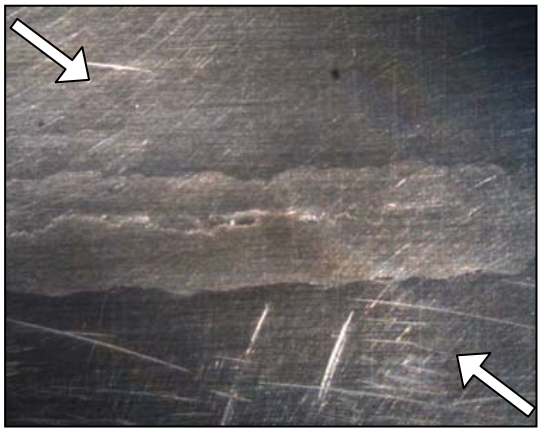

Figure B.111 - Sample 6
Spotlighting from Indicated Directions

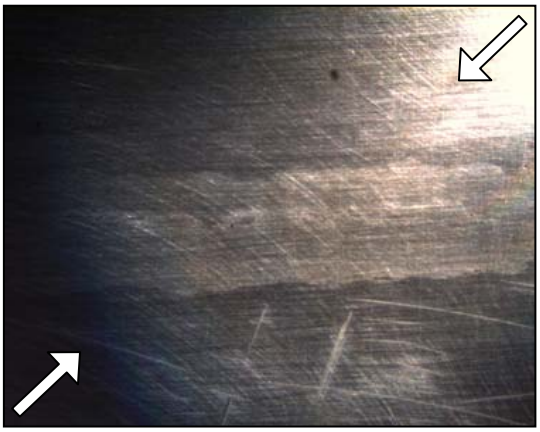

Figure B.112 - Sample 6
Spotlighting from Indicated Directions

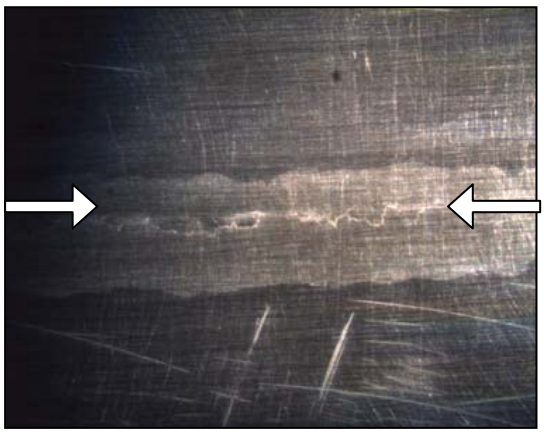

Figure B.113 - Sample 6
Spotlighting from Indicated Direction

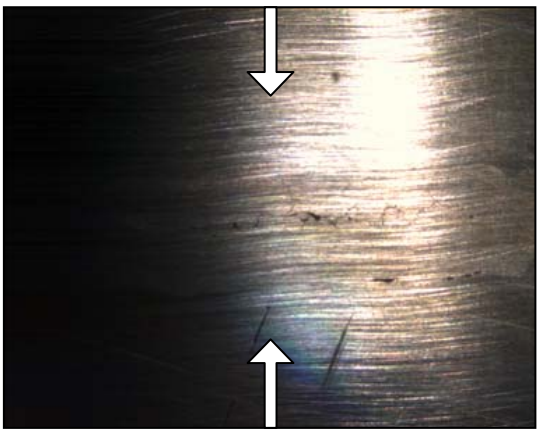

Figure B.114 - Sample 6
Spotlighting from Indicated Direction

Sample 6 – Vertical Scratching – 50-µm Crack Opening Dimension

Figure B.115 - Sample 6
Diffuse On-Axis Lighting

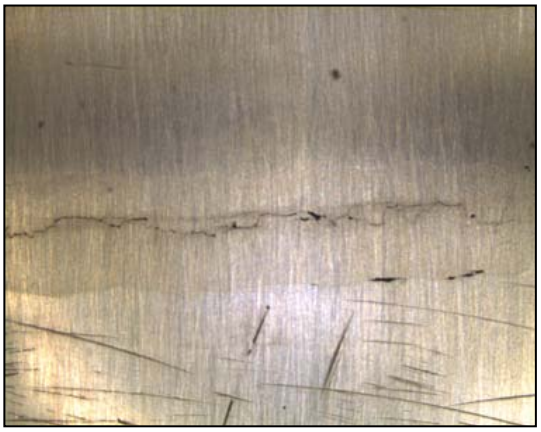

Figure B.116 - Sample 6
Diffuse Ring Lighting

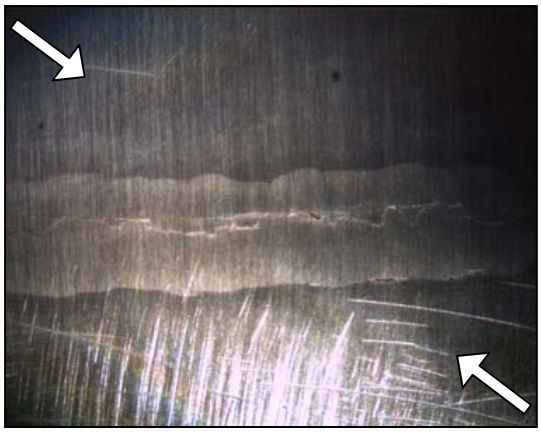

Figure B.117 - Sample 6
Spotlighting from Indicated Directions

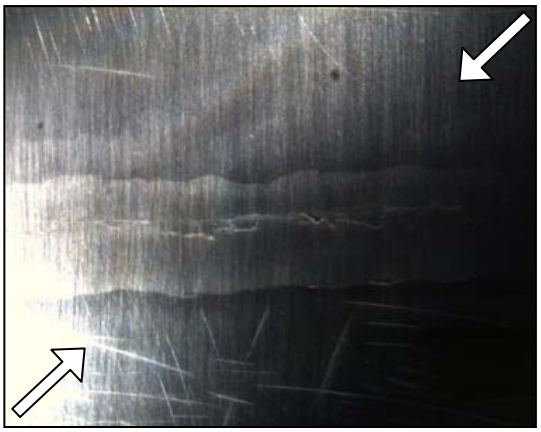

Figure B.118 - Sample 6
Spotlighting from Indicated Directions

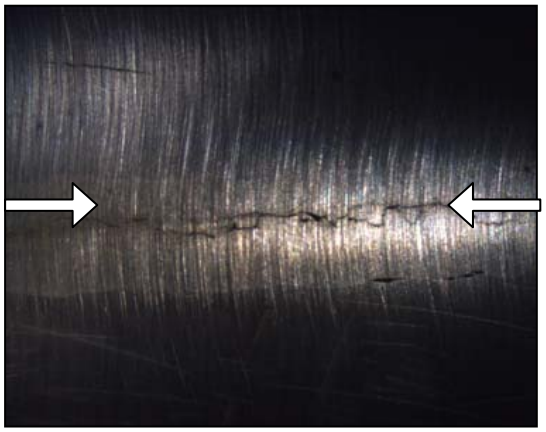

Figure B.119 - Sample 6
Spotlighting from Indicated Direction

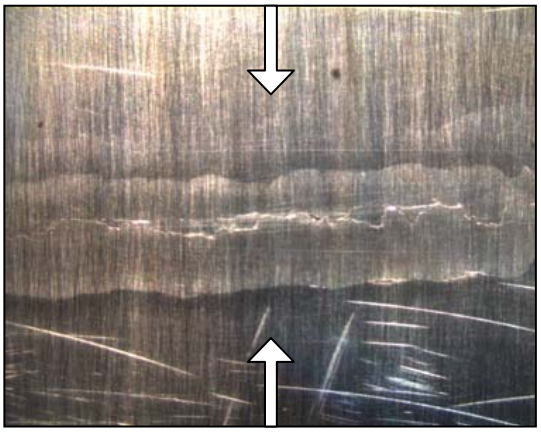

Figure B.120 - Sample 6
Spotlighting from Indicated Direction

Sample 7 – Unpolished – 10- to 75-µm Crack Opening Dimension

Figure B.121 - Sample 7
Diffuse On-Axis Lighting

Figure B.122 - Sample 7
Diffuse Ring Lighting

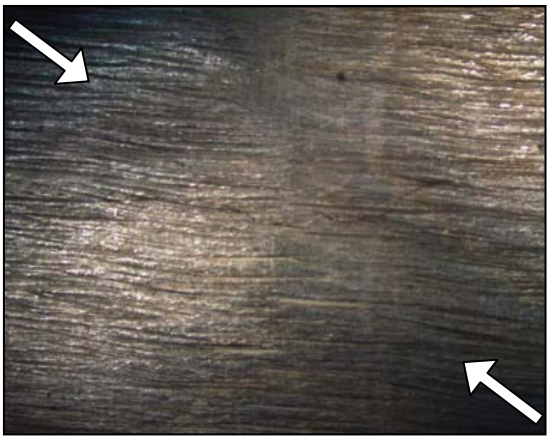

Figure B.123- Sample 7
Spotlighting from Indicated Directions

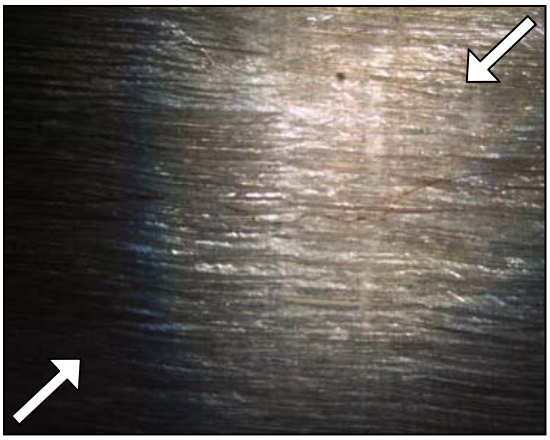

Figure B.124 - Sample 7
Spotlighting from Indicated Directions

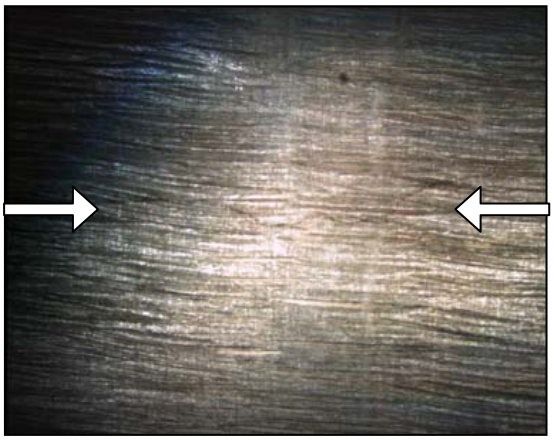

Figure B.125 - Sample 7
Spotlighting from Indicated Direction

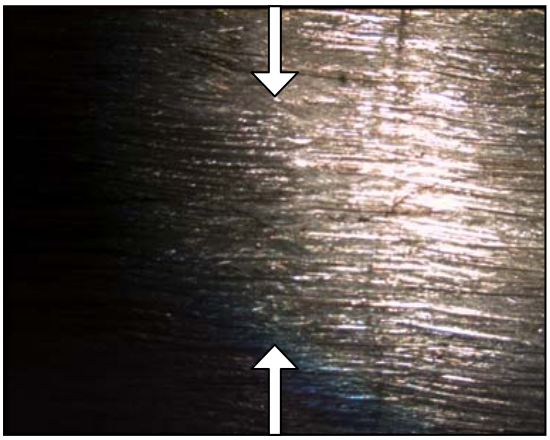

Figure B.126 - Sample 7
Spotlighting from Indicated Direction

Sample 7 – Polished – 10- to 75-µm Crack Opening Dimension

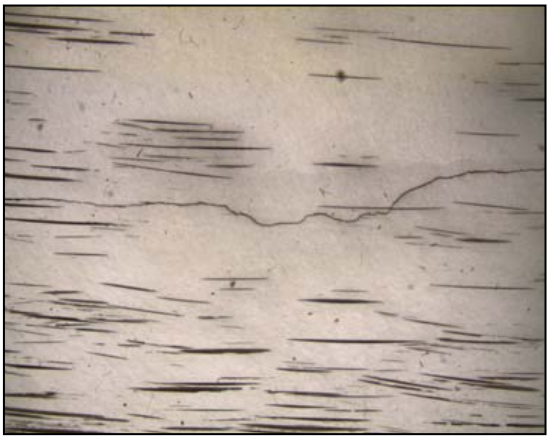

Figure B.127 - Sample 7
Diffuse On-Axis Lighting

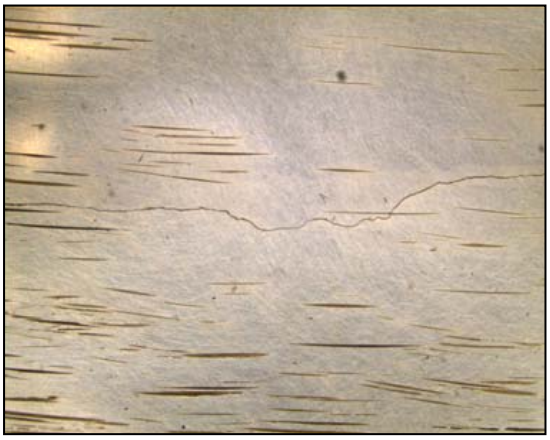

Figure B.128 - Sample 7
Diffuse Ring Lighting

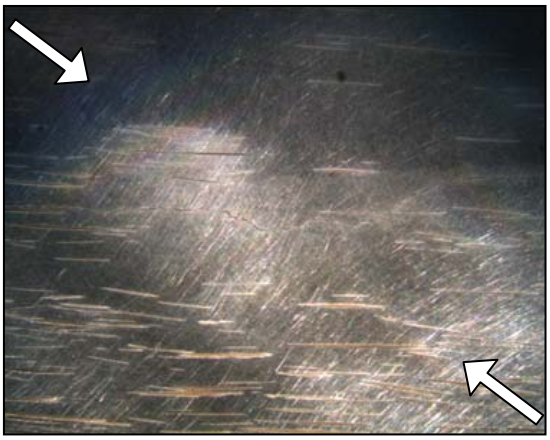

Figure B.129 - Sample 7
Spotlighting from Indicated Directions

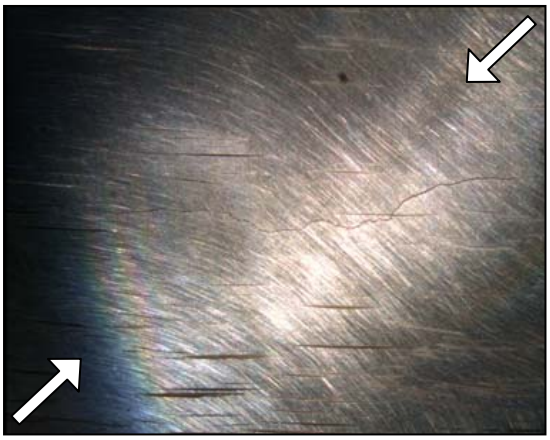

Figure B.130 - Sample 7
Spotlighting from Indicated Directions

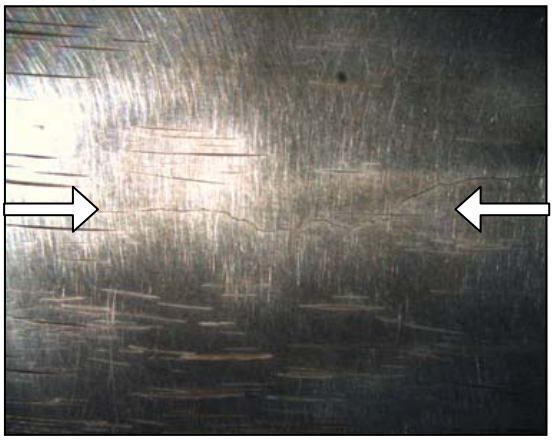

Figure B.131 - Sample 7
Spotlighting from Indicated Direction

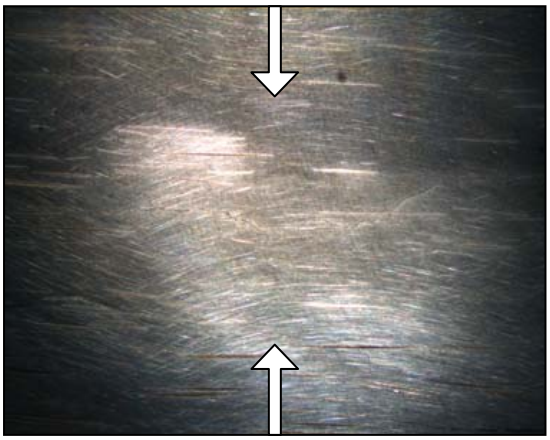

Figure B.132 - Sample 7
Spotlighting from Indicated Direction

Sample 7 – Horizontal Scratching – 10- to 75-µm Crack Opening Dimension

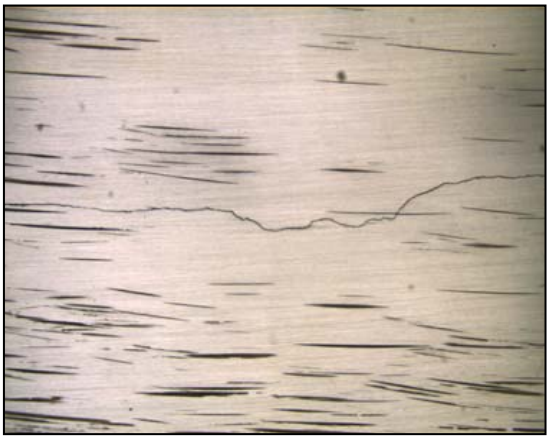

Figure B.133 - Sample 7
Diffuse On-Axis Lighting

Figure B.134 - Sample 7
Diffuse Ring Lighting

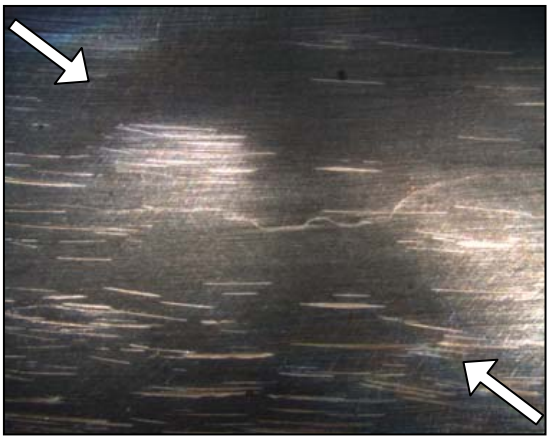

Figure B.135 - Sample 7
Spotlighting from Indicated Directions

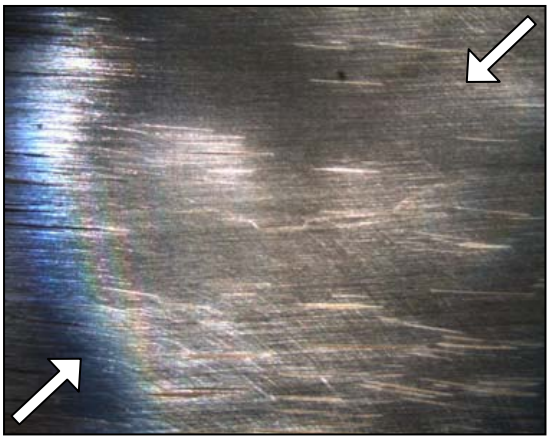

Figure B.136 - Sample 7
Spotlighting from Indicated Directions

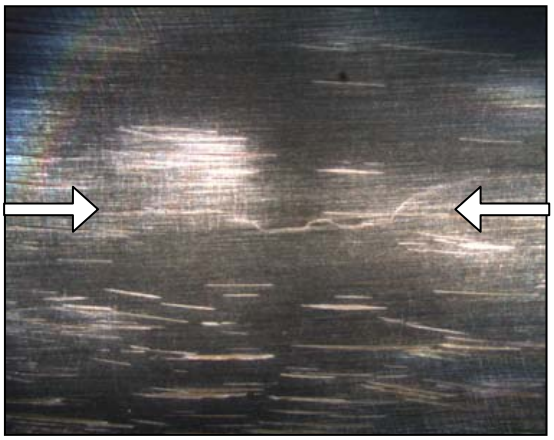

Figure B.137 - Sample 7
Spotlighting from Indicated Direction

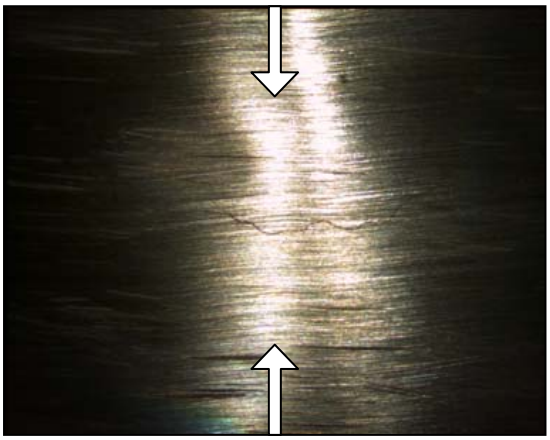

Figure B.138 - Sample 7
Spotlighting from Indicated Direction

Sample 7 – Vertical Scratching – 10- to 75-µm Crack Opening Dimension

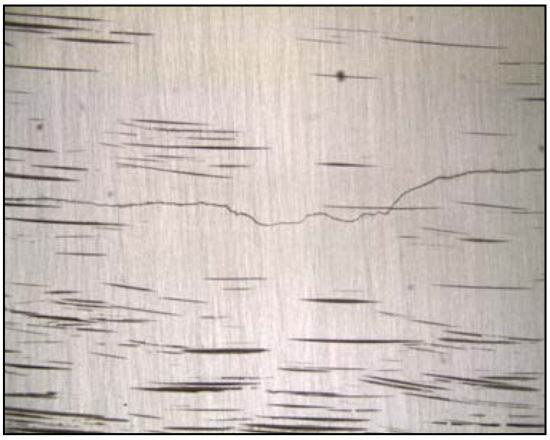

Figure B.139 - Sample 7
Diffuse On-Axis Lighting

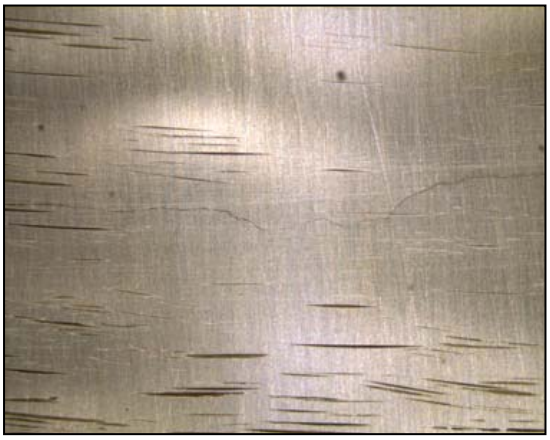

Figure B.140 - Sample 7
Diffuse Ring Lighting

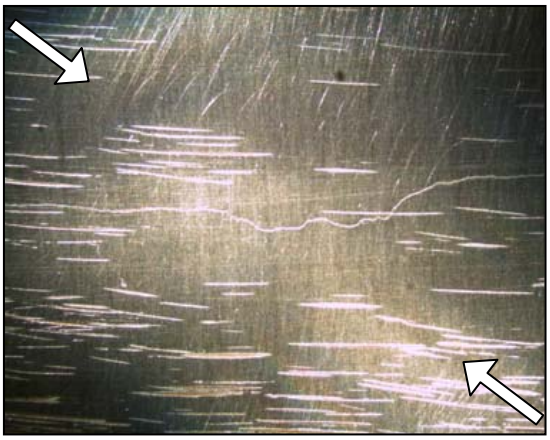

Figure B.141 - Sample 7
Spotlighting from Indicated Directions

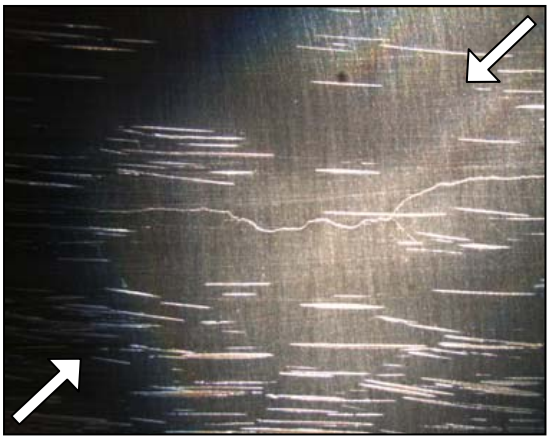

Figure B.142 - Sample 7
Spotlighting from Indicated Directions

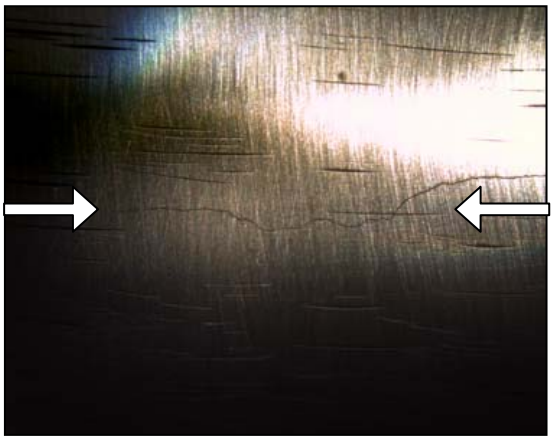

Figure B.143 - Sample 7
Spotlighting from Indicated Direction

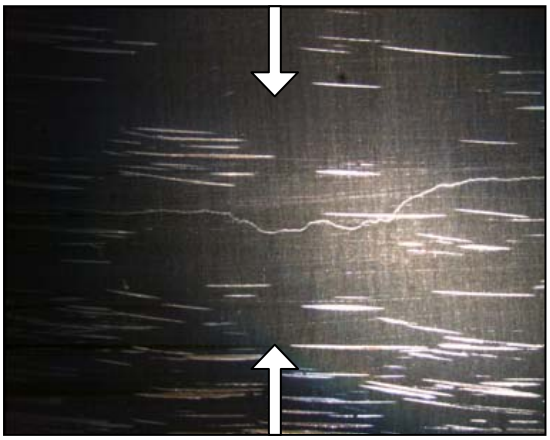

Figure B.144 - Sample 7
Spotlighting from Indicated Direction

Sample 8 – Unpolished – 125-µm Crack Opening Dimension

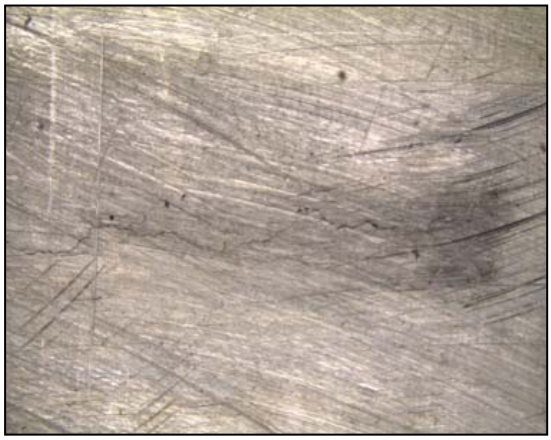

Figure B.145 - Sample 8
Diffuse On-Axis Lighting

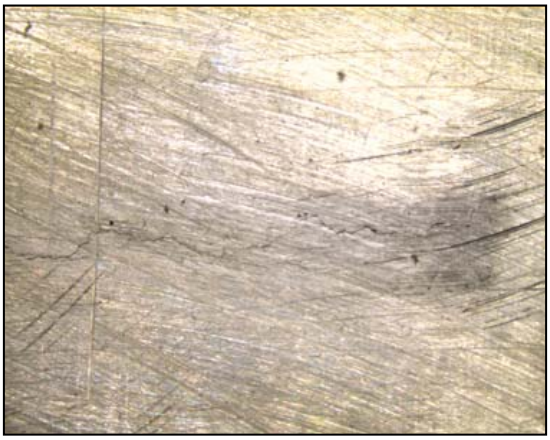

Figure B.146 - Sample 8
Diffuse Ring Lighting

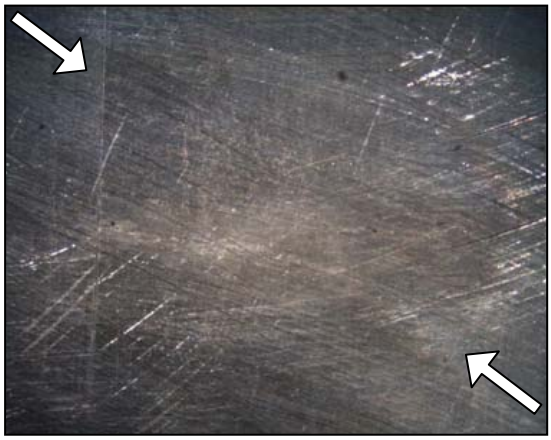

Figure B.147 - Sample 8
Spotlighting from Indicated Directions

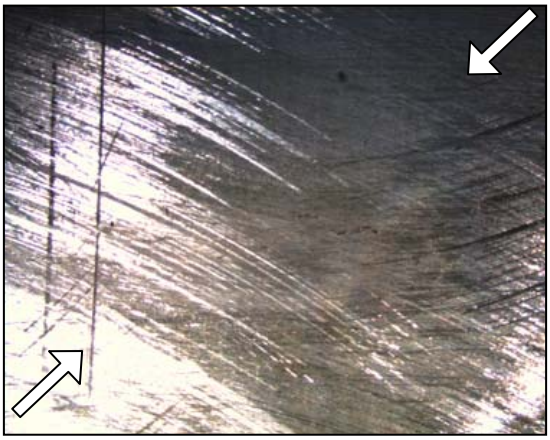

Figure B.148 - Sample 8
Spotlighting from Indicated Directions

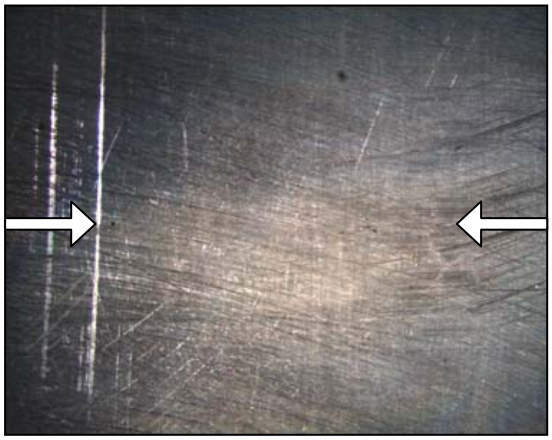

Figure B.149 - Sample 8
Spotlighting from Indicated Direction

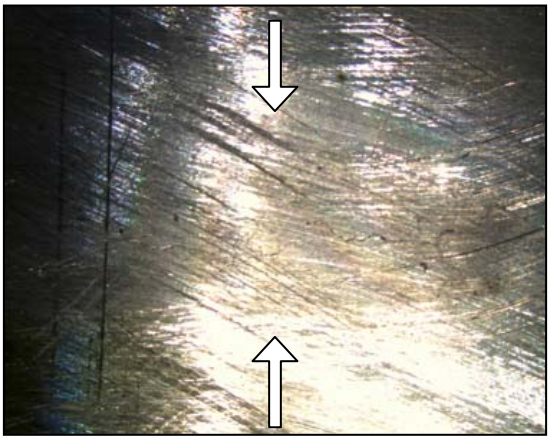

Figure B.150 - Sample 8
Spotlighting from Indicated Direction

Sample 8 – Polished – 125-µm Crack Opening Dimension

Figure B.151 - Sample 8
Diffuse On-Axis Lighting

Figure B.152 - Sample 8
Diffuse Ring Lighting

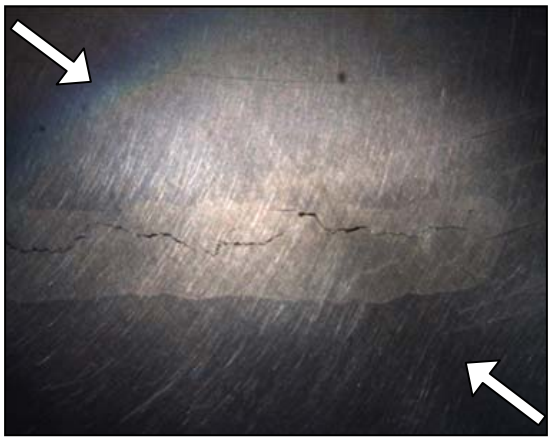

Figure B.153 - Sample 8
Spotlighting from Indicated Directions

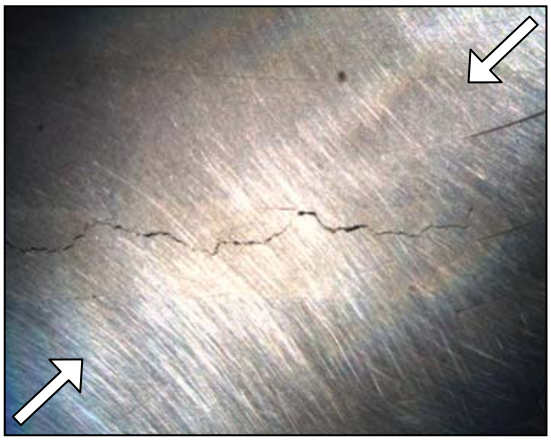

Figure B.154 - Sample 8
Spotlighting from Indicated Directions

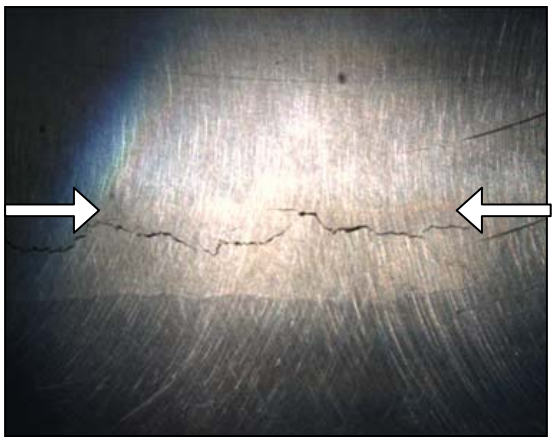

Figure B.155 - Sample 8
Spotlighting from Indicated Direction

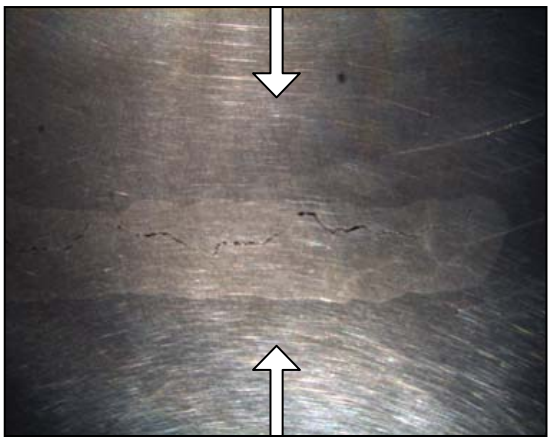

Figure B.156 - Sample 8
Spotlighting from Indicated Direction

Sample 8 – Horizontal Scratching – 125-µm Crack Opening Dimension

Figure B.157 - Sample 8
Diffuse On-Axis Lighting

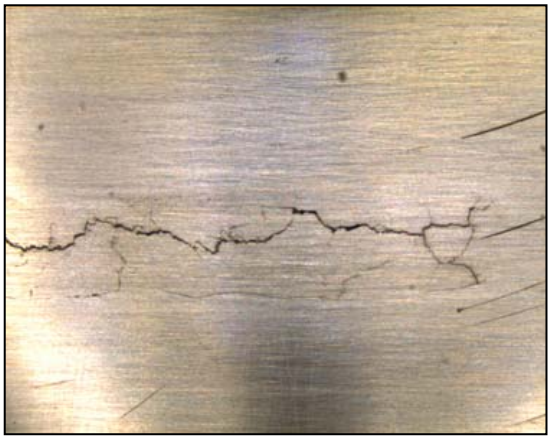

Figure B.158 - Sample 8
Diffuse Ring Lighting

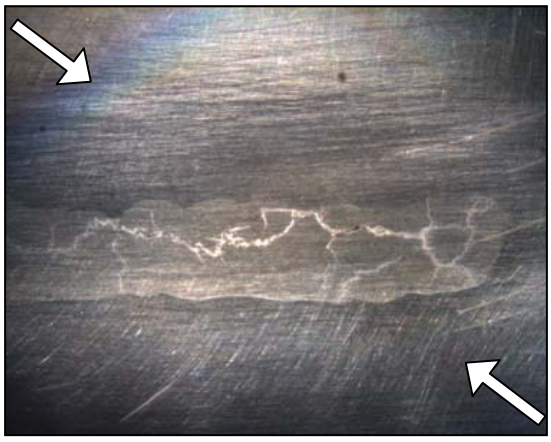

Figure B.159 - Sample 8
Spotlighting from Indicated Directions

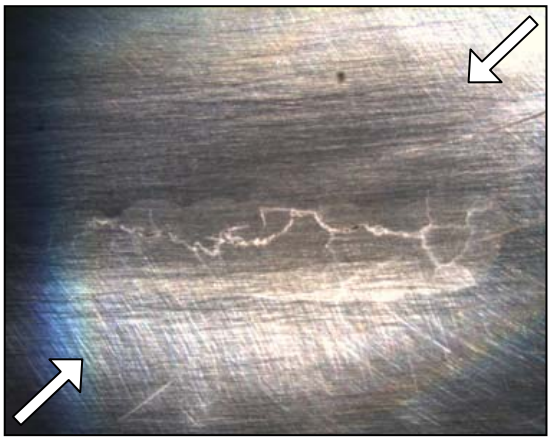

Figure B.160 - Sample 8
Spotlighting from Indicated Directions

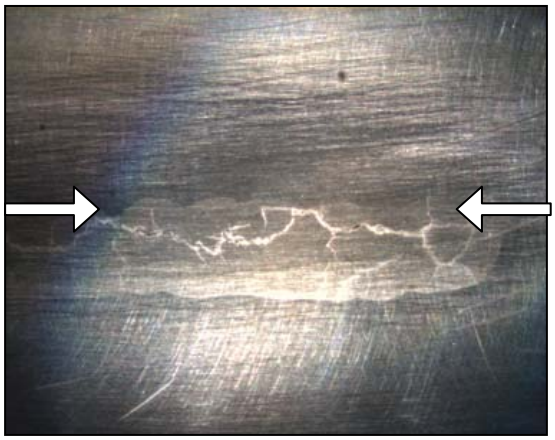

Figure B.161 - Sample 8
Spotlighting from Indicated Direction

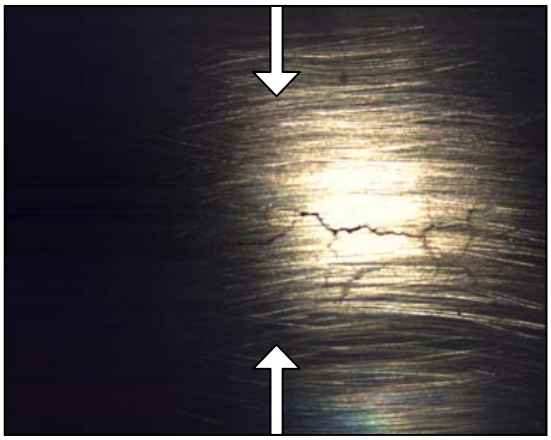

Figure B.162 - Sample 8
Spotlighting from Indicated Direction

Sample 8 – Vertical Scratching – 125-µm Crack Opening Dimension

Figure B.163 - Sample 8
Diffuse On-Axis Lighting

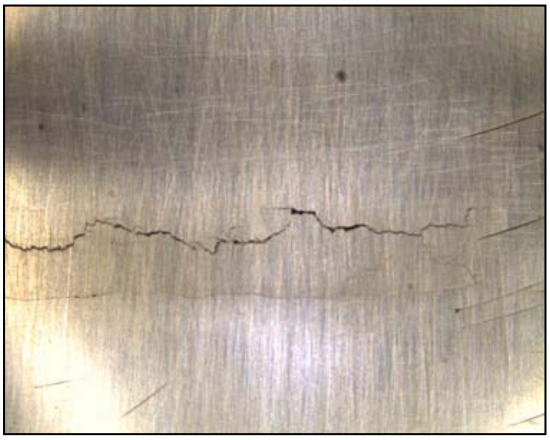

Figure B.164 - Sample 8
Diffuse Ring Lighting

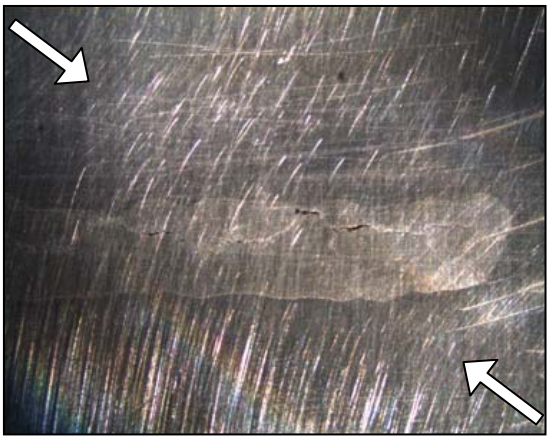

Figure B.165 - Sample 8
Spotlighting from Indicated Directions

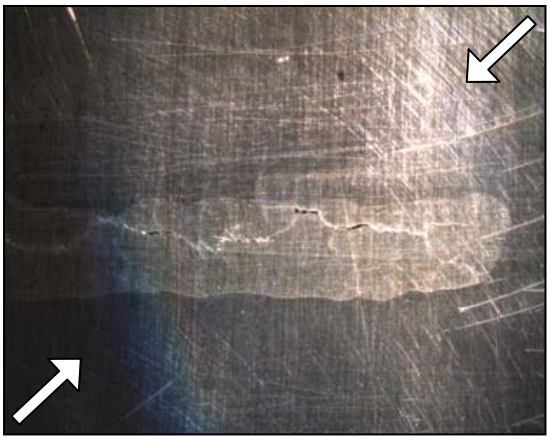

Figure B.166 - Sample 8
Spotlighting from Indicated Directions

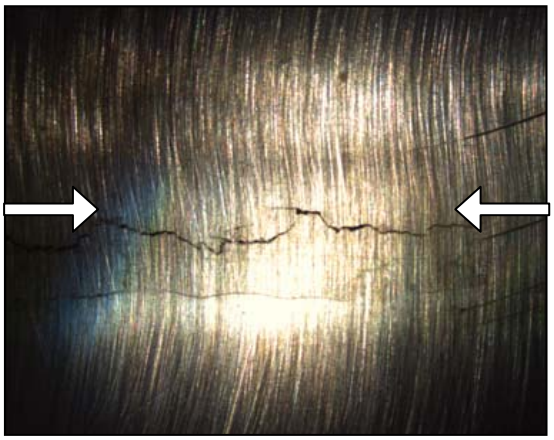

Figure B.167 - Sample 8
Spotlighting from Indicated Direction

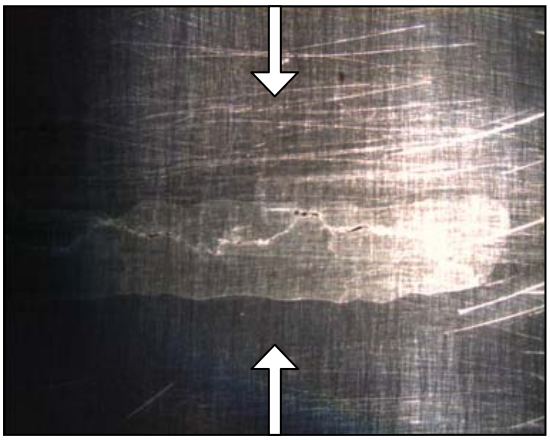

Figure B.168 - Sample 8
Spotlighting from Indicated Direction

Sample 9 – Unpolished – 125-µm Crack Opening Dimension

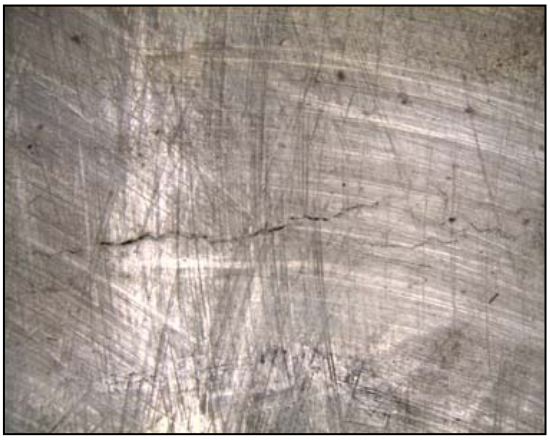

Figure B.169 - Sample 9
Diffuse On-Axis Lighting

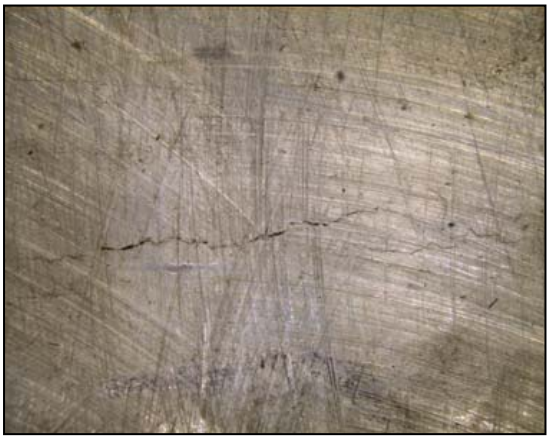

Figure B.170 - Sample 9
Diffuse Ring Lighting

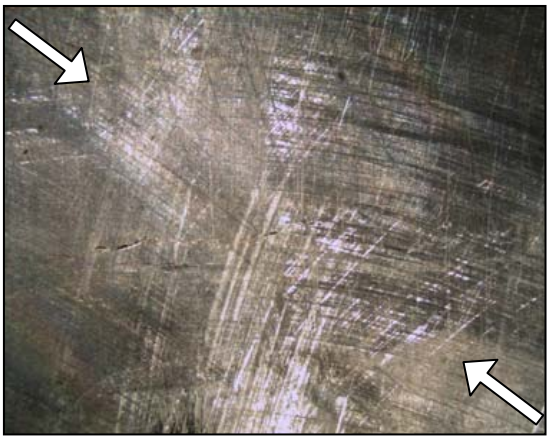

Figure B.171 - Sample 9
Spotlighting from Indicated Directions

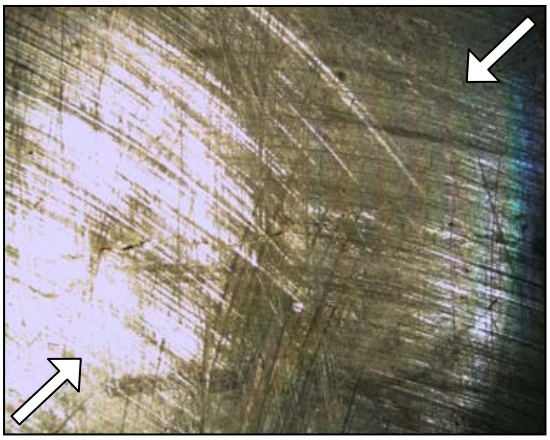

Figure B.172 - Sample 9
Spotlighting from Indicated Directions

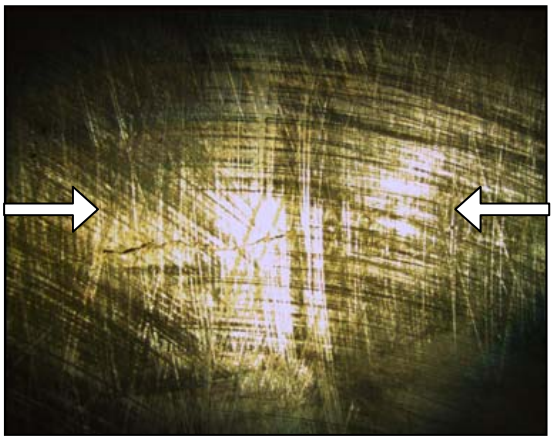

Figure B.173 - Sample 9
Spotlighting from Indicated Direction

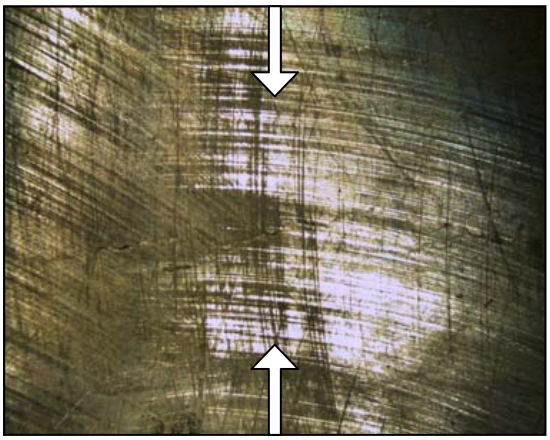

Figure B.174 - Sample 9
Spotlighting from Indicated Direction

Sample 9 – Polished – 125-µm Crack Opening Dimension

Figure B.175 - Sample 9
Diffuse On-Axis Lighting

Figure B.176 - Sample 9
Diffuse Ring Lighting

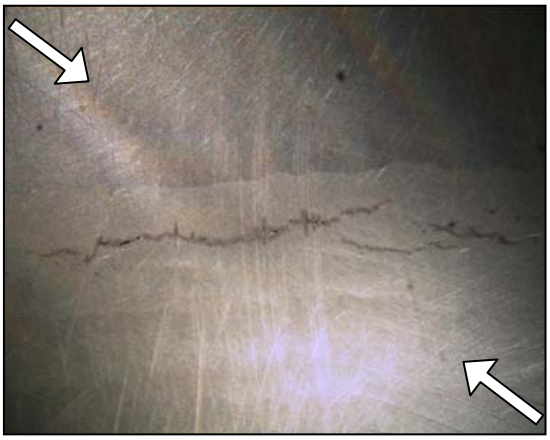

Figure B.177 - Sample 9
Spotlighting from Indicated Directions

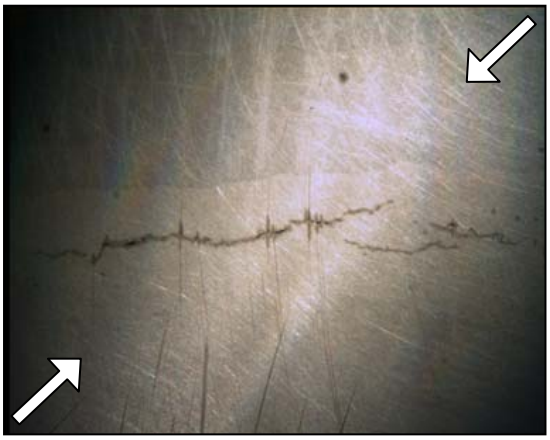

Figure B.178 - Sample 9
Spotlighting from Indicated Directions

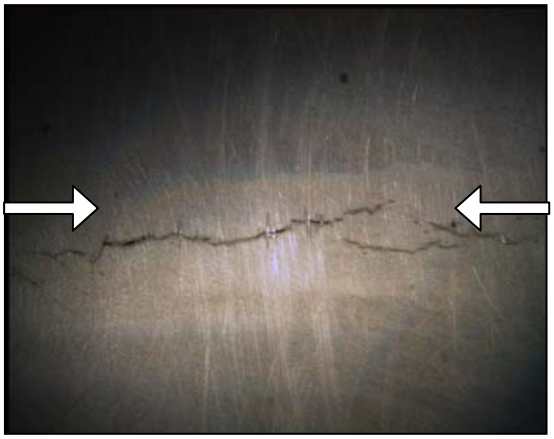

Figure B.179 - Sample 9
Spotlighting from Indicated Direction

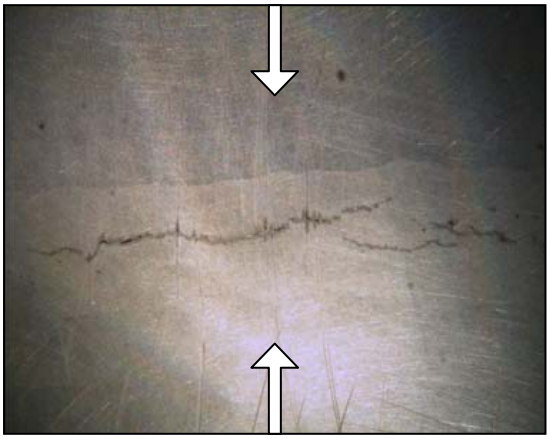

Figure B.180 - Sample 9
Spotlighting from Indicated Direction

Sample 9 – Horizontal Scratching – 125-µm Crack Opening Dimension

Figure B.181 - Sample 9
Diffuse On-Axis Lighting

Figure B.182 - Sample 9
Diffuse Ring Lighting

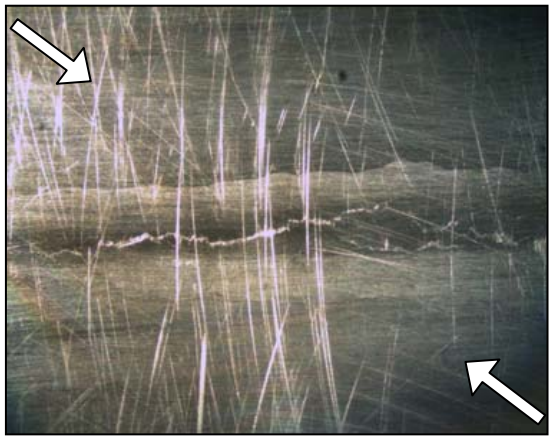

Figure B.183 - Sample 9
Spotlighting from Indicated Directions

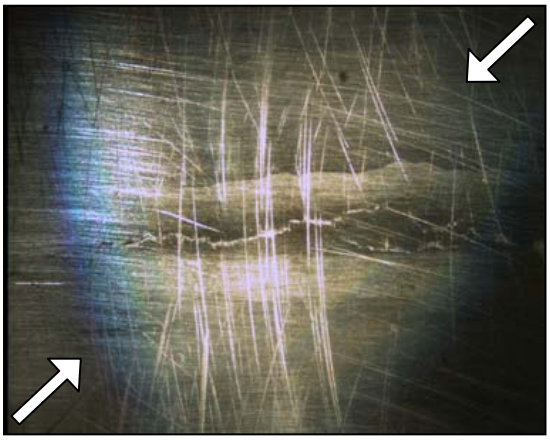

Figure B.184 - Sample 9
Spotlighting from Indicated Directions

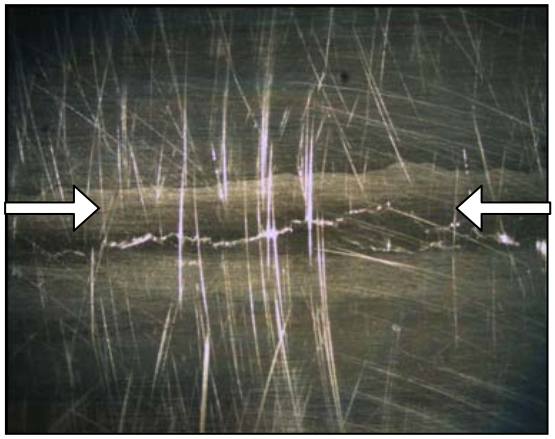

Figure B.185 - Sample 9
Spotlighting from Indicated Direction

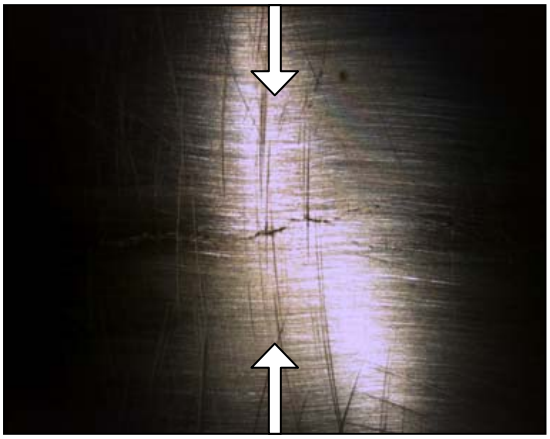

Figure B.186 - Sample 9
Spotlighting from Indicated Direction

Sample 9 – Vertical Scratching – 125-µm Crack Opening Dimension

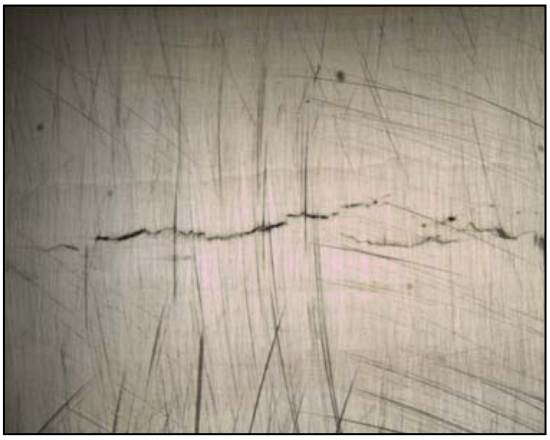

Figure B.187 - Sample 9
Diffuse On-Axis Lighting

Figure B.188 - Sample 9
Diffuse Ring Lighting

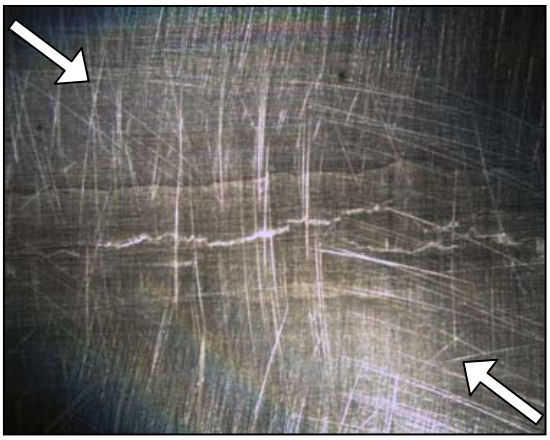

Figure B.189 - Sample 9
Spotlighting from Indicated Directions

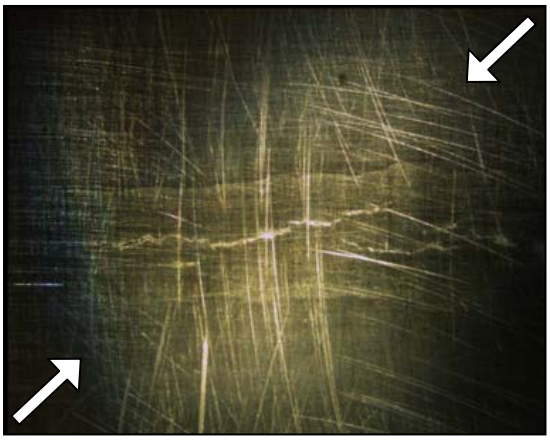

Figure B.190 - Sample 9
Spotlighting from Indicated Directions

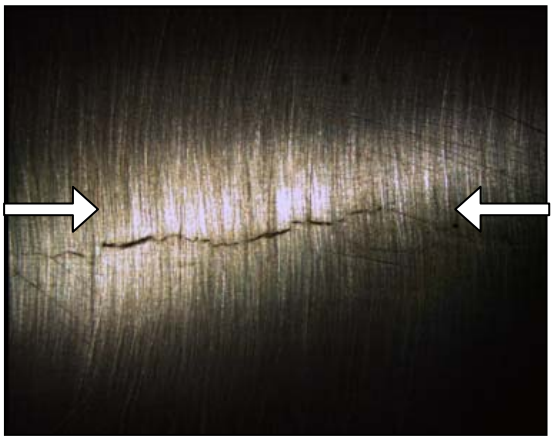

Figure B.191 - Sample 9
Spotlighting from Indicated Direction

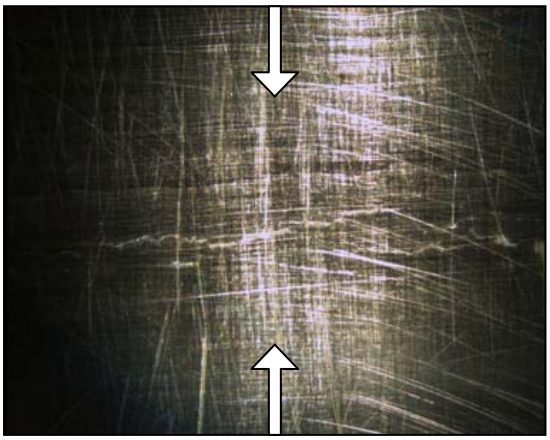

Figure B.192 - Sample 9
Spotlighting from Indicated Direction